

# The Upsilon spectrum and the determination of the lattice spacing from lattice QCD including charm quarks in the sea

R. J. Dowdall,<sup>1,\*</sup> B. Colquhoun,<sup>1</sup> J. O. Daldrop,<sup>1,†</sup> C. T. H. Davies,<sup>1,‡</sup> I. D. Kendall,<sup>1</sup> E. Follana,<sup>2</sup> T. C. Hammant,<sup>3</sup> R. R. Horgan,<sup>3</sup> G. P. Lepage,<sup>4</sup> C. J. Monahan,<sup>3,§</sup> and E. H. Müller<sup>5</sup>

(HPQCD Collaboration)<sup>||</sup>

<sup>1</sup>*SUPA, School of Physics and Astronomy, University of Glasgow, Glasgow, G12 8QQ, UK*

<sup>2</sup>*Departamento de Física Teórica, Universidad de Zaragoza, Cl. Pedro Cerbuna 12, E-50009 Zaragoza, Spain*

<sup>3</sup>*DAMTP, University of Cambridge, Wilberforce Road, Cambridge CB3 0WA, UK*

<sup>4</sup>*Laboratory of Elementary-Particle Physics, Cornell University, Ithaca, New York 14853, USA*

<sup>5</sup>*SUPA, School of Physics, University of Edinburgh, King's Buildings, Edinburgh, EH9 3JZ, UK*

(Received 1 November 2011; published 21 March 2012)

We give results for the Upsilon spectrum from lattice QCD using an improved version of the nonrelativistic QCD action for  $b$  quarks which includes radiative corrections to kinetic terms at  $\mathcal{O}(v^4)$  in the velocity expansion. We also include for the first time the effect of up, down, strange and charm quarks in the sea using “second generation” gluon field configurations from the MILC Collaboration. Using the  $Y\ 2S - 1S$  splitting to determine the lattice spacing, we are able to obtain the  $1P - 1\bar{S}$  splitting to 1.4% and the  $3S - 1S$  splitting to 2.4%. Our improved result for  $M(Y) - M(\eta_b)$  is 70(9) MeV and we predict  $M(Y') - M(\eta'_b) = 35(3)$  MeV. We also calculate  $\pi$ ,  $K$  and  $\eta_s$  correlators using the highly improved staggered quark action and perform a chiral and continuum extrapolation to give values for  $M_{\eta_s}(0.6893(12)$  GeV) and  $f_{\eta_s}(0.1819(5)$  GeV) that allow us to tune the strange quark mass as well as providing an independent and consistent determination of the lattice spacing. Combining the non-relativistic QCD and highly improved staggered quark analyses gives  $m_b/m_s = 54.7(2.5)$  and a value for the heavy quark potential parameter of  $r_1 = 0.3209(26)$  fm.

DOI: 10.1103/PhysRevD.85.054509

PACS numbers: 12.38.Gc, 11.15.Ha, 14.40.Nd, 14.40.Pq

## I. INTRODUCTION

Lattice QCD calculations have developed rapidly both in accuracy and in scope in the last few years. This growth has built on the first demonstration that numerical simulations including  $u$ ,  $d$  and  $s$  quarks in the sea with light enough  $u/d$  quarks give results in agreement with experiment for simple “gold-plated” quantities across the full range of hadron physics [1]. Errors at the level of a few % make this highly nontrivial. A key element of those calculations was the determination of the  $Y$  spectrum because there are many gold-plated states below threshold for strong Zweig-allowed decay. In addition radial and orbital excitation energies are very insensitive to quark masses (including that of the  $b$  itself) making them useful for determining the lattice spacing,  $a$ , without a complicated tuning process. A further incentive for lattice  $Y$  studies is the importance of testing  $b$  quark physics from lattice QCD

so that the same action can be used for results in  $B$  physics required, in conjunction with experiment, for the determination of elements of the Cabibbo-Kobayashi-Maskawa matrix. Here we give new results for the  $Y$  spectrum improving on those earlier results in several ways to keep pace with improvements in other areas of lattice QCD. We have improved statistical errors, improved the nonrelativistic QCD (NRQCD) action and we are also now using “second generation” gluon field configurations that include charm quarks in the sea.

The  $b$  quarks in these first calculations that included the full effect of sea quarks [2,3] were implemented using lattice NRQCD with an action accurate through  $v^4$  in the velocity expansion for the  $b$  quark [4]. The coefficients of the  $v^4$  terms were matched to full QCD at tree level, having removed the most significant source of radiative corrections, that of tadpole diagrams generated in lattice QCD from the form of the lattice gluon field, by the use of “tadpole-improvement” [5]. The gluon field configurations used were generated by the MILC Collaboration [6] using a Symanzik-improved gluon action in which radiative corrections at  $\mathcal{O}(\alpha_s a^2)$  were included except for radiative corrections from quark loops [7] ( $\mathcal{O}(n_f \alpha_s a^2)$  where  $n_f$  is the number of sea quark flavors), which were omitted. Configurations at three different values of the lattice spacing were available: “supercoarse” ( $a \approx 0.18$  fm);

\*Rachel.Dowdall@glasgow.ac.uk

†Current address: Helmholtz Institut für Strahlen und Kernphysik and Bethe Centre for Theoretical Physics, Universität Bonn, 53115 Bonn, Germany

‡c.davies@physics.gla.ac.uk

§Current address: Department of Physics, College of William and Mary, Williamsburg, VA 23187, USA

||URL: <http://www.physics.gla.ac.uk/HPQCD>

“coarse” ( $a \approx 0.12$  fm) and “fine” ( $a \approx 0.09$  fm).  $u/d$  and  $s$  sea quarks were included using the improved staggered (asqtad) action [8–10] which is numerically relatively fast. A range of  $u/d$  masses (taken to be the same) were used ranging down to a ratio with the  $s$  sea quark mass of around 0.2. The key mass splittings in the bottomonium spectrum studied were those between the ground  $S$ -wave states and the first radially excited  $S$ -wave states, the  $2S - 1S$  splitting, and that between the first  $P$ -wave states and the ground  $S$ -wave states, the  $1P - 1S$  splitting. The statistical errors from the lattice calculation for these splittings were 1–2% (i.e. 5–10 MeV) and systematic errors were estimated to be similar to this or smaller, depending on the lattice spacing. Within these errors, agreement with experiment was confirmed.

More recently the  $Y$  spectrum has been calculated using the same NRQCD action on gluon configurations at a “coarse” ( $a \approx 0.11$  fm) and a “fine” ( $a \approx 0.09$  fm) lattice spacing generated by the RBC/UKQCD Collaboration using the Iwasaki gluon action and  $2 + 1$  flavors of sea quarks implemented with the domain wall formalism [11,12]. Results in close agreement and with similar errors to those found on the MILC configurations are obtained, confirming the independence of the results from the sea quark formalism.

The systematic errors in the calculation of the  $Y$   $2S - 1S$  and  $1P - 1S$  splittings were studied in some detail in [2]. Sources of error there were missing radiative corrections to the  $v^4$  terms in the lattice NRQCD action (beyond tadpole-improvement), as well as radiative corrections to discretization correction terms and from higher order ( $v^6$ ) missing relativistic corrections. In addition systematic errors from the missing radiative corrections to the improvement terms in the gluon action were estimated. These errors were typically each of order 1% in the  $1P - 1S$  splitting on the fine lattices and about half that for the  $2S - 1S$  splitting because of some cancellation between  $1S$  and  $2S$  states. Errors were similar for the radiative and relativistic errors on coarser lattices but of course the discretization errors were larger.

Subsequent to this, we have made estimates of the effect of missing  $c$  quarks in the sea [13,14]. These have negligible effect on mesons apart from bottomonium, where internal momenta can be large enough to generate  $c$  quarks from the vacuum. We found the shift in the ground-state  $S$  wave masses might be of  $\mathcal{O}(5$  MeV) [14] (it is spin independent) with approximately half the shift for  $2S$  states because of a smaller “wave function at the origin” and no shift for  $1P$  states. This would give rise to systematic errors of 0.5% for the  $2S - 1S$  splitting and 1% for the  $1P - 1S$  splitting, similar to the systematic errors from other effects quoted above.

The conclusion from these results is that the errors in bottomonium masses and radial and orbital mass splittings have been pinned down and tested from this NRQCD

action at the level of 5–10 MeV. There is also a contribution to systematic errors at the same level coming from the gluon field configurations. The NRQCD systematic errors also feed in to the calculation of  $B$ ,  $B_s$  and  $B_c$  meson masses using NRQCD  $b$  quarks. The state-of-the-art calculation for the masses of these mesons has  $\mathcal{O}(10$  MeV) errors dominated by systematic errors from this NRQCD action [14,15].

In the last five years, however, other lattice QCD calculations have become increasingly accurate. For example the mass of the  $D_s$  meson was recently calculated by HPQCD with combined statistical and systematic errors of 3 MeV and its decay constant calculated to 1% [13]. These errors are at the level where we must allow for missing electromagnetism from lattice QCD.

There have been several contributions to this progress. Advances in computational speed have meant better statistical errors from calculating many more meson correlators on larger samples of configurations. It has also been possible to generate lattices with smaller lattice spacing, so that the  $D_s$  calculation includes “superfine” ( $a \approx 0.06$  fm) and “ultrafine” ( $a \approx 0.045$  fm) lattices [6]. Significant improvements have been made to relativistic quark actions too. For example, the  $D_s$  meson mass calculation used the highly improved staggered quark (HISQ) action for both valence quarks. The HISQ action [16] has smaller discretization errors than the asqtad action by about a factor of 3 and can be used for quarks as heavy as charm on lattices with a lattice spacing of 0.15 fm or smaller. This has revolutionized charm physics calculations [17] in lattice QCD and is having an impact also on calculations for mesons containing a  $b$  quark through a combination of extrapolations in the mass of the heavy HISQ quark acting as the “ $b$ ” to the physical point for the real  $b$  quark, combined with extrapolations to the continuum ( $a \rightarrow 0$ ) limit from results at many values of  $a$  [18]. The heavy HISQ calculations are computationally much more expensive than those using NRQCD and this currently limits their utility. The results for  $B_s$  and  $B_c$  meson masses have comparable errors to the existing NRQCD results, but are dominated by statistical and  $a \rightarrow 0$  extrapolation uncertainties. They then provide a complementary way of testing  $b$  physics to that of NRQCD and it is clear that combining the strengths of both methods will be optimal in future.

Meanwhile the MILC Collaboration have moved on to the production of “second generation” gluon field configurations which have a number of improvements over the earlier ensembles [19]. They include a more highly improved gluon action [20], HISQ quarks in the sea with the addition of  $c$  quarks as well as  $u$ ,  $d$  and  $s$  and with lighter  $u$  and  $d$  masses than before.

The availability of these configurations along with the incentives discussed above to improve errors in  $Y$  and  $B$  physics using NRQCD  $b$  quarks has meant that we have

begun a new programme of improved NRQCD calculations. Here we present the first results, giving the radial and orbital splittings in the  $Y$  spectrum, tuning the lattice  $b$  quark mass and determining the lattice spacing from the  $(2S - 1S)$  splitting. As well as using the second generation gluon field configurations we have improved the NRQCD action by adding radiative corrections to the  $v^4$  kinetic terms including discretization errors. We also have improved statistics and improved methods for tuning the  $b$  quark mass. This has meant that we can test the effect of radiative corrections to the  $v^4$  kinetic terms on the meson dispersion relation. Using both perturbative and nonperturbative methods for determining the radiative corrections to spin-dependent terms we are able to improve the determination of the  $Y$  hyperfine splitting.

A useful complementary method for determining the lattice spacing was developed in [21]. It uses the fictitious  $s\bar{s}$  pseudoscalar particle known as the  $\eta_s$ . This particle does not exist in the real world because of mixing with light quarks to form the  $\eta$  and  $\eta'$  but on the lattice this can be prevented. The mass and decay constant of the  $\eta_s$  can be determined accurately in a lattice QCD calculation using the HISQ action and their physical values fixed from  $M_\pi$ ,  $M_K$ ,  $f_\pi$  and  $f_K$  from a simultaneous chiral and continuum extrapolation. Here we update the results of [21] for these  $2 + 1 + 1$  configurations and use these also to give a determination of the lattice spacing.

The two different methods for determining the lattice spacing can be combined through the use of a third quantity,  $r_1$  [22], which can be derived accurately from determination of the heavy quark potential [23].  $r_1/a$  values are provided for these configurations by the MILC Collaboration [24].  $r_1/a$  provides a good determinant of the relative lattice spacing between different sets of gluon configurations but its physical value must be determined from other quantities. From the separate determination of the lattice spacing from the two methods above we have two sets of results for  $r_1$  in fm as a function of lattice spacing. From this we are able to test that the two methods give the same result in the continuum and chiral limits (which they do) and provide a physical value of  $r_1$  that could be used, in the absence of either of the other

methods, to determine the lattice spacing on other ensembles with  $2 + 1 + 1$  flavors of sea quarks.

We also combine results for tuned  $b$  quark masses in NRQCD and tuned  $s$  quark masses from HISQ along with one-loop renormalization constants to give a value for  $m_b/m_s$  for comparison to other results obtained purely from the HISQ action.

The layout of the paper is as follows. Section II discusses the second generation gluon field ensembles giving more details of the improvements present there. Section III describes the improvements to the NRQCD calculations and results for the  $Y$  spectrum. Section IV discusses the  $\pi$ ,  $K$ ,  $\eta_s$  analysis on these same configurations and the additional information that provides to determine the lattice spacing. This is tied together via the determination of the heavy quark potential parameter,  $r_1$ , in Sec. V and  $m_b/m_s$  in Secs. VI and VII. provides our conclusions.

## II. SECOND GENERATION $2 + 1 + 1$ GLUON FIELD ENSEMBLES

The gauge configurations used in this calculation are listed in Table I [19]. These were generated by the MILC Collaboration using a tadpole-improved Lüscher-Weisz gauge action with coefficients corrected perturbatively through  $\mathcal{O}(\alpha_s)$  including pieces proportional to  $n_f$ , the number of quark flavors in the sea [20] (see Appendix A). The gauge action is then improved completely through  $\mathcal{O}(\alpha_s a^2)$ , unlike the earlier asqtad configurations. Sea quarks are included with the HISQ action [16] which also has smaller discretization errors compared to the asqtad action (see the discussion in Sec. IV). The configurations include a sea charm quark in addition to up, down and strange. These configurations are then said to have  $2 + 1 + 1$  flavors in the sea, since the  $u$  and  $d$  quarks are taken to have the same mass, which is heavier than average  $u/d$  mass in the real world, and the  $s$  and  $c$  masses are tuned as closely as possible to their correct values at that lattice spacing. The tuning of the sea  $s$  quark mass is much more accurately done—to better than 5%—than on the previous asqtad configurations. This means that the  $u/d$  quark mass (denoted  $m_l$  here) can be more accurately

TABLE I. Details of the MILC gluon field ensembles used in this paper.  $\beta = 10/g^2$  is the  $SU(3)$  gauge coupling and  $L/a$  and  $T/a$  are the number of lattice spacings in the space and time directions for each lattice.  $am_l$ ,  $am_s$  and  $am_c$  are the light (up and down taken to have the same mass), strange and charm sea quark masses in lattice units.  $r_1/a$  is the static-quark potential parameter in lattice units determined by the MILC Collaboration [19,24]. Note that this has not been “smoothed”. The ensembles 1 and 2 will be referred to in the text as “very coarse”, 3 and 4 as “coarse” and 5 as “fine.”

Set	$\beta$	$r_1/a$	$am_l$	$am_s$	$am_c$	$L/a \times T/a$
1	5.80	2.041(10)	0.013	0.065	0.838	$16 \times 48$
2	5.80	2.0621(45)	0.0064	0.064	0.828	$24 \times 48$
3	6.00	2.574(5)	0.0102	0.0509	0.635	$24 \times 64$
4	6.00	2.623(11)	0.00507	0.0507	0.628	$32 \times 64$
5	6.30	3.549(13)	0.0074	0.037	0.440	$32 \times 96$

calibrated in terms of the  $s$  quark mass for chiral extrapolations. Here we use a ratio of  $m_l/m_s$  as low as one tenth (see Table I) whereas in our previous work on the asqtad configurations our most chiral ensemble had a ratio of the  $m_{l,\text{sea}}/m_{s,\text{physical}}$  of one quarter. This means that we have a much smaller chiral extrapolation to do to reach the physical  $u/d$  mass (where  $m_l = m_s/27$  [6]) than before.

The sea quarks are included with the standard method of incorporating the determinant of the quark matrix raised to the one quarter power for each flavor, in order to implement the correct counting for sea staggered quarks. The algorithm used for including the sea quarks has now been improved by MILC to the exact RHMC algorithm [19], i.e. all errors in the time step for the updating algorithm have been removed.

The configurations are separated by 5 trajectories in the time units of the updating algorithm for the very coarse and coarse ensembles and by 6 trajectories for the fine ensemble. In Secs. III B and IV A we will study the auto-correlations in our meson correlators to show how independent the configurations are for different observables.

The  $r_1/a$  values given in Table I are determined by the MILC Collaboration after extraction of the potential between two infinitely heavy (static) quarks at separation  $r/a$  in lattice units.  $r_1/a$  is defined [22] as the point where the force  $F(r)$  derived from the derivative of the potential satisfies

$$r^2 F(r) = 1. \quad (1)$$

The values of  $r_1/a$  for these ensembles have been chosen to match approximately those of the previous results including 2 + 1 flavors of asqtad quarks and can be used to determine the lattice spacing if the physical value for  $r_1$  is known. Using the  $r_1$  value determined previously on configurations with 2 + 1 flavors of sea quarks, this means that the lattice spacing values will be approximately 0.15 fm, 0.12 fm and 0.09 fm. The physical spatial size of the lattices then exceeds 2.5 fm and is as high as 3.8 fm on the ensembles that correspond to  $m_l/m_s = 0.1$ . In Sec. V we will derive a physical value for  $r_1$  based on the results from Secs. III and IV to calibrate more accurately the lattice spacing values for these configurations.

### III. THE UPSILON SPECTRUM

#### A. The NRQCD action

The spectrum of bottomonium mesons is extracted by computing appropriate correlators constructed from  $b$ -quark propagators on the gluon field ensembles listed in Table I. We make use of NRQCD, an effective field theory that gives an expansion of the Dirac action in powers of the heavy quark velocity,  $v$ . This is discretized onto a space-time lattice as lattice NRQCD [4,25] and is a good formalism to use for  $b$  quarks since they are known to be very nonrelativistic inside their bound states ( $v^2 \approx 0.1$ ).

As used on the lattice, NRQCD has the advantage that propagators can be generated using a simple time evolution equation rather than having to invert the Dirac matrix. The quark and antiquark fields are separated in this formalism as 2-component spinors.

The NRQCD Hamiltonian we use is given by:

$$\begin{aligned} aH &= aH_0 + a\delta H; \quad aH_0 = -\frac{\Delta^{(2)}}{2am_b}, \\ a\delta H &= -c_1 \frac{(\Delta^{(2)})^2}{8(am_b)^3} + c_2 \frac{i}{8(am_b)^2} (\nabla \cdot \tilde{\mathbf{E}} - \tilde{\mathbf{E}} \cdot \nabla) \\ &\quad - c_3 \frac{1}{8(am_b)^2} \sigma \cdot (\tilde{\nabla} \times \tilde{\mathbf{E}} - \tilde{\mathbf{E}} \times \tilde{\nabla}) \\ &\quad - c_4 \frac{1}{2am_b} \sigma \cdot \tilde{\mathbf{B}} + c_5 \frac{\Delta^{(4)}}{24am_b} - c_6 \frac{(\Delta^{(2)})^2}{16n(am_b)^2}. \end{aligned} \quad (2)$$

Here  $\nabla$  is the symmetric lattice derivative and  $\Delta^{(2)}$  and  $\Delta^{(4)}$  the lattice discretization of the continuum  $\sum_i D_i^2$  and  $\sum_i D_i^4$  respectively.  $am_b$  is the bare  $b$  quark mass.  $\tilde{\mathbf{E}}$  and  $\tilde{\mathbf{B}}$  are the chromoelectric and chromomagnetic fields calculated from an improved clover term [2]. The  $\tilde{\mathbf{B}}$  and  $\tilde{\mathbf{E}}$  are made anti-Hermitian but not explicitly traceless, to match the perturbative calculations done using this action.

In terms of the velocity expansion  $H_0$  is  $\mathcal{O}(v^2)$  and  $\delta H$  is  $\mathcal{O}(v^4)$ , including discretization corrections.  $H_0$  contains the bare quark mass parameter which is nonperturbatively tuned to the correct value for the  $b$  quark as discussed below in Sec. III C. The terms in  $\delta H$  have coefficients  $c_i$  whose values are fixed from matching lattice NRQCD to full QCD. This matching takes account of high momentum modes that differ between NRQCD and full QCD and so it can be done perturbatively, giving the  $c_i$  the expansion  $1 + c_i^{(1)}\alpha_s + \mathcal{O}(\alpha_s^2)$ . In previous calculations [2] we used the tree level value of 1 for all the  $c_i$ , after tadpole-improving the gluon fields. This means dividing all the gluon fields,  $U_\mu(x)$  by a tadpole-parameter,  $u_0$ , before constructing covariant derivatives or  $\mathbf{E}$  and  $\mathbf{B}$  fields for the Hamiltonian above. The  $u_0$  parameter corrects for tadpole diagrams that arise in a universal way from the way in which the lattice gluon field is constructed. For  $u_0$  we took the mean trace of the gluon field in Landau gauge,  $u_{0L}$ . With the tadpole-improvement in place we expect the radiative corrections to the  $c_i$  coefficients to be of normal size, i.e.  $\mathcal{O}(1)$  [26]; without this they can be rather large.

Here, on top of tadpole-improvement with  $u_{0L}$ , we use  $\mathcal{O}(\alpha_s)$  corrected coefficients for the kinetic terms, i.e.  $c_1$ ,  $c_5$  and  $c_6$ , so improving on the NRQCD action used previously, and significantly reducing the systematic errors in the tuning of the  $b$  quark mass and in the determination of the radial and orbital mass splittings. The calculation of the  $c_i^{(1)}$  for  $i = 1, 5, 6$  is discussed in Appendix B [27]. Table II gives the values for  $c_1$ ,  $c_5$  and  $c_6$  that we use on the very coarse, coarse and fine lattices as a result. As expected, after tadpole-improvement, the coefficients  $c_{1,5,6}^{(1)}$



TABLE II. The coefficients  $c_1$ ,  $c_5$  and  $c_6$  used in the NRQCD Hamiltonian of Eq. (2) on the very coarse (sets 1 and 2), coarse (sets 3 and 4) and fine (set 5) ensembles. Other coefficients had values 1 except for calculations in which we specifically changed their values to test the effect, as described in the text.

Set	$c_1$	$c_5$	$c_6$
very coarse	1.36	1.21	1.36
coarse	1.31	1.16	1.31
fine	1.21	1.12	1.21

are not large and they are well behaved as a function of the  $b$  quark mass. In Sec. III C we test these coefficients through a precision study of the dispersion relation for  $Y$  and  $\eta_b$  mesons.

The other coefficients in the NRQCD action are  $c_2$ ,  $c_3$  and  $c_4$ .  $c_3$  and  $c_4$  multiply spin-dependent terms that give rise, respectively, to spin-orbit and spin-spin fine structure in the spectrum. Most of the splittings we will discuss here are “spin averaged” to remove the effect of these terms and so we will generally set  $c_3$  and  $c_4$  to their tree level values of 1. However, in Sec. III E 3 we will discuss the hyperfine splitting ( $M(Y) - M(\eta_b)$ ) and show results for both perturbatively improved and nonperturbatively determined  $c_4$ . The calculation of the appropriate  $c_4^{(1)}$  [28] is discussed in Appendix B, and the nonperturbative determination of  $c_4$  and  $c_3$  in Appendix C. The nonperturbative studies indicate that the value of  $c_3$  is very close to 1 for this NRQCD action.  $c_2$  multiplies a spin-independent term, the Darwin term, which can affect spin-independent splittings such as radial and orbital excitation energies. Because the Darwin term is field dependent we do not expect it to have such a large effect as kinetic terms, and therefore do not expect radiative corrections to  $c_2$  to be as important as for  $c_1$ ,  $c_5$  and  $c_6$ . However, in Sec. III C we will investigate the effect of changing  $c_2$  so that we can estimate concretely the systematic error from not knowing its  $\mathcal{O}(\alpha_s)$  correction.

Given the NRQCD action above, the time evolution of the heavy quark propagator is given by:

$$G(\mathbf{x}, t + 1) = \left(1 - \frac{a\delta H}{2}\right) \left(1 - \frac{aH_0}{2n}\right)^n U_t^\dagger(x) \times \left(1 - \frac{aH_0}{2n}\right)^n \left(1 - \frac{a\delta H}{2}\right) G(\mathbf{x}, t) \quad (3)$$

with starting condition:

$$G(\mathbf{x}, 0) = \phi(\mathbf{x})1. \quad (4)$$

The smearing function  $\phi(\mathbf{x})$  is used to improve the projection onto a particular state in the spectrum. Including a variety of smearing functions is essential to obtain accurate results for the splittings between the low lying excited states. Full details of the smearing functions used will be given in Sec. III B. The 1 in Eq. (4) is the unit matrix in color and (2-component) spin space. The parameter  $n$  has no physical significance, but is included for improved

TABLE III. Parameters used in the NRQCD action for our calculations that included a full  $5 \times 5$  matrix of correlators. Other parameters have been used in subsidiary test calculations as described in the text.  $am_b$  is the bare  $b$  quark mass and  $u_{0L}$  the Landau link tadpole-improvement factor used in the NRQCD action. The different number of digits given in the  $u_{0L}$  column reflect the precision with which it was determined.  $n_{\text{cfg}}$  gives the number of configurations used in each ensemble and  $n_t$  is the number of starting time sources per configuration.  $T_p$  is the time length of each propagator in lattice units.  $a_{sm}$  is the parameter for the smearing function described in Sec. III B.

Set	$am_b$	$u_{0L}$	$n_{\text{cfg}}$	$n_t$	$T_p$	$a_{sm}$
1	3.42	0.8195	1021	16	40	0.79
2	3.39	0.820 15	1000	16	40	0.80
3	2.66	0.834	1053	16	40	1.0
4	2.62	0.8349	1000	16	40	1.0
5	1.91	0.8525	874	16	48	1.37

numerical stability of high momentum modes that do not contribute to bound states [4]. In [2] it was demonstrated that radial and orbital mass splittings were the same within the statistical errors available there for  $n = 2$  and  $n = 4$  on coarse lattices. The minimum value of  $n$  for stability increases as the  $b$  quark mass in lattice units falls on finer lattices. Rather than varying  $n$  as we change the quark mass, here we use  $n = 4$  throughout which is the value appropriate to the fine lattices. At zero spatial momentum the antiquark propagator is the complex conjugate of the quark propagator for a source of the kind given in Eq. (4).

Details of various parameters used in our calculation are listed in Table III. Tuning of the bare  $b$  quark mass will be discussed in Sec. III C. The tadpole parameters  $u_{0L}$  were calculated by fixing a subset of each ensemble to lattice Landau gauge using a Fourier-accelerated steepest descents algorithm [29] to maximize the average trace link ( $\sum_{\mu=1,4;x} \text{Tr} U_\mu(x)$ ), which value, normalized, then becomes  $u_{0L}$ . The whole ensemble was then fixed to Coulomb gauge by using the same algorithm to maximize the spatial trace link ( $\sum_{i=1,3;x} \text{Tr} U_i(x)$ ) to allow us to use “wave-function” smearing operators, with parameter  $a_{sm}$  as described in Sec. III B. Propagators were calculated from 16 time sources on each configuration to minimize statistical errors. Because in NRQCD we operate a simple time evolution we can choose the time length of each propagator. This we take to be greater than or equal to half the time extent of the lattice as detailed in Table III.

## B. Smearing functions and multiexponential fits

Quark propagators are generated using three different smearing functions which we label as local, ground state and excited state. They are chosen to improve the projection onto different radially excited states and previous experience has shown that “hydrogenlike” wave functions work well [2].

TABLE IV. Smearing combinations used for either the source or the sink in the construction of  $S$ -wave correlators.

Name	Quark smearing	Antiquark smearing
l	$\phi_l$	$\phi_l$
g	$\phi_{gs}$	$\phi_l$
e	$\phi_{es}$	$\phi_l$
G	$\phi_{gs}$	$\phi_{gs}$
E	$\phi_{es}$	$\phi_{es}$

$$\begin{aligned}\phi_l(r) &= \delta_{r,0} & \phi_{gs}(r) &= \exp(-r/a_{sm}) \\ \phi_{es}(r) &= (2a_{sm} - r) \exp(-r/a_{sm}).\end{aligned}\quad (5)$$

$a_{sm}$  is the smearing radius and is chosen to be approximately the same in physical units for each ensemble. Values are given in Table III. Since a different smearing function can be applied separately to the quark and antiquark we can make five different combinations as detailed in Table IV.

A different smearing can also be applied at the source and the sink making correlator combinations labeled by, e.g. lg, le, gG. The different smearing combinations allow the construction of up to a  $5 \times 5$  matrix of correlators for the  $S$ -wave states that can be fit simultaneously. The cross-correlators provide further useful information beyond that in the diagonal terms that can be used in the fitting to extract the excited states more precisely. The correlators with quantum numbers of  $^3S_1$  or  $^1S_0$  are distinguished by the insertion of either a  $\sigma$  or a  $\mathbf{1}$  in spin space at source and sink [30].

To make  $P$ -wave states we use only the l and g smearings above and apply a symmetric difference operator,  $\Delta$  to the smeared source to give a  $P$ -“wave function”. This propagator is combined with that from a  $\delta$  function source and a derivative applied at the sink to make a  $P$ -wave meson correlator. The complete set of combinations of  $\sigma$  matrices with derivatives that are needed for the  $P$ -wave states is given in [30]. On the lattice the five-dimensional spin 2 representation is split into  $E$  and  $T_2$  representations of the lattice rotational group and we fit these representations separately since differences in mass between them can arise from discretization errors on the lattice.

For the  $S$ -wave states, statistical errors were improved further by using random wall sources in combination with the smearings discussed above. The delta function quark source is replaced with a (pseudo-)random color vector  $\eta_a(\vec{x}) \in U(1)$  at each spatial point of the initial time slice. When the meson correlator is constructed, the white noise property  $\langle \eta_a(\vec{x}) \eta_b^\dagger(\vec{y}) \rangle = \delta_{ab} \delta(\vec{x} - \vec{y})$  ensures that the random noise cancels at all points except those where the initial spatial sites are the same. This can be combined with the smearing functions by distributing the random number associated with the center of each smearing function along with the smearing function. Then once again the

white noise property will mean that the resultant correlator averages over the initial time source the effect of having a smeared source at every point [31]. Previous studies have found a significant improvement in the precision of the Upsilon ground state energy using random wall sources [21]. The improvement is less clear for excited states and therefore we did not use this technique for the  $P$ -wave states.

Propagators were calculated from 16 time sources on each configuration but to avoid correlations between time sources, the correlators were binned over all sources on the same configuration. Autocorrelations between results on successive configurations in an ensemble were studied by calculating the autocorrelation function  $C_{\Delta T}$  [32]:

$$C_{\Delta T} = \frac{\langle x_i x_{i+\Delta T} \rangle - \langle x_i \rangle \langle x_{i+\Delta T} \rangle}{\langle x_i^2 \rangle - \langle x_i \rangle^2}. \quad (6)$$

Here  $x_i$  represents a correlator on a given configuration,  $i$ .  $x_{i+\Delta T}$  is the correlator on an ensemble separated by  $\Delta T$  from  $i$  in the ordered ensemble, i.e.  $\Delta T = 1$  corresponds to neighboring configurations in the ensemble. The ensembles have been generated taking into account the fact that autocorrelations increase on finer lattices. Thus neighboring configurations are 5 trajectories apart for very coarse and coarse ensembles but 6 trajectories apart for the fine ensemble [19].  $C_{\Delta T}$  is plotted against  $\Delta T$  in Fig. 1 for the case where  $x$  is an  $Y$  correlator measured with a time separation on the lattice of approximately 0.6 fm. This value was chosen to correspond to a point where correlators were dominated by the ground state. The picture is qualitatively the same for different time separations, however.  $C_{\Delta T}$  drops to zero very rapidly, within the separation  $\Delta T = 1$ . We therefore do not have to worry about autocorrelations between configurations but can treat them all as statistically independent.

Bayesian fitting is used to extract the spectrum from the correlators [33]. The fit function

$$G_{\text{meson}}(n_{sc}, n_{sk}; t) = \sum_{k=1}^{n_{\text{exp}}} a(n_{sc}, k) a^*(n_{sk}, k) e^{-E_k t} \quad (7)$$

is used, where  $aE_k$  is the energy of the  $(k-1)$ th radial excitation in lattice units and  $a(n_{sc/sk}, k)$  are the corresponding amplitudes labeled by the smearing used at the source and sink of the correlator, i.e.  $sc, sk \in \{l, g, e, G, E\}$ . We fit the full range of  $t$  values for the correlator from 1 to  $T_p$ , where  $T_p$  values are given for  $S$  wave fits in Table III and  $T_p = 20$  for  $P$  waves. The number of terms,  $n_{\text{exp}}$ , in the fit is varied, however, and Bayesian model selection criteria are applied to determine which fit is used. In practice, this means adding additional terms to the fit until the results and the errors stabilize. An example is given in Fig. 2.

The Bayesian approach allows the inclusion of prior data into the fitting procedure. The  $\chi^2$  test function is amended to

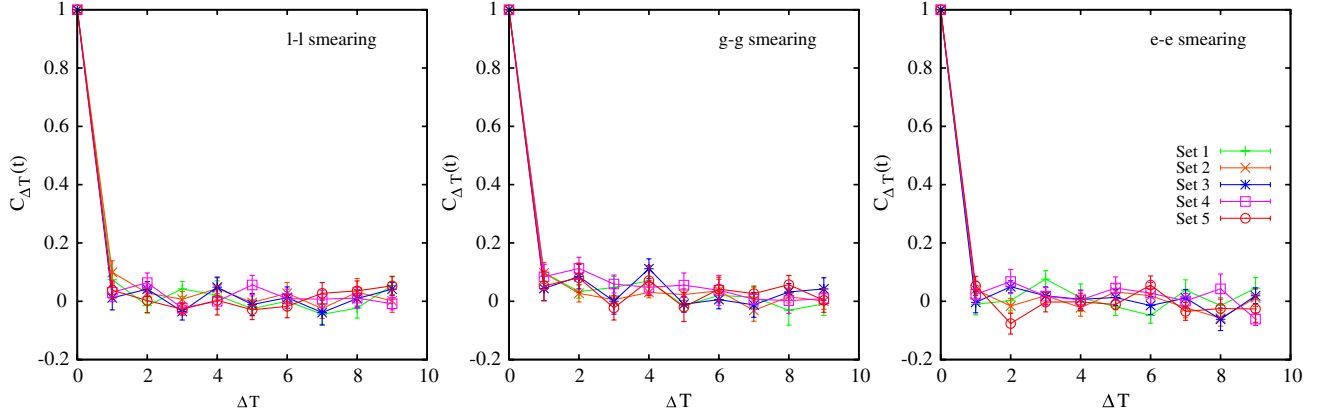


FIG. 1 (color online). Autocorrelation function  $C_{\Delta T}$  for  $\Upsilon$  correlators made from different smearing combinations, from left to right: ll, gg and ee. Different symbols are given to different ensembles according to the key on the right in the ee plot. The correlators are evaluated at lattice time separation  $t/a = 4$  on very coarse lattices (sets 1 and 2),  $t/a = 5$  on coarse lattices (sets 3 and 4) and  $t/a = 8$  on fine lattices (set 5). This corresponds to a  $t$  value where the gg correlators have reached the ground-state plateau and the ee correlators have a short plateau corresponding approximately to the first excited state mass.  $\Delta T$  gives the separation at which the autocorrelation is measured in units of numbers in the ordered ensemble list.

$$\chi_{\text{aug}}^2 = \chi^2 + \chi_{\text{prior}}^2 \quad (8)$$

and the function  $\chi_{\text{aug}}^2$  is minimized. By Bayes' theorem this corresponds to maximizing the posterior probability  $p(\text{parameters}|\text{data})$  as opposed to a standard  $\chi^2$  test which maximizes only the likelihood function  $p(\text{data}|\text{parameters})$ .  $\chi_{\text{prior}}^2$  is taken to be

$$\chi_{\text{prior}}^2 = \sum_k \frac{(p_k - \tilde{p}_k)^2}{\tilde{\sigma}_{p_k}^2} \quad (9)$$

for each fit parameter  $p_k$ . This assumes that the prior probability density function for each parameter is a

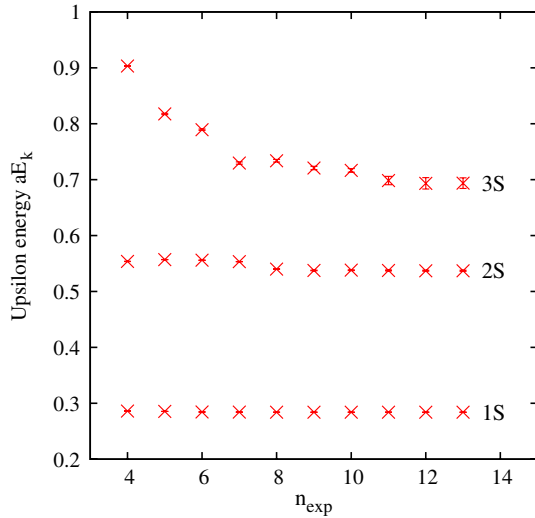


FIG. 2 (color online). Energies in lattice units of the low lying  $\Upsilon$  states for the fine ensemble, set 5, from the full  $5 \times 5$  lgeGE fit plotted against the number of exponentials,  $n_{\text{exp}}$ , included in the fit.

Gaussian with central value  $p_k$  and width  $\tilde{\sigma}_{p_k}$ . The fit parameters are: the amplitudes, which are taken to have a prior of  $0.1 \pm 1.0$ ; the ground state energies  $\ln(E_1)$  which are estimated from an effective mass plot and given a suitably wide width; and the splittings  $\ln(E_{n+1} - E_n)$  which prior information tells us should be of the order 500 MeV with a width of 250 MeV. Taking the fit parameters to be the logarithms of the energy splittings ensures that the ordering of the states is respected.

$\chi_{\text{aug}}^2$  is minimized using the singular value decomposition method. In the larger matrix fits, the correlation matrix can become ill-conditioned and it can be necessary to introduce a cutoff,  $w_{\text{cut}}$ , on the lowest eigenvalues of the correlation matrix in order to fit the data. A variation of this method is used in which, instead of setting eigenvalues below  $w_{\text{cut}} w_{\text{max}}$  to zero, they are set to  $w_{\text{max}}$  times  $w_{\text{cut}}$ . This is a less severe truncation of the correlation matrix and it improves the fits in some cases.  $w_{\text{cut}}$  was typically taken to be  $10^{-4}$  for the  $5 \times 5$  matrix fits.

In order to determine whether the inclusion of five different smearing operators actually leads to improved results, the energies of the low lying  $\Upsilon$  states are plotted in Fig. 3 for a variety of different matrix fits from the fine ensemble. The effect on the precision of the ground state is negligible but the full  $5 \times 5$  fit has significantly smaller errors for the first two excited states.

Because NRQCD is a nonrelativistic effective theory, there is an energy offset. Thus the energies obtained from correlators at zero momentum do not correspond to meson masses. Energy differences do correspond to mass differences, however and so, for example, the mass difference between the  $\Upsilon'$  and the  $\Upsilon$  (in lattice units) is given simply by  $aE_2 - aE_1$  from Eq. (7). To obtain absolute mass values requires the study of correlators for mesons at nonzero spatial momentum as discussed in Sec. III C.

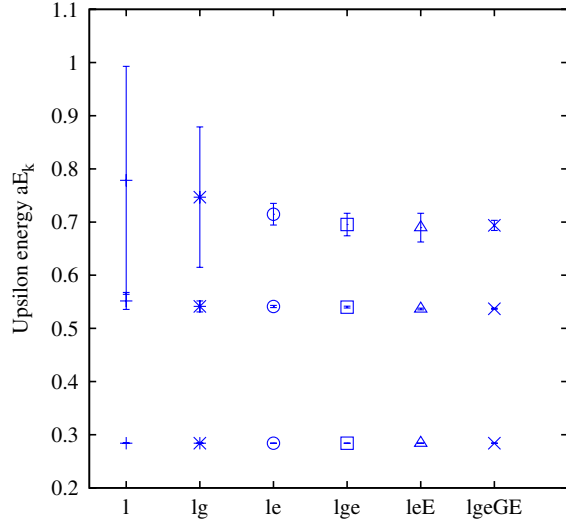


FIG. 3 (color online). Comparison of the effect of different smearing combinations for extraction of the energies of the ground and first two radially excited  $Y$  states. The energy in lattice units from the fine ensemble is shown for a  $1 \times 1 \times 1$  fit (plus),  $2 \times 2$  fits lg (star) and le (circle),  $3 \times 3$  fits lge (square) and leE (triangle), and the  $5 \times 5$  fit containing all sources lgeGE (cross).

### C. NRQCD systematics in tuning the $b$ quark mass

In this calculation the parameters of QCD that need to be determined are the  $b$  quark mass and  $\Lambda_{\text{QCD}}$ . In practice this translates into the fact that we need to tune the  $b$  quark mass parameter in the lattice NRQCD Hamiltonian until we obtain the correct value for one calibration hadron mass and we need to determine the lattice spacing from another calibration hadron mass. After that is done all other hadron masses are determined with no further tuning. The two calibration hadrons should be chosen with rather different properties. The mass chosen to fix the  $b$  quark mass should ideally be very sensitive to that value; the mass chosen to determine the lattice spacing should be as independent of the  $b$  quark mass as possible to avoid a complicated iterative tuning process. To determine the lattice spacing we choose the radial excitation energy of the  $Y$ , i.e.  $M(Y') - M(Y)$ . This is known from experiment to be very insensitive to the heavy quark mass since it changes by only 4% between the  $b$  and the equivalent quantities for the  $c$  quark, which has a mass a factor of 4.5 smaller. The determination of the lattice spacing from this quantity will be discussed in Sec. III E. Here we focus on the tuning of the  $b$  quark mass and, in particular, on the effect of the improvements to the NRQCD action which we have implemented here for the first time.

As discussed in Sec. III B the fitted energy from a zero momentum hadron correlator made from NRQCD propagators is not the hadron's mass because there is an energy offset. Instead we must determine the “kinetic mass” from the energy-momentum dispersion relation:

$$aM_{\text{Kin}} = \frac{a^2 P^2 - (a\Delta E)^2}{2a\Delta E}, \quad (10)$$

where  $a\Delta E$  is the energy difference between the meson with momentum  $Pa$  in lattice units and the meson at rest. Equation (10) assumes a fully relativistic dispersion relation, i.e.

$$aE(P) = aE(0) + \sqrt{a^2 P^2 + a^2 M_{\text{Kin}}^2}. \quad (11)$$

Systematic errors will then be present in the kinetic mass for lattice NRQCD both because the action is only accurate to a specific order in the expansion in  $v^2/c^2$  and from lattice discretization errors. Here we study both of these effects. First it is worth briefly recapitulating a discussion from the literature (see, for example, [34]) on how the kinetic mass is built up in a nonrelativistic approach as successive orders in  $v^2/c^2$  are added to the nonrelativistic expansion, because it provides a useful handle on systematic errors.

By definition the mass of a meson is given by the sum of the masses of its constituent quarks plus the binding energy. The binding energy has contributions from the internal kinetic energy, i.e. the motion of the constituent quarks relative to the center of mass, and from the interaction energy. If we write the meson dispersion relation in the standard nonrelativistic expansion as

$$E(\mathbf{P}) = M_1 + \frac{\mathbf{P}^2}{2M_2} + \dots, \quad (12)$$

then  $M_1$  is known as the static mass and  $M_2$  is the kinetic mass, equal to  $M_{\text{Kin}}$  in Eq. (10) up to relativistic corrections. It should be possible to construct the correct meson mass from both  $M_1$  and  $M_2$ , i.e. the binding energy contribution needs to feed correctly into both of them.

To see how this works in outline it is sufficient to study two free particles. The total energy of the two particle system is the sum of the masses,  $m_i$ , plus the kinetic energies,  $\mathbf{q}_i^2/2m_i$  for each particle. In the center of mass frame ( $\mathbf{P} = 0$ ) this is simply  $m_1 + m_2$  plus the internal kinetic energy. As is well-known, the internal kinetic energy can be written to leading nonrelativistic order as  $\mathbf{p}^2/2\mu$  where  $\mathbf{p}$  is the momentum of either particle in this frame and  $\mu$  is the reduced mass ( $1/\mu = 1/m_1 + 1/m_2$ ). Thus  $M_1$  takes the expected form for this two particle system. To study  $M_2$  we must include the motion of the center of mass and expand the sum of the two particle kinetic energies to  $\mathcal{O}(\mathbf{P}^2)$ . For  $M_2$  to have the correct form including the leading piece of the internal kinetic energy we need  $E(P)$  to take the form

$$E(P) = m_{q1} + m_{q2} + \frac{\mathbf{p}^2}{2\mu} + \dots + \frac{\mathbf{P}^2}{2(m_{q1} + m_{q2})} \times \left(1 - \frac{\mathbf{p}^2}{2\mu(m_{q1} + m_{q2})} + \dots\right), \quad (13)$$



i.e. we need to locate a  $\mathbf{P}^2\mathbf{p}^2$  term in the sum of the individual particle kinetic energies. This requires the individual kinetic energies to be expanded beyond leading order in the nonrelativistic expansion to include terms at fourth order in the momentum. Thus  $M_2$  will have the correct form to leading order in the internal kinetic energy if the individual kinetic energy terms are correct through next-to-leading order in momentum. In an interacting theory we also need the interaction terms to be correct through  $\mathcal{O}(v^4)$  to have the binding energy correctly included in the kinetic mass.

These issues are discussed in some detail in [34] for heavy quarks using the clover action since there are important differences in discretization errors there between choosing  $M_1$  or  $M_2$  as the appropriate meson mass against which to tune the quark mass. In NRQCD we must use  $M_2$  ( $M_{\text{Kin}}$ ). The quark Hamiltonian given in Eq. (2) has no quark mass term, so to reconstruct the meson mass from  $M_1$  would require adding back in the zero of energy. This is perturbatively calculable but we wish to tune the quark mass fully nonperturbatively.  $M_2$  on the other hand acquires its quark mass pieces from the quark kinetic energy terms and so has no zero of energy problem. As discussed above,  $M_2$  will also correctly include the internal kinetic energy if the  $v^4$  relativistic corrections to the kinetic energy are included in the quark Hamiltonian, as they are in Eq. (2). Indeed we are now including the radiative corrections to the  $v^4$  kinetic terms through adjustments to  $c_1$ ,  $c_5$  and  $c_6$ , and we will show below the effect that this has.

We can determine the kinetic mass very precisely by use of propagators made starting with a random wall source patterned by an  $\exp(i\mathbf{p} \cdot \mathbf{x})$  factor to give the quark momentum [31]. We use only a  $\delta(\mathbf{x})$  smearing function for these calculations so they are very fast, but we must evolve both a quark and an antiquark propagator because the complex conjugate of a quark propagator of momentum  $\mathbf{p}$  is an antiquark of momentum  $-\mathbf{p}$ . Typically we take quark and antiquark momenta to be equal so that the meson momentum, when they are combined, is  $\mathbf{P} = 2\mathbf{p}$ .

We fit the meson correlator of momentum  $\mathbf{P}$  simultaneously with the meson correlator at rest so that the energy difference  $a\Delta E$  between the ground state energies can be determined directly by the fit taking the correlations into account. In this way we obtain  $a\Delta E$  values with errors typically in the 5th decimal place. To avoid cluttering the main body of the text, the detailed tables of values for  $Y$  and  $\eta_b$  energies as a function of momentum and  $aM_{\text{kin}}$  are collected in Appendix D. Propagators were calculated for the full number of configurations given for each ensemble in Table III, but in some cases we used fewer time sources per configuration than is given there.

We can then plot out the kinetic mass for a range of meson momenta to study systematic effects in Eq. (10) which would show up as a disagreement between kinetic masses obtained from different momentum values.

Previous calculations saw no significant differences in kinetic mass values for momenta up to  $P^2a^2 = 9$  with errors of around 1% [2]. This is equivalent to a test, as a function of momentum, of the constancy of the “speed of light”. Here we are able to achieve errors down to 0.1%, depending on the momentum. Then systematic variations of  $aM_{\text{Kin}}$  with momentum can be seen at the 0.5% level.

$aM_{\text{Kin}}$  values for  $Y$  and  $\eta_b$  mesons on the coarse lattices, set 3, are plotted in Fig. 4 and show several features. One is that there is a systematic difference between the values of  $aM_{\text{Kin}}$  for on-axis (those in one lattice direction only) and off-axis momenta. This was hinted at in [2] but the errors were too large for it to be clear. The on-axis kinetic masses are higher, and this reflects a breaking of rotational invariance on the lattice which is a discretization error. It is particularly obvious for the momenta with components along the spatial directions labeled by integers (3,0,0) and (2,2,1), both of which have  $P^2a^2 = 9(2\pi a/L)^2$ . The difference is tiny but visible. We will return to this point below.

Another feature of Fig. 4 is that the kinetic mass for the  $\eta_b$  is above that of the  $Y$  which is the opposite way round to the energy difference at zero momentum and to experiment. A similar but somewhat smaller effect is seen on the fine lattices. The discussion above on the way in which the meson kinetic mass is built up order by order in the non-relativistic expansion shows how this has happened. It results from the fact that the  $\sigma \cdot B$  term that gives rise to the hyperfine splitting is only included at leading order in our NRQCD action, Eq. (2). Relativistic corrections to this term would be needed for it to feed correctly into the

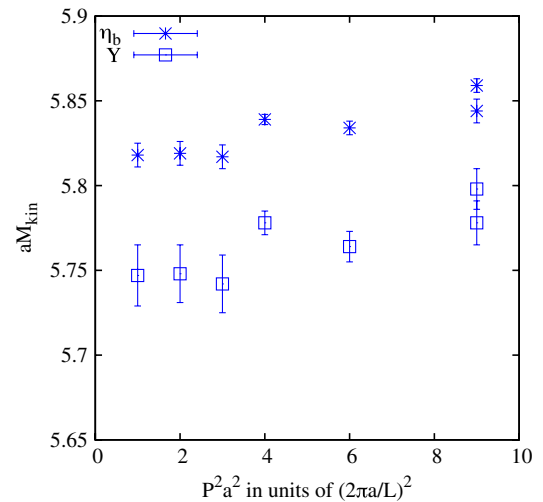


FIG. 4 (color online). Kinetic mass values in lattice units obtained on the coarse ensemble, set 3, for the  $a m_b$  and  $c_i$  values given in Tables II and III. Kinetic mass values are given separately for the  $Y$  and  $\eta_b$  and plotted against the square of the lattice momentum in units of  $2\pi a/L$ . The two results at  $x$ -axis value of 9 correspond to momenta with indices (3, 0, 0) and (2, 1, 1). The higher one is (3, 0, 0).

kinetic mass,  $M_2$ . The effect of the  $\sigma \cdot B$  term splitting is correctly incorporated in the meson energy at zero momentum ( $M_1$ ), however, and it is from differences in  $M_1$  for  $Y$  and  $\eta_b$  that we determine the hyperfine splitting (see Sec. III E 3). This small but nonzero systematic error in  $M_2$  is simply removed by working instead with the spin-averaged kinetic mass of the  $Y$  and  $\eta_b$ :

$$\bar{M}_{\text{Kin}}(1S) = \frac{(3M_{\text{Kin}}(Y) + M_{\text{Kin}}(\eta_b))}{4} \quad (14)$$

and using this to fix the  $b$  quark mass.

The above arguments also allow insight into the effect of radiative corrections to the  $v^4$  kinetic terms in the NRQCD Hamiltonian that we include here for the first time. Changing the coefficient of the  $p^4/8m_b^3$  term,  $c_1$ , from 1 to  $1 + \mathcal{O}(\alpha_s)$  will modify the amount of the internal kinetic energy that is incorporated into the meson kinetic mass, effectively correcting for an  $\mathcal{O}(\alpha_s)$  mismatch between this contribution to  $M_1$  and  $M_2$  from binding energy effects. The effect of this radiative correction is seen clearly in Fig. 5 where we compare the spin-averaged kinetic mass with all  $c_i$  set to 1 to that from having the radiatively improved coefficients given in Table II. The difference would be expected to be  $\mathcal{O}(\alpha_s \times B)$  where  $B$  is the binding energy of  $\mathcal{O}(500 \text{ MeV})$ . This could in principle be as large as 150–200 MeV. From Fig. 5 we see that the effect is somewhat smaller than this on the coarse ensemble set 3—a shift of kinetic mass of 0.05 in lattice units corresponds to around 80 MeV on these lattices. The shift is clearly visible, however. The radiative correction acts to increase the kinetic mass for a given bare  $b$  quark mass. This is because  $c_1 > 1$  and the binding energy is positive.

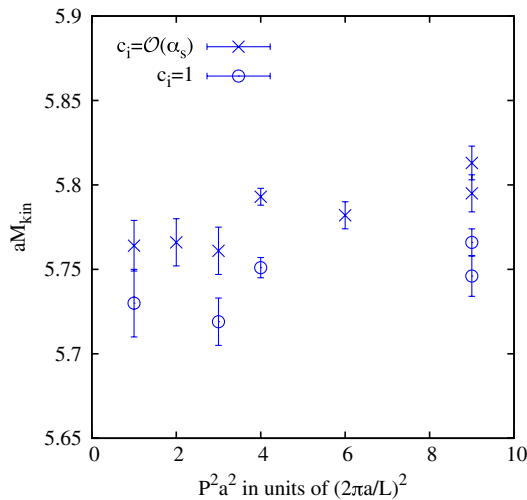


FIG. 5 (color online). Spin-averaged values for the kinetic mass in lattice units obtained on the coarse ensemble, set 3, for  $am_b = 2.66$  (as in Table III). Results for the  $c_i$  values given in Table II are compared to the results for  $c_i = 1$ . The kinetic mass is plotted against the square of the lattice momentum in units of  $2\pi a/L$ .

Thus the correctly tuned quark mass will be lower (by the same percentage shift as that for the kinetic mass) when radiative corrections are included. A similar shift is observed on the fine lattices as shown in Fig. 6.

Remaining systematic errors from higher order radiative corrections to  $v^4$  terms in the NRQCD action will be suppressed by a further power of  $\alpha_s$  beyond the shift seen here. We therefore expect the remaining error in the kinetic mass from this source to be  $\mathcal{O}(0.3\%)$ . Systematic errors from missing higher order,  $v^6$ , terms at tree level in the NRQCD action are a factor of  $v^2$ , or 10%, smaller than the size of the effect of  $v^4$  terms, and therefore of similar size to missing  $\alpha_s^2 v^4$  terms. They will also have the effect of correcting for momentum dependence in  $M_{\text{Kin}}$ . From Fig. 5 we can see that there is a sign of an upward drift of  $M_{\text{Kin}}$  with momentum but the effect is smaller than the shift of  $M_{\text{Kin}}$  with the radiative correction to the  $c_i$  coefficients.

We now return to the issue of discretization errors in the kinetic mass. These arise from the replacement of time and space derivatives in the NRQCD action with finite differences on the lattice. The terms with coefficients  $c_5$  and  $c_6$  contain  $a^2 v^4$  and  $av^4$  correction terms to remove these errors. With the inclusion of radiative corrections to  $c_5$  and  $c_6$ , the remaining errors are at  $\mathcal{O}(\alpha_s^2 a^2 v^4)$  in this calculation. The term with coefficient  $c_5$ , i.e. the term proportional to  $\Delta^{(4)}$  is of interest because this is rotationally noninvariant. The signal for a lack of continuum rotational invariance in our results is a disagreement between the kinetic mass for on-axis momenta, that typically have a high value for  $P_i^4$ , and off-axis momenta. This was seen in Fig. 4 for the coarse lattices. Less variation is evident on the fine lattices (Fig. 6), as expected for a discretization effect.

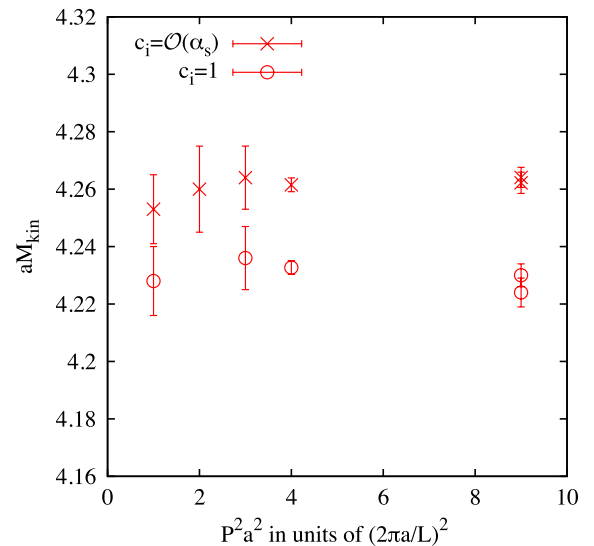


FIG. 6 (color online). Spin-averaged values for the kinetic mass in lattice units obtained on the fine ensemble, set 5, for the  $am_b$  and  $c_i$  values given in Tables II and III, compared to the results for  $c_i = 1$ . The kinetic mass is plotted against the square of the lattice momentum in units of  $2\pi a/L$ .

To make clearer the way in which the rotationally non-invariant discretization errors depend on the lattice spacing Fig. 7 plots the energy difference in physical units between mesons with momentum (3, 0, 0) and (2, 2, 1) as a function of  $a^2$  using results from all three values of the lattice spacing.  $P^2 a^2 = 9(2\pi a/L)^2$  corresponds to approximately the same physical momentum at all three lattice spacing values, so the results should be a good test of how rotational invariance is restored as  $a \rightarrow 0$ . In fact the energy difference is tiny on all except the very coarse lattices, where it reaches 1 MeV. The case in which the  $c_{1,5,6}$  coefficients are set to their tree level values of 1 is plotted as well as the case with the  $c_{1,5,6}$  coefficients taking the radiatively improved values that we have used for the rest of our calculation here. The radiatively improved values give very slightly smaller energy splittings, since they have improved the  $a^2$  contribution to this error by one order in  $\alpha_s$  to  $\alpha_s^2 a^2 v^4$ . The energy difference between mesons with momentum (3, 0, 0) and (2, 2, 1) also has contributions at  $\mathcal{O}(a^4 v^6)$ , however, and both the effect of radiative improvement and the shape of the curve in Fig. 7 tend to imply that these  $a^4$  terms dominate over any remaining  $a^2$  terms.

Rotationally invariant discretization errors would give rise to a kinetic mass that varied with  $P^2$ . This is the same effect as that of relativistic errors, because the correcting operators are the same. Discretization errors require an  $a$ -dependent coefficient to correct them. However, as discussed above under relativistic corrections, there is no sign in our results of such errors to better than 0.5%.

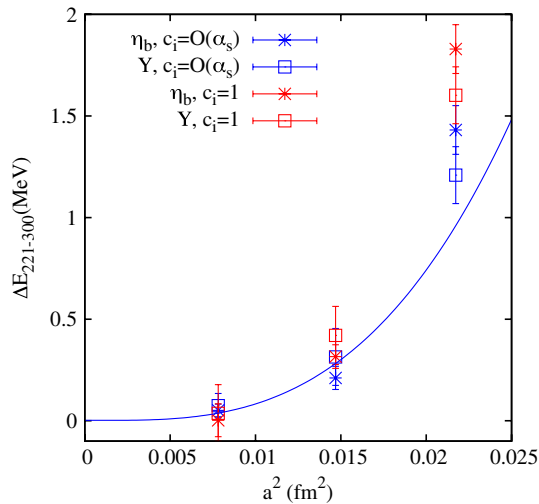


FIG. 7 (color online). The energy difference in MeV between mesons with momentum (3, 0, 0) and (2, 2, 1) in units of  $2\pi a/L$  on the lattice plotted against the square of the lattice spacing in fm. Results are shown for the case  $c_{1,5,6} = 1$  as well as for  $c_{1,5,6}$  taking their  $\alpha_s$ -improved values. An example fit curve with  $a^4$  and  $a^6$  dependence is shown through the  $Y$  data for  $c_{1,5,6}$   $\alpha_s$  improved.

The conclusion from this section is that, to minimize systematic errors, we should tune the  $b$  quark mass by calculating the spin-averaged kinetic mass  $\bar{M}_{\text{Kin}}(1S)$  and matching that to experiment. We do this from the comparison of meson energies at zero momentum and the “maximally off-axis” momentum (1, 1, 1) to minimize discretization errors. Table V gives results for this kinetic mass on all ensembles for the given values of the  $b$  quark mass and coefficients,  $c_i$ . To convert these results to physical units we need a value for the lattice spacing to be determined in Sec. III E. Table V gives statistical/fitting errors on the values. As discussed above, remaining systematic errors from missing radiative, relativistic and discretization errors amount to a total of 0.5%. We are able to pin down the size of these systematic errors by using the improved methods described here to study the dispersion at this level of detail.

Figure 8 compares the results for the spin-averaged kinetic mass on the coarse ensemble, set 3 for a variety of different choices for the coefficients in the NRQCD action to show the size of variations in the kinetic mass. The figure shows that we can see the difference between taking tree-level values for  $c_{1,5,6}$  and radiatively improved values. Changing  $c_2$  (the coefficient of the Darwin term) has very little effect. The effect of changing  $c_4$  (the coefficient of the  $\sigma \cdot \mathbf{B}$  term which should be spin averaged away at leading order in this kinetic mass) is also not large. Another check of this is given in Table V on set 1.

The experimental result for the  $Y$  mass is 9.4603(3) GeV and that of the  $\eta_b$ , 9.391(3) GeV, [35] giving a spin average of 9.443(1) GeV. The real world includes effects that are missing from our lattice calculation, however, and so we

TABLE V. Summary of the kinetic masses obtained on different ensembles for a variety of parameter values. We use the energy difference between lattice momentum zero and momentum  $a\mathbf{p} = (1, 1, 1)$  in units of  $2\pi a/L$ . The column  $c_{1,5,6}$  denotes whether the  $\mathcal{O}(\alpha_s)$  improved coefficients were used in the action and the columns  $c_2, c_4$  indicate additional values of those coefficients that were run on coarse set 3 and very coarse set 1 to estimate systematic errors.

Set	$am_b$	$c_{1,5,6}$	$c_2$	$c_4$	$aM_{\text{Kin}}(Y)$	$aM_{\text{Kin}}(\eta_b)$	$a\bar{M}_{\text{Kin}}(1S)$
1	3.42	$\alpha_s$	1	1	7.269(18)	7.405(10)	7.303(15)
1	3.42	$\alpha_s$	1	1.22	7.271(22)	7.472(10)	7.321(18)
2	3.39	$\alpha_s$	1	1	7.228(10)	7.345(4)	7.257(8)
2	3.42	$\alpha_s$	1	1	7.310(14)	7.423(7)	7.338(13)
3	2.66	1	1	1	5.703(17)	5.767(7)	5.719(14)
3	2.66	$\alpha_s$	1	1	5.742(17)	5.817(7)	5.761(14)
3	2.66	$\alpha_s$	1.25	1	5.748(8)	5.823(4)	5.766(7)
3	2.66	$\alpha_s$	1	1.25	5.767(10)	5.889(4)	5.798(8)
4	2.62	$\alpha_s$	1	1	5.706(9)	5.761(4)	5.719(7)
4	2.66	$\alpha_s$	1	1	5.778(11)	5.833(5)	5.792(10)
5	1.91	1	1	1	4.230(13)	4.252(6)	4.236(11)
5	1.91	$\alpha_s$	1	1	4.256(14)	4.287(6)	4.264(11)
5	2.0	$\alpha_s$	1	1	4.431(11)	4.466(5)	4.439(10)

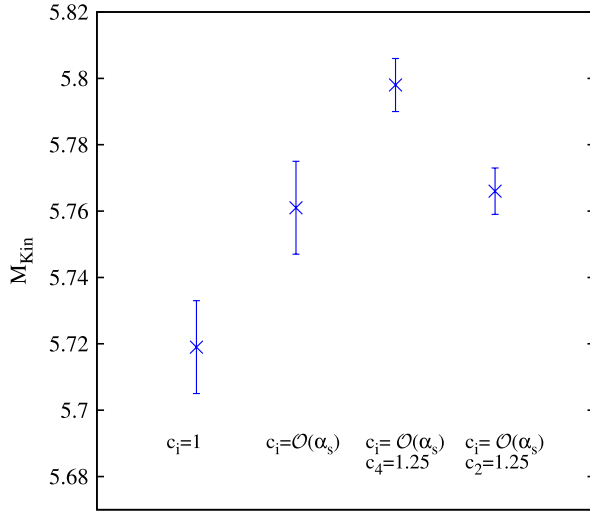


FIG. 8 (color online). Comparison of values obtained for the kinetic mass from a variety of different parameter values on coarse set 3.

must correct for this. Electromagnetism affects the  $\Upsilon$  and  $\eta_b$  approximately equally and, from a potential model we estimate that it reduces their masses by 1.6 MeV [14]. In addition the  $\eta_b$  can annihilate to gluons and we estimate that this effect also reduces its mass by 2.4 MeV, taking the same value as that estimated for the  $\eta_c$  [16]. The “experimental” mass that we should compare our results to is then increased from above to 9.445(2) GeV where we allow for a 100% error in our estimate of the shifts in the masses [36].

#### D. NRQCD systematics in radial and orbital splittings

Here we discuss the remaining sources of systematic error in our calculation of the radial and orbital excitation energies. These systematic errors will feed subsequently into the determination of the lattice spacing from the  $\Upsilon$   $2S - 1S$  splitting.

Radial and orbital excitation energies arise at leading order from the time derivative and  $H_0$  in the NRQCD

action [Eq. (2)]. The relativistic corrections at  $v^4$  in  $\delta H$  thus provide relative  $\mathcal{O}(v^2) \approx 10\%$  corrections to these splittings. Missing radiative corrections to the  $v^4$  terms dominated the errors in earlier calculations [2,11], since  $\alpha_s v^2 \approx 2 - 3\%$  is larger than  $v^4 \approx 1\%$  from missing higher order relativistic corrections. We now include for the first time the radiative corrections to most of the  $v^4$  terms in  $\delta H$ . The remaining errors are then largely at relative  $\mathcal{O}(\alpha_s^2 v^2)$ , i.e. less than 1%.

Table VI lists the remaining systematic errors from spin-independent terms in the  $2S - 1S$  and  $1P - 1S$  splittings in more detail following [2]. The errors were determined using a potential model to make estimates of the energy shifts in each of the  $1S$ ,  $2S$  and  $1P$  states. For example, radiative corrections at  $\mathcal{O}(\alpha_s^2)$  to the  $p^4/(8m_b^3)$  term in the NRQCD action give shifts of size  $\alpha_s^2 \langle p^4 \rangle / 4m_b^3$  where  $\langle p^4 \rangle$  is the expectation value of  $p^4$  in that state.

The effects of the Darwin term appear at  $\mathcal{O}(\alpha_s v^4)$  since we have not included a radiative correction to  $c_2$ . However, since this term vanishes in the free theory it is already suppressed by an additional power of  $\alpha_s$ . Its effects are proportional to the square of the wave function at the origin so it does not affect  $P$ -wave states. A very similar term arises from missing spin-independent 4-quark operators. The spin-dependent 4-quark operators are discussed in Appendix B along with the coefficients they have in order to match NRQCD to QCD. The spin-independent ones arise from the same diagrams and the calculation of their coefficients is in progress. Here we take an error from missing these 4-quark operators which is of the same size as the error from radiative corrections to the Darwin term.

Note that errors cancel to a significant extent between the  $2S$  and  $1S$  states because of their similarities [2]. This is the reason for focussing on the  $2S - 1S$  splitting to determine the lattice spacing, because it has the smallest systematic error.

We see from Table VI that the largest remaining systematic error is now that from missing  $v^6$  terms. The key kinetic term at  $v^6$  that would appear in a higher order NRQCD action is  $-(\Delta^{(2)})^3/(16(am_b)^5)$  at tree level. This

TABLE VI. An estimate of systematic errors in the  $2S - 1S$  and  $1P - 1S$  splittings in the  $\Upsilon$  in our lattice QCD calculation arising from missing higher order relativistic and radiative corrections to the NRQCD action that we use (Eq. (2)).

Correction	Relativistic	Radiative kinetic	Radiative Darwin	4-quark spin-independent	Total relativistic + radiative
Form	$\delta p^6/(m_b)^5$	$\alpha_s^2 \delta p^4/4(m_b)^3$	$4\pi\alpha_s^2 \psi(0)^2/(3m_b^2)$	$\alpha_s^2 \psi(0)^2/m_b^2$	
Est. percentage in $2S - 1S$					
Very coarse	0.5	0.2	0.4	0.4	0.8
Coarse	0.5	0.15	0.3	0.3	0.7
Fine	0.5	0.1	0.2	0.2	0.6
Est. percentage in $1P - 1S$					
Very coarse	1.0	0.7	0.9	0.9	1.8
Coarse	1.0	0.5	0.7	0.7	1.5
Fine	1.0	0.3	0.4	0.4	1.2



TABLE VII. An estimate of systematic errors in the  $2S - 1S$  and  $1P - 1S$  splittings in the  $\Upsilon$  in our lattice QCD calculation arising from discretization errors in the NRQCD and gluon actions.

Correction	Discretization in NRQCD action (i)	Discretization in NRQCD action (ii)	Discretization in Gluon action	Total Discretization
Form	$\alpha_s^2 a \delta p^4 / 8n(m_b)^2$	$\alpha_s^2 a^2 \delta p_i^4 / 12m_b$	$4\pi\alpha_s^2 a^2 \psi(0)^2 / 15$	
Est. percentage in $2S - 1S$				
Very coarse	0.2	0.4	0.3	0.5
Coarse	0.1	0.2	0.15	0.3
fine	0.05	0.06	0.05	0.1
Est. percentage in $1P - 1S$				
Very coarse	0.7	2.0	1.0	2.3
Coarse	0.4	1.0	0.5	1.2
Fine	0.2	0.3	0.1	0.4

term is proportional to  $+(v^2)^3$  and so, if it dominates the  $v^6$  errors, they will have the same sign at every value of the lattice spacing. Including this  $v^6$  term would act in the direction of reducing both the  $2S - 1S$  and  $1P - 1S$  splitting but the  $1P - 1S$  splitting would be reduced the most.

Table VII similarly quantifies remaining systematic errors from missing  $\alpha_s^2$  radiative corrections to the discretization correction terms with coefficients  $c_5$  and  $c_6$ . These are significantly reduced over our earlier calculations [2] now that the  $\alpha_s$  radiative corrections are included. In addition the gluon action is now improved completely through  $\mathcal{O}(\alpha_s^2 a^2)$  [20] and this means that the discretization errors coming from the gluon action are similarly reduced.

We can estimate the size of  $a^4$  errors from the analysis in Sec. III C where we study discretization errors in the kinetic mass. The energy difference between mesons of momenta (3, 0, 0) and (2, 2, 1) in units of  $2\pi a/L$  can be taken as a measure of at least the rotationally noninvariant  $a^4$  errors, as discussed there. The energy difference (Fig. 7) is barely visible except on the very coarse lattices where it amounts to 1 MeV, or 0.2% of the  $2S - 1S$  splitting. This is much less than the estimate of remaining  $a^2$  errors in that case so we do not include it in Table VII.

## E. Results

### 1. Radial and orbital excitation energies

Our main results for the fitted energies for the ground-state and first two radial excitations of the  $\Upsilon$  and  $\eta_b$  are given in Table VIII. The values come from multi-exponential fits to a  $5 \times 5$  matrix of correlators for each meson as described in Sec. III B. We take 9 exponentials on sets 1, 2 and 3; 11 exponentials on set 4 and 12 on set 5. We also give the fitted ground-state energy for the  $h_b(1P)$  state on sets 3 and 5 from a 5 exponential fit to  $2 \times 2$  matrix of correlators. The  $b$  quark masses and coefficients,  $c_i$ , used in the NRQCD action are those of Tables II and III. Errors are very small on the ground-state  $S$ -wave masses but increase rapidly with the radial excitation number. The

table also includes energy splittings in lattice units for radial and orbital excitations.

As explained earlier we can use the radial excitation energy,  $M(Y') - M(Y)$ , to fix the lattice spacing, by setting

$$a^{-1}(\text{GeV}) = \frac{0.5630(9)}{aE(2^3S_1) - aE(1^3S_1)}. \quad (15)$$

0.5630(4) GeV is the experimental mass difference and we have increased the error to allow for a possible relative shift in the two masses as a result of the electromagnetic attraction between quark and antiquark missing in our calculation. As discussed earlier, a potential model estimate would give a shift of 1.6 MeV to the  $\Upsilon$  from the electrostatic attraction between quark and antiquark, and somewhat less for the  $Y'$  since typical separations between quark and antiquark are larger. We do not shift the result but allow for an error of 0.8 MeV.

As long as we deal with spin-averaged splittings we do not have to consider errors in spin-dependent terms. However, for the  $2S - 1S$  splitting the match to experiment cannot be spin averaged since no experimental information is available for the  $\eta_b(2S)$ . In that case we have to consider sources of systematic error in the hyperfine splitting that will induce errors in the  $\Upsilon$  and  $Y'$  energies. This will be discussed further in Sec. III E 3.

The main source of error is from missing radiative corrections when we take the coefficient of the  $\sigma \cdot B$  term,  $c_4$ , to be 1. In Sec. III E 3 we compare results for  $c_4 = 1$  to those from  $c_4$  corrected perturbatively through  $\mathcal{O}(\alpha_s)$  and nonperturbatively, to give the correct  $1^3P$  fine structure. Both methods for correcting  $c_4$  give values above 1 and increase the lattice result for the hyperfine splitting (which is proportional to  $c_4^2$  at leading order). Thus with  $c_4 = 1$  the  $\Upsilon$  energy is too low. Since  $M(Y) = M(1\bar{S}) + (M(Y) - M(\eta_b))/4$ , the shift from  $c_4$  in the  $\Upsilon$  mass is one quarter of the change in the hyperfine splitting. In Sec. III E 3 we also determine the ratio of the  $2S$  hyperfine splitting to that of the  $1S$  hyperfine splitting and find a result close to 0.5, independent of  $c_4$ . Thus the shift from a

TABLE VIII. Radial, orbital and  $S$ -wave fine structure splittings in lattice units for sets 1 to 5 for the NRQCD parameters and coefficients given in Tables II and III.  $c_3 = c_4 = 1.0$ . Errors are statistical/fitting only.  $R_S$ ,  $R_P$  and  $R_H$  are defined in the text.

	1	2	3	4	5
$aE(1^1S_0)$	0.25080(5)	0.25361(3)	0.26096(3)	0.26524(2)	0.25851(2)
$aE(2^1S_0)$	0.6898(16)	0.6909(8)	0.6235(8)	0.6246(6)	0.5248(7)
$aE(3^1S_0)$	0.975(14)	0.940(22)	0.849(9)	0.854(4)	0.677(11)
$aE(1^3S_1)$	0.28532(6)	0.28809(3)	0.29245(3)	0.29681(2)	0.28405(2)
$aE(2^3S_1)$	0.7078(14)	0.7074(8)	0.6416(7)	0.6393(9)	0.5370(9)
$aE(3^3S_1)$	0.988(16)	0.975(8)	0.855(11)	0.867(10)	0.693(10)
$aE(2\bar{S} - 1\bar{S})$	0.4266(11)	0.4238(7)	0.3525(6)	0.3467(7)	0.2563(7)
$aE(3\bar{S} - 1\bar{S})$	0.708(12)	0.687(8)	0.569(9)	0.575(8)	0.411(8)
$aE(2^1S_0 - 1^1S_0)$	0.4390(16)	0.4373(8)	0.3626(8)	0.3594(6)	0.2663(7)
$aE(3^1S_0 - 1^1S_0)$	0.724(14)	0.687(22)	0.588(9)	0.588(4)	0.418(11)
$aE(2^3S_1 - 1^3S_1)$	0.4225(14)	0.4193(8)	0.3492(7)	0.3425(9)	0.2530(9)
$aE(3^3S_1 - 1^3S_1)$	0.703(16)	0.687(8)	0.563(11)	0.570(10)	0.409(10)
$R_S$	1.664(38)	1.638(19)	1.611(32)	1.665(31)	1.617(40)
$a\Delta$	0.001 90(1)	0.001 90(1)	0.001 51(1)	0.001 51(1)	0.000 91(1)
$aE(1^1P_1)$	...	...	0.5654(23)	...	0.4833(10)
$aE(1^1P_1 - 1\bar{S})$	...	...	0.2809(22)	...	0.2056(10)
$R_P$	...	...	0.808(7)	...	0.816(5)
$aE(1^3S_1 - 1^1S_0)$	0.034 52(8)	0.034 48(4)	0.031 49(4)	0.031 57(3)	0.025 54(3)
$aE(2^3S_1 - 2^1S_0)$	0.0180(21)	0.0165(11)	0.0181(11)	0.0147(10)	0.0122(11)
$R_H$	0.521(62)	0.479(33)	0.575(35)	0.465(34)	0.478(45)

change in  $c_4$  to the  $2S - 1S$  splitting is one eighth of change in the  $1S$  hyperfine splitting. An increase in  $c_4$  above 1 reduces the  $2S - 1S$  splitting. From Table XIV we can compare results for the  $1S$  hyperfine splitting for  $c_4 = 1$  to the value obtained for  $c_4$  improved through  $\mathcal{O}(\alpha_s)$  for sets 1, 3 and 5. Dividing by 8 then gives shifts in lattice units that can be applied to correct the  $2S - 1S$  splitting on very coarse, coarse and fine lattices. These shifts are denoted by  $a\Delta$  in Table VIII, and are to be subtracted from the  $2S - 1S$  splitting to give the corrected lattice result. It can be seen that  $a\Delta$  is not much larger than the statistical errors on the  $2S - 1S$  splitting. The statistical error in  $a\Delta$  is negligible, but there is a systematic error which is taken as  $0.5 \times a\Delta$ . This accounts for the errors in the hyperfine splitting from 4-quark operators, higher order radiative corrections to  $c_4$  and relativistic corrections to the  $\sigma \cdot \mathbf{B}$  term. This error is then included in the systematic error for the corrected  $2S - 1S$  splitting.

Note that we do not expect the spin-orbit term with coefficient  $c_3$  to have significant effect on the  $S$ -wave states. In any case our nonperturbative determination of  $c_3$  discussed in Appendix C gives a result consistent with the value of 1.0 that we are using. Possible errors from radiative corrections to  $c_2$  are included in our systematic error budget for NRQCD (Table VI).

Table X gives the values of the lattice spacing in fm obtained from the  $2S - 1S$  splitting on each ensemble, along with their associated statistical/fitting error and systematic error. The systematic errors are combined in quadrature from Tables VI and VII and from  $a\Delta$  in Table VIII. The systematic errors are dominated by those from missing

higher order relativistic corrections to the NRQCD action and these will be correlated to some extent between ensembles. There is an additional overall systematic error of 0.2% coming from the experimental value for the splitting and electromagnetic effects missing from our calculation.

In Table IX we give results for cases where  $c_4$  is set to its nonperturbatively tuned value on sets 3, 4 and a test value of 1.10 on set 5 (the nonperturbatively tuned value is in fact 1.18, see Appendix C). Changing  $c_4$  shifts the fitted energies of all the states but this is simply because the zero of energy has changed. As expected, changing  $c_4$  has very little effect on splittings between spin-averaged  $S$  wave states or between the  $1^1P_1$  mass and the spin-averaged  $1S$  state.

An important test of the results is whether, using these values for the lattice spacing, we get results in agreement with experiment for other mass differences, i.e. whether ratios of splittings are correct. In our previous work on  $2 + 1$  flavor gluon configurations [2] agreement with experiment was found within 3% statistical/systematic errors. Here we have substantially improved errors, including improved statistical errors, so we can improve on our earlier analysis.

Table VIII gives values for the ratios of the  $\Upsilon$   $3S - 1S$  and  $1^1P_1 - 1\bar{S}$  splittings to the  $\Upsilon$   $2S - 1S$  splitting from our results for  $c_4 = 1$ . Table IX gives the same ratios for the case where  $c_4$  takes its nonperturbatively tuned value. In forming the ratio  $R_P = (1^1P_1 - 1\bar{S})/(2^3S_1 - 1^3S_1)$  for the case  $c_4 = 1$  we correct the denominator for  $c_4$  errors using the  $a\Delta$  values in Table VIII. The numerator should not be sensitive to  $c_4$  because the  $S$ -state energies have

TABLE IX. Radial, orbital and  $S$ -wave fine structure splittings in lattice units for sets 3, 4 and 5 with NRQCD coefficients and parameters as in Tables II and III. In addition  $c_4$  is nonperturbatively tuned taking values from Table XIII.  $c_3 = 1$  for all results. Errors are statistical/fitting only. Reduced statistics of 400 configurations were used for the  $S$ -wave states from set 5.  $R_S$ ,  $R_P$  and  $R_H$  are defined in the text.

	3	4	5
$c_3$	1.0	1.0	1.0
$c_4$	1.25	1.25	1.10
$aE(1^1S_0)$	0.20943(3)	0.21289(2)	0.23204(2)
$aE(2^1S_0)$	0.5796(6)	0.5777(7)	0.5021(12)
$aE(3^1S_0)$	0.788(12)	0.802(6)	0.660(12)
$aE(1^3S_1)$	0.25628(4)	0.25978(2)	0.26206(3)
$aE(2^3S_1)$	0.6022(7)	0.5999(7)	0.5170(18)
$aE(3^3S_1)$	0.827(7)	0.821(5)	0.663(24)
$aE(2\bar{S} - 1\bar{S})$	0.3520(6)	0.3463(6)	0.2584(13)
$aE(3\bar{S} - 1\bar{S})$	0.573(6)	0.568(4)	0.405(18)
$aE(2^1S_0 - 1^1S_0)$	0.3702(6)	0.3648(7)	0.2701(12)
$aE(3^1S_0 - 1^1S_0)$	0.579(12)	0.589(6)	0.428(12)
$aE(2^3S_1 - 1^3S_1)$	0.3460(7)	0.3401(7)	0.2549(18)
$aE(3^3S_1 - 1^3S_1)$	0.571(7)	0.561(5)	0.401(24)
$R_S$	1.651(20)	1.650(15)	1.573(95)
$aE(1^1P_1)$	0.5247(22)	0.5253(20)	...
$aE(1^1P_1 - 1\bar{S})$	0.2801(22)	0.2773(20)	...
$R_P$	0.810(7)	0.815(6)	...
$aE(1^3S_1 - 1^1S_0)$	0.04684(5)	0.04689(3)	0.03003(4)
$aE(2^3S_1 - 2^1S_0)$	0.0226(9)	0.0222(10)	0.0149(22)
$R_H$	0.482(19)	0.473(21)	0.496(73)

been spin averaged and the  $1^1P_1$  state is unaffected by  $c_4$ , as discussed in Appendix C. Both the  $Y\ 3S - 1S$  and  $2S - 1S$  splittings will have some sensitivity to  $c_4$ . However, any shifts will cancel between the two splittings up to an amount equal to one quarter of the difference in the  $3S$  and  $2S$  hyperfine splittings. This is negligible compared to statistical errors in this ratio. The ratio  $R_S = (3^3S_1 - 1^3S_1)/(2^3S_1 - 1^3S_1)$  in Table VIII is therefore not corrected for  $c_4$ .

The ratio  $R_S$  from Table VIII, where we have results for all five sets, is plotted against the square of the lattice spacing in Fig. 9. We see very little dependence on lattice spacing and on the  $u/d$  sea quark mass (the  $s$  and  $c$  sea quark masses are already well-tuned to their physical values, see Sec. IV). Figure 9 also shows results for  $R_P$ , combining results from Tables VIII and IX since we have results for only 2 ensembles in each table. The results change very little between the ensembles, however, as Fig. 9 shows.

To derive a physical value for each ratio we can use the results to fit for the dependence on these two quantities and then determine the result at physical sea quark mass and at  $a = 0$  to compare to experiment. For the sea  $u/d$  quark mass dependence a simple polynomial in  $m_l/m_s$  (values in Table I) suffices because the  $m_l$  values are already very

TABLE X. Lattice spacing values in fm determined from several methods. The first column gives results from the  $Y\ 2S - 1S$  splitting. The first error is from statistics/fitting, the second from remaining systematic errors from the NRQCD action (from Tables VI and VII) and the third is a correlated 0.2% error from experiment and electromagnetic corrections. The second column gives lattice spacing values from the decay constant of the  $\eta_s$  meson as described in Sec. IV. The first error is from statistics/fitting and the second is a correlated 0.3% error from the uncertainty in the physical value of  $f_{\eta_s}$  as discussed in Sec. IV. The third column gives lattice spacing values determined from  $r_1/a$  values in Table I. The first error is from statistics/fitting and the second is a correlated 0.8% error from the uncertainty in the physical value of  $r_1$  as discussed in Sec. V.

Set	$a_Y$ (fm)	$a_{\eta_s}$ (fm)	$a_{r_1/a}$ (fm)
1	0.1474(5)(14)(2)	0.1546(10)(5)	0.1569(8)(13)
2	0.1463(3)(14)(2)	0.1526(6)(5)	0.1553(3)(13)
3	0.1219(2)(9)(2)	0.1234(7)(4)	0.1244(2)(10)
4	0.1195(3)(9)(2)	0.1218(5)(4)	0.1221(5)(10)
5	0.0884(3)(5)(1)	0.0899(6)(3)	0.0902(3)(7)

close to the physical point with  $m_l/m_s = 0.1$  and  $0.2$ . The dependence on the lattice spacing is more complicated because in NRQCD we must allow for unphysical  $a$  dependence coming from  $am_b$ -dependent radiative corrections to discretization errors. This  $am_b$  dependence is mild when  $am_b$  is sufficiently large, as here, and this is seen explicitly in the radiative corrections that are included in our calculation for  $c_5$  and  $c_6$  (Table II).

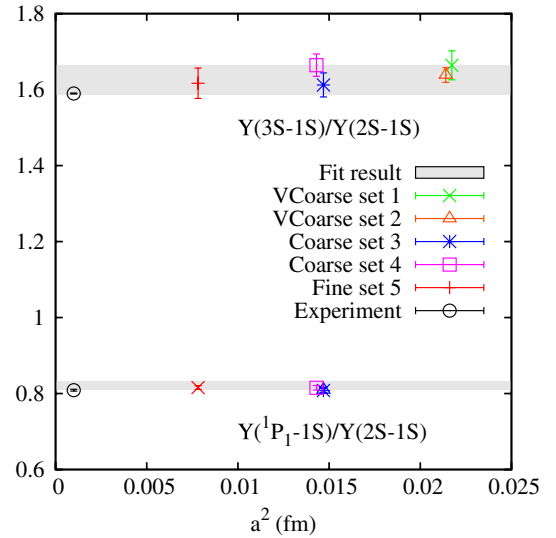


FIG. 9 (color online). Results for the ratio of the  $3S - 1S$  and  $1P - 1S$  splittings to the  $2S - 1S$  in the  $Y$  system plotted against the square of the lattice spacing determined from the  $2S - 1S$  splitting. The grey shaded bands give the physical result obtained from a fit to the data as described in the text. The black open circles slightly offset from  $a = 0$  are from experiment [35].

We therefore fit each ratio,  $R$ , to the following functional form:

$$R = R_{\text{phys}} \left[ 1 + \sum_{j=1,2} c_j (a\Lambda)^{2j} (1 + c_{jb} \delta x_m + c_{jbb} (\delta x_m)^2) + 2b_l \delta x_l (1 + c_l (a\Lambda)^2) \right]. \quad (16)$$

Here  $\delta x_l$  is  $(am_l/am_s) - (m_l/m_s)_{\text{phys}}$  for each ensemble.  $(m_l/m_s)_{\text{phys}}$  is taken from lattice QCD as 27.2(3) [6]. The strange sea quark mass is tuned to better than 3% with the lattice spacing taken from the  $Y$   $2S - 1S$  splitting so we can ignore any effects from this mistuning since sea quark mass effects are so small.  $\delta x_m$  allows for variation in the value of  $am_b$  over the range we are using and therefore a change in the NRQCD radiative corrections to discretization errors. We choose  $\delta x_m$  to vary from  $-0.5$  to  $+0.5$  over our full range of masses by setting  $\delta x_m = (am_b - 2.65)/1.5$ .  $\Lambda$  sets the scale for physical  $a$  dependence. We take it to be 500 MeV.

The fit prior on  $R_{\text{phys}}$  is taken to be  $0.8 \pm 0.1$  for  $R_P$  and  $1.6 \pm 0.2$  for  $R_S$ . Since tree-level  $a^2$  errors have been removed in this calculation we take the prior on  $a^2$  terms to be  $0.0 \pm 0.3$ ; we take  $0.0 \pm 1.0$  for higher order terms in  $a$ .  $c_l$  allows for  $\mathcal{O}(\alpha_s a^2)$  staggered quark taste-changing discretization errors. For  $b_l$  we take  $0.0 \pm 0.015$  allowing for a 3% shift if the  $u/d$  quarks were as heavy as strange. Previous results [2] saw a 10% shift in results in the quenched approximation.

Good fits using the form in Eq. (17) are easily obtained for both  $R_P$  and  $R_S$ . For  $\chi^2/\text{dof}\{\text{dof}\}$  we obtain 0.2{4} and 0.4{5} for  $R_P$  and  $R_S$ , respectively. The physical results we obtain are

$$\frac{1^1P_1 - 1\bar{S}}{(2S - 1S)_Y} = 0.820(12) \quad \frac{(3S - 1S)_Y}{(2S - 1S)_Y} = 1.625(39). \quad (17)$$

These values are plotted along with the lattice results in Fig. 9.

The complete error budget for the two ratios is given in Table XI. Most of the errors are obtained directly from our fit. The NRQCD systematic error in  $R_P$  is taken from combining results in Tables VI and VII. Since these errors are correlated between the numerator and denominator of  $R_P$  we take the systematic error in  $R_P$  to be the difference between them. The total NRQCD systematic error at each lattice spacing is then included in our fit as a correlated error on the data. In fact we find no significant difference whether we include it as a correlated or uncorrelated error. We obtain the error in our final result from this systematic error by observing the change in the final answer from including it or not including it. Variation in the NRQCD systematic errors as a function of  $am_b$  is included in our fit form and the error from this estimated from the variation of  $\chi^2$  in the fit. We use the same approach for  $R_S$  and take the NRQCD systematic error to be the same as for  $R_P$ . We

TABLE XI. Complete error budget for the ratios of mass splittings,  $R_P = (1^1P_1 - 1\bar{S})/(2S - 1S)_Y$  and  $R_S = (3S - 1S)_Y/(2S - 1S)_Y$ . Errors are given as a percentage of the ratio. Errors which are negligible compared to the others are indicated by “0”.

	$R_P$	$R_S$
Stats/fitting	1.0	1.8
$a$ dependence	0.6	1.2
$m_l$ dependence	0.6	0.5
NRQCD $am_b$ dependence	0.1	0.2
NRQCD systematics	0.5	1.0
Finite volume	0	0
$m_b$ tuning	0	0
Electromagnetism/ $\eta_b$ annihilation	0.2	0.2
Total	1.4	2.4

might expect some further cancellation of errors within  $R_S$  because of the similarity between the  $S$ -wave states. However, this is less true when comparing  $3S$  to  $1S$  than for  $2S$  and  $1S$  so we ignore that possibility to be conservative.

We believe that errors from any mistuning of  $m_b$  are completely negligible.  $R_P$  and  $R_S$  change experimentally very little between  $b$  and  $c$  and we have very well-tuned  $b$  masses except on the very coarse lattices where our mistuning amounts to 4%.

We also believe that finite volume errors are negligible. A study using the heavy quark potential derived from a quenched lattice QCD calculation in [37] calculated wave functions for radially excited  $Y$  states. None of the wave functions for the states being considered here extended beyond a radius of 1.5 fm and the  $2S$  and  $1P$  extended little beyond 1.0 fm. When sea quarks are included, as here, the size of the states will be smaller because the Coulomb coefficient in the heavy quark potential is larger. Thus 1.5 fm is an overestimate for the size of the states. The physical extent of our lattices range from 2.3 fm for set 1 to 3.8 fm for set 4, so should be large enough to contain the  $Y$  states without any finite-volume errors from their being squeezed.

In Table XI we include a 0.2% error from electromagnetic effects and the possibility of  $\eta_b$  annihilation, neither of which is included in our calculation. Electromagnetic effects we estimated earlier at 1.6 MeV in the  $1S$  mass and 0.8 MeV (correlated) in the  $2S$  mass. If we take the effects on the  $1P$  and  $3S$  masses to be much smaller then we arrive at a possible error in  $R_S$  and  $R_P$  of the order of 0.1% to 0.2%.  $\eta_b$  annihilation affects the spin-averaged  $1S$  mass, shifting it by approximately 0.5 MeV. This amounts to a possible 0.1% effect in  $R_P$ , whereas  $R_S$  is unaffected.

Our result for the ratio  $R_P$  of 0.820(12) is to be compared with the experimental result 0.8088(23). Agreement is good within our 1.4% errors. Similarly we obtain 1.625(39) for  $R_S$  to be compared with the experimental result



1.5896(12). Again agreement is good, but now with 2.4% errors, dominated by our statistical/fitting error because the  $3S$  state is a doubly excited state. The fact that our central value is slightly higher than experiment for both  $R_S$  and  $R_P$  is consistent with the expected effect of missing  $\nu^6$  terms, included in our errors, as discussed in Sec. III D.

Our result for  $R_P$  can be converted to a result for  $M(h_b) - M(1\bar{S}) = 0.461(7)$  GeV. This can be compared to the result  $0.440 \pm 17^{+10}_{-0}$  GeV with over double the error obtained on configurations including  $2 + 1$  flavors of sea quarks using the Fermilab heavy quark action [38]. The experimental result for  $M(h_b) - M(1\bar{S})$  is 0.4553 (17) GeV [35,39].

Our result for  $R_S$  gives  $M(Y'') - M(Y) = 0.914(23)$  GeV compared to an experimental result of 0.8949(6) GeV [35]. We have not included in our error budget any effect from coupling of the  $Y''$  to virtual decay channels. The  $Y''$  is 200 MeV below threshold for real decay to a pair of  $B$  mesons. This is considered large enough for the  $Y''$  to be "gold-plated" and for the decay channel to have no impact on the mass.

## 2. Tuned $b$ quark masses

We now return to the tuning of the  $b$  quark mass. Although not an issue for the mass splittings just discussed, it is an important source of systematic error for spin-dependent mass splittings. We use our determination of the lattice spacing from the  $Y(2S - 1S)$  splitting, given in Table X to convert the kinetic mass values given in Sec. III C to physical units. As described in Sec. III C the appropriate experimental value for comparison is 9.445(2) GeV.

When this is done we see that the masses are very well-tuned except on the very coarse lattices where they are 4% high. For small changes in the  $b$  quark mass the change in kinetic mass is approximately twice the change in quark mass, as can be seen from Table V. For the slight changes that we need to make this is a sufficiently good approximation. We simply adjust the quark mass by one half the error in the kinetic mass to obtain the tuned quark mass values in lattice units given in Table XII.

Three errors are given in Table XII. The first is from the statistical error in the kinetic mass determined on each ensemble. The second error comes from the total error in the determination of the lattice spacing in Table X. This includes both statistical and systematic errors in determining the  $2S - 1S$  splitting. The third error is a 0.5% systematic error from NRQCD in the kinetic mass obtained from analysis of the dispersion relation in Sec. III C.

## 3. The hyperfine splitting

The mass difference between the  $^3S_1$  and  $^1S_0$  states is an important test of our calculations because it is statistically very precise for the ground-state mesons. Controlling systematic errors is the key issue, and the main one is that of

TABLE XII. Tuned  $b$  and  $s$  quark masses in lattice units on each set of configurations. The second column gives  $am_b$  and the third  $am_s$  using the  $Y(2S - 1S)$  splitting to determine the lattice spacing. The first two errors in these two columns come from statistical errors and systematic errors, respectively, in the lattice spacing determination. The third and fourth errors in the  $am_b$  case are the statistical and systematic errors in determining the kinetic mass. Statistical errors in the determination of  $am_s$  mass are negligible. The third error in the  $am_s$  case is a correlated 0.3% error from the square of the physical value of the  $\eta_s$  mass. The fourth column gives  $am_s$  using the  $\eta_s$  decay constant to determine the lattice spacing. The first error is from statistics/fitting and the second is a correlated 0.6% error from the square of the physical value of the  $\eta_s$  decay constant.

Set	$am_b(a_Y)$	$am_s(a_Y)$	$am_s(a_{\eta_s})$
1	3.297(11)(35)(7)(16)	0.0641(4)(12)(2)	0.0705(9)(4)
2	3.263(7)(35)(4)(16)	0.0636(3)(12)(2)	0.0692(5)(4)
3	2.696(4)(22)(7)(13)	0.0528(2)(8)(2)	0.0541(6)(3)
4	2.623(7)(22)(7)(13)	0.0512(3)(8)(2)	0.0531(4)(3)
5	1.893(6)(12)(5)(9)	0.0364(2)(4)(1)	0.0376(5)(2)

radiative corrections to  $c_4$ , the coefficient of the  $\sigma \cdot \mathbf{B}$  term in the NRQCD action. At leading order the hyperfine splitting is proportional to  $c_4^2$ . Our previous calculation [2], with  $c_4 = 1$ , gave a prediction for  $M(Y) - M(\eta_b)$  of 61(14) MeV with the error dominated by the then-unknown radiative corrections to  $c_4$ .

For this calculation we have results for  $c_4$  including  $\mathcal{O}(\alpha_s)$  corrections as well as  $c_4$  tuned nonperturbatively. These determinations of  $c_4$  are described in Appendix B and C, respectively. The values obtained by the two methods for  $c_4$  are given in Table XIII. The nonperturbative values are slightly larger than the perturbative ones, but the differences are well within the expectations from additional  $\alpha_s^2$  corrections to the perturbative values and/or systematic errors in the nonperturbative values. Both sets of values get closer to 1 on the finer lattices, as expected, because they are functions of the strong coupling constant at a scale related to the inverse of the lattice spacing.

Table XIV gives results for the energies of the  $Y$  and  $\eta_b$  for various combinations of values of coefficients in the NRQCD action. We also give the mass difference between the  $Y$  and  $\eta_b$  which is the hyperfine splitting. This can be more precise than either mass separately because we fit both meson correlators together and extract the difference directly from the fit taking into account the correlations. Where we have fits to a  $5 \times 5$  matrix of correlators, as in Tables VIII and IX, we give those results. In other cases we calculated only a single local correlator for each of the  $Y$  and  $\eta_b$  which is quite sufficient to extract a splitting between the ground state masses. Results are not as precise for splittings between radially excited states in those cases, however, and we do not give them.

We see from Table XIV that changing  $c_4$  does have a large effect on the hyperfine splitting, approximately in

TABLE XIII. Values for the coefficient of the  $\sigma \cdot \mathbf{B}$  term,  $c_4$ , for different lattice spacing values. The error on the perturbative values is  $1 \times \alpha_s^2$ . The errors on the nonperturbative values are statistics, experiment and NRQCD systematics, respectively. We did not extract a nonperturbative value on the very coarse lattices.

Sets	$c_4^{\text{pert}}$	$c_4^{\text{nonpert}}$
Fine	1.16(5)	1.18(2)(1)(5)
Coarse	1.20(7)	1.28(7)(1)(5)
Very coarse	1.22(8)	-

line with the expectation of variation as  $c_4^2$ . We also see that, on sets 3 and 5 where we have data for comparison, changing  $c_{1,5,6}$  to their  $\mathcal{O}(\alpha_s)$  improved values does increase the hyperfine splitting slightly. It is a small effect, however, of order 2%. Changing the coefficient of the Darwin term,  $c_2$  also has a small effect of order 1(1)%.

We conclude from this that we have controlled all of the coefficients of  $v^4$  terms in our NRQCD action at a level required to give few percent errors in the hyperfine splitting from these sources. We have not, however, included 4-quark operators in our NRQCD Hamiltonian and they can have an impact on the hyperfine splitting at an order equivalent to that of  $\alpha_s$  corrections to  $c_4$  [28].

TABLE XV. Corrections to the 1S and 2S hyperfine splittings from spin-dependent 4-quark operators missing from our NRQCD action. We use Eq. (B14) inserting values for  $\psi(0)$  from our fitted results and values for  $\alpha_V(\pi/a)$  from Table XXII. We convert to physical units using lattice spacing values from Table X.

Sets	Correction to 1S hyperfine (MeV)	Correction to 2S hyperfine (MeV)
Fine	-1.7	-1.0
Coarse	5.2	3.4
Very coarse	12.9	8.3

In Appendix C we give coefficients for the 4-quark operators and a formula in Eq. (B14) for the correction that they would induce in the hyperfine splitting. Table XV gives values for this correction, to be added to the results from Table XIV, on the very coarse, coarse and fine ensembles based on using a spin-averaged value of the “wave function-at-the-origin”,  $\psi(0)$ , for the  $\Upsilon$  and  $\eta_b$  from our fits. This varies only very little with  $c_4$ , falling by at most 2% from  $c_4 = 1$  to our nonperturbative  $c_4$  values, so we ignore this variation. Our correlators are normalized by dividing by 6 after summing over 2 spins and 3 colors. Then  $\psi(0)$  is given by the amplitude of our correlator fits;  $a(l, 1)$  for the 1S and  $a(l, 2)$  for the 2S from Eq. (7).

TABLE XIV. Fitted energies for ground state  $\Upsilon$  and  $\eta_b$  mesons on all configuration sets. The column  $c_{1,5,6}$  denotes whether the  $\mathcal{O}(\alpha_s)$  improved coefficients were used in the action. Various values of  $c_2$  and  $c_4$  have also been used as indicated.  $c_3 = 1$  except for the case indicated by \* in which  $c_3 = 0.96$ . Where possible the result from the full  $5 \times 5$  matrix fit was taken. Otherwise, the values from the kinetic mass fits were used. In those cases a smaller number of configurations and/or time sources was sometimes used and this is reflected in the statistical errors.

Set	$am_b$	$c_{1,5,6}$	$c_2$	$c_4$	$aE_{\eta_b}$	$aE_{\Upsilon}$	$aE_{\Upsilon} - aE_{\eta_b}$
1	3.42	$\alpha_s$	1	1	0.250 80(5)	0.285 32(6)	0.034 52(8)
1	3.42	$\alpha_s$	1	1.22	0.214 32(5)	0.264 00(6)	0.049 68(7)
1	3.5	$\alpha_s$	1	1	0.250 15(6)	0.283 92(9)	0.033 77(10)
2	3.39	$\alpha_s$	1	1	0.253 61(3)	0.288 09(3)	0.034 48(4)
2	3.42	$\alpha_s$	1	1	0.253 44(5)	0.287 59(5)	0.034 16(6)
3	2.66	1	1	1	0.255 29(4)	0.286 26(6)	0.030 97(7)
3	2.66	$\alpha_s$	1	1	0.260 96(3)	0.292 45(3)	0.031 49(4)
3	2.66	$\alpha_s$	1.25	1	0.256 27(24)	0.287 28(33)	0.031 01(41)
3	2.66	$\alpha_s$	1	1.25	0.209 43(3)	0.256 28(3)	0.046 84(5)
3	2.66	$\alpha_s$	1	1.20	0.220 40(5)	0.263 94(7)	0.043 54(4)
3	2.68	$\alpha_s$	1	1	0.261 08(7)	0.292 49(9)	0.031 41(11)
3	2.7	1	1	1	0.243 75(8)	0.274 83(11)	0.031 08(13)
4	2.62	$\alpha_s$	1	1	0.265 24(2)	0.296 81(2)	0.031 57(3)
4	2.62	$\alpha_s$	1	1.25	0.212 89(2)	0.259 78(2)	0.046 89(2)
4	2.66	$\alpha_s$	1	1	0.265 46(3)	0.296 62(4)	0.031 16(5)
5	1.91	1	1	1	0.246 52(3)	0.271 53(5)	0.025 01(6)
5	1.91	$\alpha_s$	1	1	0.258 51(2)	0.284 05(2)	0.025 54(3)
5	1.91	$\alpha_s$	1	1.10	0.232 04(2)	0.262 06(3)	0.030 03(4)
5	1.91	$\alpha_s$	1	1.15*	0.217 72(22)	0.249 84(40)	0.032 13(30)
5	1.91	$\alpha_s$	1	1.16	0.215 19(2)	0.248 02(4)	0.032 83(2)
5	2.0	$\alpha_s$	1	1	0.259 35(3)	0.283 97(4)	0.024 62(5)

We see from Table XV that the correction is substantial on the very coarse lattices and very small on the fine lattices, because of the variation of the coefficients  $d_1$  and  $d_2$  with  $am_b$ . The corrected results are shown in Fig. 10 along with the uncorrected results for  $c_4 = 1$ . We see that there is a substantial difference between the results coming from the change in  $c_4$  and, to a lesser extent, from the correction for the 4-quark operator. The strong dependence on the lattice spacing seen in the  $c_4 = 1$  results is reduced, in line with the expectation that improving an effective theory should reduce the cutoff dependence.

An additional small factor in Fig. 10 is that we have corrected results for slight mistuning of the  $b$  quark mass and we have included the error from the quark mass tuning in the hyperfine splitting error. The hyperfine splitting is expected to be approximately inversely proportional to the quark mass and this is seen in Table XIV. We assume this relationship to make small adjustments based on the tuned  $b$  masses from Table XII. The largest effect is a 4% one on the very coarse lattices. The lattice spacing error from the quark mass tuning is correlated with the lattice spacing error on the hyperfine splitting because of this inverse

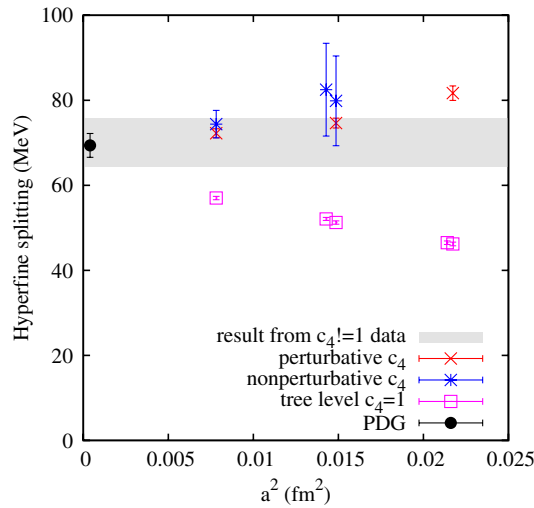


FIG. 10 (color online). Results for the hyperfine splitting,  $M(Y) - M(\eta_b)$  plotted against the square of the lattice spacing. We show results for  $c_4 = 1$  (cyan squares) as well as results for  $c_4$  set equal to its perturbatively improved (red crosses) and nonperturbatively improved values (blue stars). The  $c_4 = 1$  results include statistical errors only and are shown purely for comparison purposes—they are not included in the fit. The results for perturbative and nonperturbative  $c_4$  include a correction for missing 4-quark operators and  $m_b$  mistuning. The errors on these points are from statistics, the lattice spacing and the tuning of  $m_b$ . The results for nonperturbative  $c_4$  also include statistical errors in the determination of  $c_4$ . Our final physical result including our full error budget is given by the grey shaded band. The full error budget includes errors from systematic uncertainties in setting  $c_4$  and from missing  $v^6$  terms in the NRQCD action.

relationship. The lattice spacing error therefore appears with a factor of 2 in the hyperfine splitting.

To obtain a physical result for the hyperfine splitting we then combine results with perturbative and nonperturbative values of  $c_4$  allowing for systematic differences between them from uncertainties in the determination of  $c_4$ . We must also allow for uncertainties from higher-order 4-quark operator effects and for lattice spacing and sea quark mass dependence. The nonperturbative  $c_4$  results are given a correlated systematic error corresponding to the second and third errors in Table XIII and remembering that the hyperfine splitting is related to  $c_4^2$ . Similarly the results for perturbative  $c_4$  are given a separate correlated systematic error corresponding to the  $\alpha_s^2$  errors given in Table XIII. We allow for higher order 4-quark operator effects with a correlated systematic error of size  $6\alpha_s^3|\psi(0)|^2/m_b^2$  with a coefficient of possible size  $\pm 1 \pm \ln(am_b)$ . This does not assume that the small coefficient seen at  $\mathcal{O}(\alpha_s^2)$  on the fine lattices is repeated at higher order.

We allow for lattice spacing and sea quark mass effects as in the fit function of Eq. (17). The prior on sea quark mass effects is now taken to allow 15% effects for  $m_l \approx m_s$ . This reflects the fact that a 40% difference was seen between quenched and dynamical results in [2]. In fact sea quark mass effects in our data are small. Figure 11 shows a comparison of the hyperfine splitting as a function of the light sea quark mass for the case  $c_4 = 1$  where we have a complete set of data. Although these results are *not* used to determine our final answer for the hyperfine splitting they do provide a useful comparison between ensembles at the same lattice spacing and different light quark mass since the effects of  $c_4$  are independent of sea quark mass. The results are adjusted for  $b$  quark mass mistuning and include errors from the  $b$  quark mass and the lattice spacing. Variation with light quark mass is at most 2 MeV. Note that we are using much lighter sea quark masses than in previous calculations [2,12]; indeed  $m_l$  is within a factor of 3 of its physical value.

We obtain a physical value for the hyperfine splitting from the above fit of 70(6) MeV. Fitting the results for perturbative  $c_4$  on their own gives a consistent 67(7) MeV and the results for nonperturbative  $c_4$  alone gives 75(9) MeV. Our best result therefore comes from combining the two. An additional 10% error must be allowed for higher order ( $v^6$ ) spin-dependent terms in the NRQCD action, giving a final result of:

$$M(Y) - M(\eta_b) = 70(9) \text{ MeV.} \quad (18)$$

Our complete error budget is given in Table XVI. The shift for the effect of  $\eta_b$  annihilation is included in our 4-quark operator correction (as discussed in Appendix C) but we separate out an error for that from the rest of the 4-quark operator error.

In Fig. 12 we compare our new result for the hyperfine splitting to earlier full lattice QCD results and to experiment [35]. Earlier results using NRQCD are:

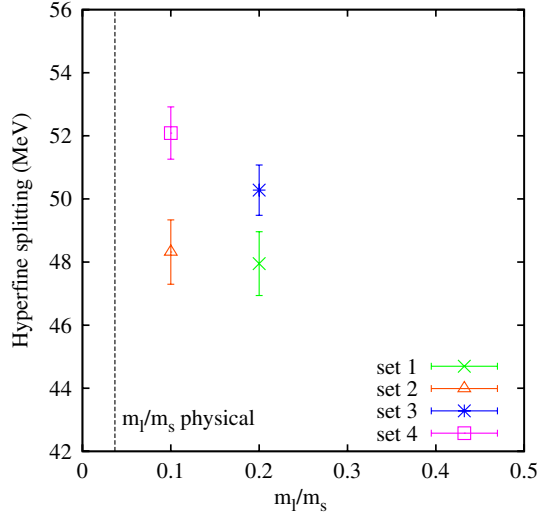


FIG. 11 (color online). Results for the hyperfine splitting obtained for  $c_4 = 1$  (not used in our fit for the physical hyperfine splitting) compared as a function of sea light quark mass in units of the strange quark mass. Results are given for two values of  $m_l/m_s$  on very coarse (sets 1 and 2) and coarse (sets 3 and 4) lattices. The errors on the points include statistical/fitting errors, lattice spacing errors and  $m_b$  tuning errors.

61(14) MeV from [2] with a tree-level  $v^4$  NRQCD action and 60.3(7.7) MeV from [12] using an NRQCD with  $v^6$  spin-dependent terms and  $c_4$  determined from  $P$ -wave splittings but with no 4-quark operator corrections, which are potentially more significant than  $v^6$  terms, or errors from them. The result obtained from the Fermilab heavy quark action [38] is 54.0(12.4) MeV. For this action the hyperfine splitting is sensitive to the coefficient of the  $\mathcal{O}(a)$  improvement term known as the clover term. In principle

TABLE XVI. Complete error budget for the  $1S$  hyperfine splitting and the ratio of the  $2S$  to the  $1S$  hyperfine splittings. Errors are given as a percentage of the final result.

	$M(Y) - M(\eta_b)$	$R_H$
Stats/fitting	0.1	4
$a$ dependence	1.5	5
$a$ uncertainty	0.5	0
$m_l$ dependence	3	3.5
NRQCD $am_b$ dependence	2	0.5
NRQCD $v^6$	10	5
NRQCD $c_4$ uncertainty	7	0
NRQCD 4-quark uncertainty	2	1
$m_b$ tuning <sup>a</sup>	0.1	0
$\eta_b$ annihilation	1	0.5
Total	13	9

<sup>a</sup>Note that the  $m_b$  tuning uncertainty does not include the lattice spacing uncertainty in  $m_b$ . Since that is correlated with the  $a$  uncertainty on converting the hyperfine splitting from lattice to physical units, they must be handled together and both are included in the  $a$  uncertainty.

this coefficient does not have to be tuned but the approach to the continuum limit is slow. Here it was taken to have its tree-level value after tadpole-improvement and the quark mass was tuned using the spin-averaged kinetic mass of the  $B_s$  and  $B_s^*$  mesons.

All four lattice QCD results agree well with the current experimental average of 69.3(2.8) MeV [35] obtained from averaging results from experiments on radiative transitions to  $\eta_b$  from  $Y'$  and  $Y''$  [40–42]. Preliminary experimental results using radiative transitions from the  $h_b$  indicate a somewhat lower value [43].

Our new result above contains the most complete analysis at  $\mathcal{O}(v^4)$  in the NRQCD action. To improve it would require the inclusion of spin-dependent operators at  $\mathcal{O}(v^6)$ . The effect of spin-dependent  $v^6$  operators was studied in [12], taking ratios of the hyperfine splitting to  $P$ -wave spin splittings to cancel the effect of  $c_4$ . Those results indicate that spin-dependent  $v^6$  terms tend to reduce the hyperfine splitting by about 10%. We have included a (symmetric) 10% error in our results to account for missing  $v^6$  terms.

The hyperfine splitting has also been calculated using continuum QCD perturbation theory [44]. A considerably smaller result is obtained of 41(14) MeV. This is not in disagreement with the nonperturbative lattice QCD results given the size of the errors. It has been suggested, however,

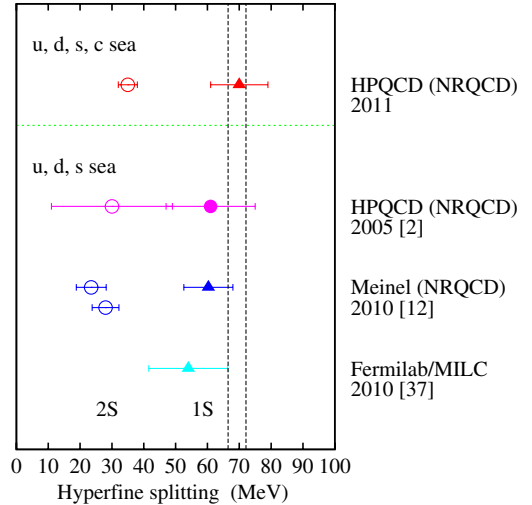


FIG. 12 (color online). Comparison of results for the hyperfine splittings,  $M(Y) - M(\eta_b)$  and  $M(Y') - M(\eta'_b)$ , from different full lattice QCD calculations. Filled symbols indicate the  $1S$  hyperfine and open symbols, the  $2S$  hyperfine. Circles indicate predictions and triangles postdictions. The top (red) points are the new results from this paper, and the points below that (pink) are from [2], when the  $1S$  hyperfine was a prediction. The third line gives results from [12]. Two results are given for the  $2S$  hyperfine; that from a ratio to the  $1S$  hyperfine, as here, and that from a ratio to the combination of  $P$ -wave spin splittings sensitive to  $c_4$  (see Appendix C). The top three results use the NRQCD formalism for  $b$  quarks; the bottom (cyan) result uses the Fermilab heavy quark action [38]. The black dashed lines mark the current experimental average [35].



that the inclusion of radiative corrections to  $c_4$  in the lattice NRQCD calculation would reduce the value of the hyperfine splitting obtained [45]. That expectation was based on an incorrect analysis of the form of  $c_4$  in the lattice NRQCD calculation and we see indeed from the results given here that the inclusion of radiative corrections to  $c_4$  has had the opposite effect and increased our value for the hyperfine splitting.

The best way to study the 2S hyperfine splitting,  $M(Y') - M(\eta'_b)$  is through the ratio to the 1S hyperfine splitting. We define:

$$R_H = \frac{M(Y') - M(\eta'_b)}{M(Y) - M(\eta_b)}. \quad (19)$$

Then  $c_4$  effects cancel as can be seen in the numbers in Tables VIII and IX and plotted in Fig. 13. In the Figure we have corrected the results for missing 4-quark operator effects which are slightly different in the 1S and 2S states and so have an effect on the ratio. This is at most 4%, on the very coarse lattices. We have made no correction for the slight mistunings of  $m_b$  since they should largely cancel in this ratio.

Again we extract a physical result for  $R_H$  by allowing for  $m_l$  and  $a$  dependence as in Eq. (17). Here we relaxed the priors on the  $a$  dependence so that they all had the form  $0.0 \pm 1.0$ . The prior on  $m_l$  dependence (in units of  $m_s$ ) was taken as  $0.0 \pm 0.15$  as for the 1S hyperfine, allowing a 15% change from  $m_l = m_s$  down to the physical point.

Our final physical value is

$$R_H = 0.499(42). \quad (20)$$

The full error budget is given in Table XVI where we allow a 5% error for missing spin-dependent  $v^6$  terms, allowing

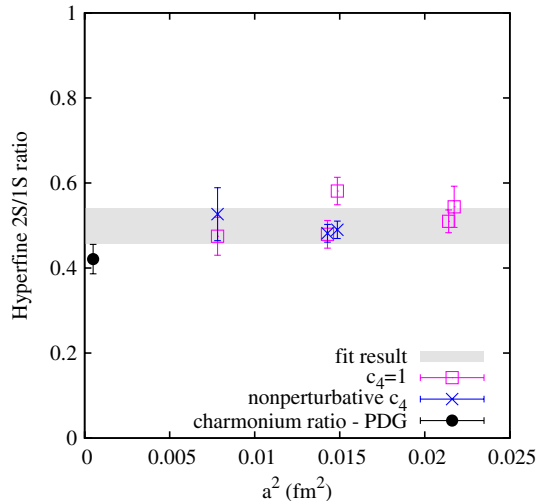


FIG. 13 (color online). The ratio of hyperfine splittings for 2S and 1S states,  $(M(Y') - M(\eta'_b))/(M(Y) - M(\eta_b))$ , plotted against the square of the lattice spacing. Points have been corrected for missing 4-quark operator effects. The shaded band shows our final physical result including our full error budget.

for some cancellation of  $v^6$  effects between the 1S and 2S hyperfine splittings.

Combining our result for  $R_H$  with the current experimental average for the 1S hyperfine splitting gives a result for the 2S hyperfine splitting of 35(3)(1) MeV, where the second error comes from the experimental 1S splitting. We predict the mass for the  $\eta'_b$  to be 9.988(3) GeV.

Figure 12 compares our result for the 2S hyperfine splitting to earlier predictions. Meinel [12] gives 23.5 (4.7) MeV from a ratio to  $P$ -wave spin splittings and 28.0 (4.7) from a ratio to the 1S hyperfine splitting, as used here. He includes the effect of spin-dependent  $v^6$  operators but without such a complete analysis as we have done here of  $v^4$  operators. The conclusion from Fig. 12 is that lattice QCD results give a fairly clear prediction of the 2S hyperfine splitting around 30 MeV, half the result for the 1S hyperfine splitting.

Figure 13 compares our result for the bottomonium ratio of 2S to 1S hyperfine splittings to the experimental charmonium ratio of 0.421(35). Our bottomonium result is somewhat higher, but not in disagreement with this value. This indicates that the heavy quark mass dependence in the 1S and 2S hyperfine splittings is very similar over the wide range of quark masses from  $c$  to  $b$  so that the ratio remains the same.

The  $S$ -wave hyperfine splittings can be compared to the much smaller result for the  $P$ -wave states. In Appendix C we determine the  $P$ -wave hyperfine splitting to be 2 (2) MeV, consistent with zero.

#### IV. THE $\eta_s$ MASS AND DECAY CONSTANT

To complement the computation in the previous section, the lattice spacing was also determined using the decay constant of the fictitious  $\eta_s$  meson,  $f_{\eta_s}$ . This is a pseudo-scalar particle consisting of an  $s\bar{s}$  pair whose properties can easily be computed in lattice QCD. It is particularly suitable for fixing the lattice spacing since there are no  $u/d$  valence quarks meaning that the error coming from the chiral extrapolation to physical  $u/d$  masses is small. The “physical” values of the  $M_{\eta_s}$  and  $f_{\eta_s}$  have to be fixed by comparison to  $M_\pi$ ,  $M_K$ ,  $f_\pi$  and  $f_K$  as in [21]. This requires a simultaneous chiral and continuum extrapolation for the masses and decay constants of the  $\pi$ ,  $K$  and  $\eta_s$ . Previously we found, on ensembles including 2 + 1 flavors of sea quarks, that properties of the  $\eta_s$  were very close to those expected from leading order chiral perturbation theory, i.e.  $M_{\eta_s}^2 \approx 2M_K^2 - M_\pi^2$  and  $f_{\eta_s} \approx 2f_K - f_\pi$ . We reexamine that issue here on these ensembles containing 2 + 1 + 1 sea quarks.

##### A. Simulation details and fitting

$s$  and  $u/d$  valence quark propagators were calculated on the ensembles given in Table I using the same HISQ action as used for the sea quarks. The HISQ action [16] is a

further improved version of the improved staggered (asqtad) action that reduces discretization errors coming from staggered taste effects for that action by about a factor of 3. The improved staggered action smears the gluon fields that appear in the quark action in a very specific way to reduce high-momentum taste-exchange interactions but without increasing discretization errors [10]. The HISQ action takes this one step further by performing two smearing steps. The original version of the HISQ action used an SU(3) projection of the smeared links between the two smearing steps. However, this caused difficulties for the updating algorithm when these quarks were included as sea quarks [19]. Instead the sea quarks here use the HISQ action but with only a U(3) projection between the smearing steps. Whether U(3) or SU(3) projection it makes very little difference to the spectrum of mesons from HISQ quarks and so all the good features of the HISQ action demonstrated in [16] remain essentially unaltered. Note that the HISQ action does not use tadpole-improvement—the U(3) (or SU(3)) projection effectively takes care of large tadpole contributions in the same way that the use of the  $u_0$  parameter does in the NRQCD and gluon actions.

The parameters of the valence quark propagators are listed in Table XVII. We took the light quark mass to be the same as that in the sea (except for a small difference on set 3), but we retuned the valence strange quark masses slightly to allow for mistuning of the strange sea quark mass (of course the final well-tuned  $s$  quark mass values cannot be decided until a value for the lattice spacing is determined so we will revisit this issue at the end of this section). We used delta function random wall sources as for the l-smear  $b$  quark propagators discussed in Sec. III. We also used 16 evenly-spaced time sources per configuration to increase statistics. The starting position of these time sources was shifted from configuration to configuration in the ensemble.

The light meson pseudoscalar correlators are calculated by combining the light and strange quark propagators. Here we use the Goldstone mesons, made with the local

TABLE XVII. Valence light and strange quark mass parameters on each ensemble. The valence light quark masses are the same as in the sea (given in Table I), except for a slight difference on set 3. The valence strange quark masses have been retuned slightly to be closer to the physical values. Columns 4 and 5 give the number of configurations used from each ensemble and the number of time sources for propagators per configuration.

Set	$am_l^{\text{val}}$	$am_s^{\text{val}}$	$n_{\text{cfg}}$	$n_t$
1	0.013	0.0688	1021	16
2	0.0064	0.0679	1000	16
3	0.010 44	0.0522	1053	16
4	0.005 07	0.0505	1000	16
5	0.0074	0.0364	1008	16

$\gamma_5$  operator. Then the correlators are simply given by the squared modulus of the propagators summed over a time-slice to project onto zero momentum. The correlators were binned over all time sources on a configuration.

To study the autocorrelations between configurations we proceed as in Sec. IIIB to calculate the autocorrelation function  $C_{\Delta T}$ . Figure 14 shows  $C_{\Delta T}$  against  $\Delta T$  for both the  $\pi$  and  $\eta_s$  correlators at a source-sink lattice time separation appropriate to our fits. This time separation is increased as the lattice spacing decreases to remain approximately physical. We see from the Figure that the  $\eta_s$  shows little autocorrelation, although more than was visible for the  $Y$  in Fig. 1. We expect longer autocorrelation times for lighter mesons because they have a larger spatial extent and therefore decorrelation of the gluon field configuration on relevant spatial scales takes longer in Monte Carlo time. The  $\pi$  correlators on the coarse and very coarse lattices show a similar autocorrelation function to the  $\eta_s$ . However, on the fine lattices where autocorrelations might be expected to be worst, there are clear signs that neighboring configurations in time are correlated. Note the difference between our result and that of [19]. There very little autocorrelation was seen in the  $\pi$  meson correlator, but fewer time sources were used per configuration (typically 4). Both here and in [19] the time sources are moved randomly from one configuration to the next. However, with 16 time sources there is not much scope for a large shift in time between configurations. To reduce autocorrelations we bin all of our fine light meson correlators by a factor of 8 in configuration number before fitting. From Fig. 14 this can be seen to reduce the autocorrelation function well below  $e^{-1}$ .

The fitting method used for the correlators was the same as for the Upsilon correlators but with only a single source and sink smearing. For meson correlators made from relativistic quarks the fit function takes a “cosh” form rather than simple exponentials because of propagation in both time directions. For staggered quarks in general we have to include an additional oscillating term from opposite parity mesons that couple through the time-doubler quark. The fit function then becomes:

$$G_{\text{meson}}(t) = \sum_{k=0}^{n_{\text{exp}}} a_k (e^{-E_k t} + e^{-E_k (T-t)}) - (-1)^{t/a} \times \sum_{ko=0}^{n_{\text{exp}}} a_{ko} (e^{-E_{ko} t} + e^{-E_{ko} (T-t)}). \quad (21)$$

The oscillating piece is absent for the  $\pi$  and  $\eta_s$  because the valence quark and antiquark have equal mass and the oscillation cancels. It is necessary to include it for the  $K$  meson. For each ensemble a simultaneous fit to all three correlators was performed using the appropriate form for each. This allowed us to take into account the correlations between the fit results for each meson in our subsequent chiral extrapolations. We use the full range of  $t$  values in the fit apart from the first 3–5 time-slices. Priors for

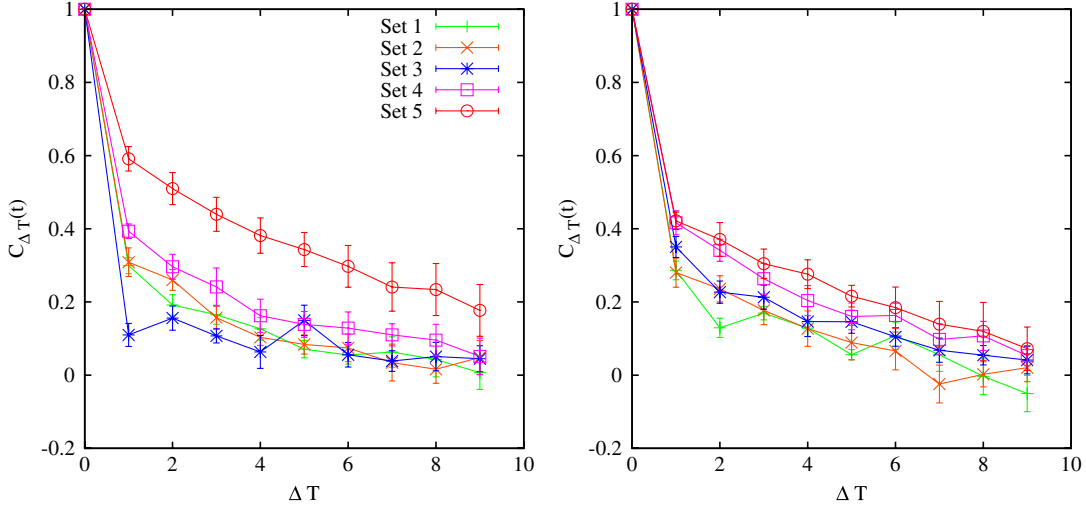


FIG. 14 (color online). Autocorrelation function  $C_{\Delta T}$  for  $\pi$  (left) and  $\eta_s$  (right) correlators. These are made with a  $\delta$  function random wall as described in the text. The key to the results from different ensembles is set 1, green plus; set 2, orange cross; set 3 blue star; set 4 pink open square; set 5, red open circle. The correlators are evaluated at lattice time separation  $t/a = 6$  on very coarse lattices (sets 1 and 2),  $t/a = 8$  on coarse lattices (sets 3 and 4) and  $t/a = 10$  on fine lattices (set 5). This corresponds to a  $t$  value, approximately constant in physical units across the lattice spacing values, where the  $\pi$  and  $\eta_s$  correlators have reached the ground-state plateau.  $\Delta T$  is given in units of configuration number in the ordered list for each ensemble.

energies and amplitudes are chosen as for the  $Y$  fits described in Sec. III B. We take results from 4 exponential fits, where ground-state masses and their errors have clearly stabilized.

The results that we use are the ground-state meson masses and amplitudes, i.e.  $k = 0$  in Eq. (21). The meson masses are given by the parameter  $E_0$  from each fit, since there is no energy offset for staggered quarks as there is for NRQCD. The decay constants are extracted from the fit using

$$f_{ab} = (m_a + m_b) \sqrt{\frac{2a_0}{E_0^3}} \quad (22)$$

for a meson containing quarks  $a$  and  $b$  with masses  $m_a, m_b$ , ground state mass  $E_0$  and ground state amplitude,  $a_0$ , from the fit form above. Equation (22) uses the partially conserved axial current relation, valid for staggered quarks, to relate the matrix element of the pseudoscalar density to that of the temporal axial current and therefore the decay constant. The existence of the partially conserved axial current relation means that the temporal axial current is absolutely normalized and there is no uncertainty from

lattice to continuum current matching factors as there can be in some other quark formalisms.

## B. Results and chiral extrapolations

Our results for the  $\pi$ ,  $K$ , and  $\eta_s$  meson masses and decay constants are listed in Tables XVIII and XIX. We also give various ratios that are useful indicators of the sensitivity of the  $\eta_s$  parameters to the chiral extrapolation in the  $u/d$  sea quark mass, and to the lattice spacing.

We fit the three decay constants and meson masses simultaneously using SU(3) chiral perturbation theory, adapted to include discretization effects. The usual approach is to use values for the decay constant and meson mass in GeV, having chosen a value of the lattice spacing on each ensemble. Extrapolation to the point where  $M_\pi$  and  $M_K$  take their physical values then allows comparison to experiment of the resulting values for  $f_\pi$  and  $f_K$ . Here instead we use values for  $r_1/a$  to fix the relative lattice spacing between ensembles and keep the physical value of  $r_1$  as a parameter to be obtained from the fit. The value for  $r_1$  is determined by the requirement to match  $f_\pi$  and  $f_K$  from experiment in the chiral limit where the experimental

TABLE XVIII. Values for the ground state masses in lattice units ( $E_0$  from Eq. (21)) for  $\pi$ ,  $K$  and  $\eta_s$  mesons. The fourth row gives the ratio of the square of the  $\eta_s$  mass to a combination of  $\pi$  and  $K$  masses that would be 1 in leading order chiral perturbation theory.

Set	1	2	3	4	5
$aM_\pi$	0.236 37(15)	0.166 15(7)	0.191 53(9)	0.134 13(5)	0.140 70(9)
$aM_K$	0.411 95(17)	0.390 82(9)	0.327 81(10)	0.307 57(7)	0.239 33(11)
$aM_{\eta_s}$	0.533 61(14)	0.527 97(8)	0.423 51(9)	0.414 76(6)	0.308 84(11)
$M_{\eta_s}^2/(2M_K^2 - M_\pi^2)$	1.004 26(43)	1.003 17(28)	1.006 36(34)	1.004 74(26)	1.006 60(27)

TABLE XIX. Values for the ground state decay constants in lattice units (derived from  $a_0$  in Eq. (21) as described in the text) for  $\pi$ ,  $K$  and  $\eta_s$  mesons. We also give various ratios of decay constants obtained from the simultaneous fit. The sixth row gives the ratio of the  $\eta_s$  decay constant to a combination of  $\pi$  and  $K$  decay constants that would be 1 in leading order chiral perturbation theory.

Set	1	2	3	4	5
$af_\pi$	0.111 83(9)	0.105 11(5)	0.090 75(5)	0.084 51(4)	0.066 21(5)
$af_K$	0.126 89(8)	0.122 68(4)	0.101 85(5)	0.097 88(3)	0.074 27(4)
$af_{\eta_s}$	0.141 99(6)	0.140 26(3)	0.113 12(4)	0.111 19(2)	0.082 38(4)
$f_K/f_\pi$	1.134 67(58)	1.167 17(38)	1.122 31(38)	1.158 19(35)	1.121 70(39)
$f_{\eta_s}/f_\pi$	1.269 74(80)	1.334 42(59)	1.246 53(68)	1.315 68(53)	1.244 16(69)
$f_{\eta_s}/(2f_K - f_\pi)$	1.000 31(62)	1.000 07(27)	1.001 54(45)	0.999 48(26)	1.000 61(32)
$f_{\eta_s}/M_{\eta_s}$	0.266 09(11)	0.265 66(6)	0.267 11(10)	0.268 09(6)	0.266 74(12)

values are included as extra pieces of “data” for the fit. The experimental values for  $f_\pi$  and  $f_K$  come from experimental measurement of the leptonic decay rate and values of  $V_{ud}$  and  $V_{us}$  taken from elsewhere. We use [35]

$$f_\pi = 0.1304(2) \text{ GeV} \quad f_K = 0.1561(9) \text{ GeV}. \quad (23)$$

The meson mass values that go with these decay constants in a world appropriate to lattice QCD without electromagnetism and in which  $m_u = m_d$  are [46]

$$M_\pi^2 = M_{\pi^0}^2 \quad (24)$$

$$M_K^2 = \frac{1}{2}(M_{K^0}^2 + M_{K^+}^2 - (1 + \Delta_E)(M_{\pi^+}^2 - M_{\pi^0}^2)).$$

We take  $\Delta_E$ , which parameterizes the violations of Dashen’s theorem, to have the value  $1 \pm 1$ . The decay constants are already defined to be results in pure QCD, provided electromagnetic effects have been removed from the experimental leptonic decay rates [35]. The residual error in  $f_K$  from the fact that it is the decay constant of the  $K^+$  whereas the  $K$  mass in Eq. (25) is the isospin average is less than 0.1% [46], so we ignore it here.

Our fit also returns a physical value for  $f_{\eta_s}$  and  $M_{\eta_s}$ . This can be used in subsequent analyses to tune the  $s$  quark mass and to fix the lattice spacing. It is a good meson to use for this purpose because its parameters are very insensitive to the sea quark masses, as we see in Tables XVIII and XIX.

The analysis is the same as that used in [21] except for two improvements. The first is that the fit is simplified because HISQ quarks are used in both the valence and sea sectors. The second is that we include correlations between all of the decay constants and meson masses on each ensemble by feeding into the fit the covariance matrix that resulted from the simultaneous fit to all three meson correlation functions. Below we provide a brief description of the chiral/continuum extrapolations following [21].

On each ensemble the decay constants and meson masses are a function of the masses of the valence quarks for that meson and of the masses of the sea quarks for that ensemble, with the coefficients of the mass dependence constrained to be the same for the  $\pi$ ,  $K$  and  $\eta_s$  mesons. Because the quark masses run with energy scale it

simplifies the fits to use a dependent variable related to the square of appropriate Goldstone meson masses instead of the quark mass. Thus we write

$$x_l = \frac{M_\pi^2/2}{\Lambda_\chi^2}, \quad (25)$$

where  $\Lambda_\chi$  provides the cutoff scale of the chiral expansion,

$$\Lambda_\chi = 4\pi f_\pi/\sqrt{2}. \quad (26)$$

Similarly

$$x_s = \frac{M_K^2 - M_\pi^2/2}{\Lambda_\chi^2}. \quad (27)$$

In the cases where the sea and valence quark masses differ, the  $x$  parameters for the sea quark masses are obtained from those of the valence masses by rescaling in proportion to the quark mass. Then the decay constant made from valence quarks  $a$  and  $b$  takes the functional form

$$f(x_a, x_b, x_l^{\text{sea}}, x_s^{\text{sea}}, a) = f^{\text{NLO}} + \delta f_\chi + \delta f_{\text{lat}}, \quad (28)$$

where  $f^{\text{NLO}}$  is the full partially quenched chiral perturbation theory formula at next-to-leading order [47] and  $\delta f_\chi$  and  $\delta f_{\text{lat}}$  include possible correction terms coming from higher order terms in the quark mass and finite lattice spacing corrections. Each of the terms contains a set of unknown coefficients which are given prior constraints in our fit allowing us to test their effect on our final result.

$f^{\text{NLO}}$  [47] includes terms proportional to the squares of the appropriate meson masses as well as logarithmic terms that appear in combinations such as, for example,  $(x_a + x_l^{\text{sea}}) \log(x_a + x_l^{\text{sea}})$ . The logarithmic terms are corrected for finite volume effects through the use of finite volume chiral perturbation theory. The finite volume correction is significant for  $f_\pi$ , particularly on set 1 where  $M_\pi L = 3.8$  and the finite volume correction is 1.8%. For the other sets, with  $M_\pi L > 4$ , the correction ranges from 0.4% to 0.7%. For  $f_K$  and  $f_{\eta_s}$  the correction is much smaller. It is at its largest on set 1 with 0.7% for  $f_K$  and 0.2% for  $f_{\eta_s}$ .

$\delta f_\chi$  includes polynomial dependence on various combinations of the  $x_i$  up to and including  $x_i^4$  terms [21]. Most of



these terms only matter for the  $s$  quark and they allow for differences between the  $s$  and  $l$  sectors within SU(3) chiral perturbation theory. Since  $x_s = 0.17$  including  $x_i^4$  terms means that missing terms at  $x_s^5$  are  $\mathcal{O}(10^{-4})$ , smaller than our statistical errors. It is sufficient to include polynomials because we cannot distinguish high-order logarithms from polynomials over this range in  $x_i$ .

$\delta f_{\text{lat}}$  allows for dependence on powers of the square of the lattice spacing, since this is the form that discretization errors take for staggered quarks. We include terms up to  $(a\Lambda_{\text{QCD}})^8$  where  $\Lambda_{\text{QCD}}$  is taken to be  $\mathcal{O}(0.6 \text{ GeV})$ . The coefficients of the  $a$  dependence are also allowed to have dependence on valence and sea mass dependence. This includes dependence on  $\log(x_l)$  to model discretization errors coming from staggered taste-changing effects [21].

The terms in the chiral expansion are generally written so that the coefficients are expected to be  $\mathcal{O}(1)$ . For these coefficients we take the prior in our fit to be  $0 \pm 1$ . This is true for the higher order terms in the chiral expansion that relate to  $a$  dependence and mass dependence, except where the masses involved are sea-quark masses and then the prior is taken as  $0 \pm 0.3$ , simply because sea-quark effects are typically suppressed over valence quark effects by this amount. The prior on the bare decay constant parameter in chiral perturbation theory,  $f_0$ , is taken as  $0.11 \pm 0.02$ . In fact the parameter that is tuned by the fit is  $\log(f_0)$  in order to keep  $f_0$  positive. The prior on  $\log(f_0)$  is then taken as  $-2.2 \pm 0.18$ . The priors for the coefficients  $L_{4,5,6,8}$  that multiply analytic terms at next-to-leading order in chiral perturbation theory are taken as  $0 \pm 0.01$ .

The meson masses are fitted simultaneously with the decay constants feeding in the  $6 \times 6$  covariance matrix on each ensemble. The leading behavior in chiral perturbation theory for the meson masses is now trivial. However the chiral fit, which shares some of the same coefficients as that of the decay constants [47], allows us to fix the higher order behavior as a function of sea and valence masses. In particular it allows us to fix the behavior of the  $\eta_s$  mass as the  $\pi$  and  $K$  masses vary, so that we can obtain its value at the physical point. The priors in the chiral fit for the meson masses take the same form as described above for the decay constant.

The fitting forms above were extensively tested for robustness against both real and fake data in [17,21].

The results of our fit are shown in Fig. 15. The data points, adjusted for finite volume effects and for the slight mistuning of the valence and sea strange quark masses, are plotted as a function of  $x_l/x_s$ . The fit lines at each value of the lattice spacing are shown along with the  $a = 0$  line. At the physical value for  $x_l/x_s$  we give the experimental values for  $f_\pi$  and  $f_K$ . This plot should be compared with Fig. 4 in [21]. It is evident that these “second generation” configurations have significantly smaller discretization errors [19].

The fit has a  $\chi^2/\text{dof}$  value of 0.3 for 36 degrees of freedom. The fitted value of  $f_0$  is  $\exp(-2.174 \pm 0.028)$ ,

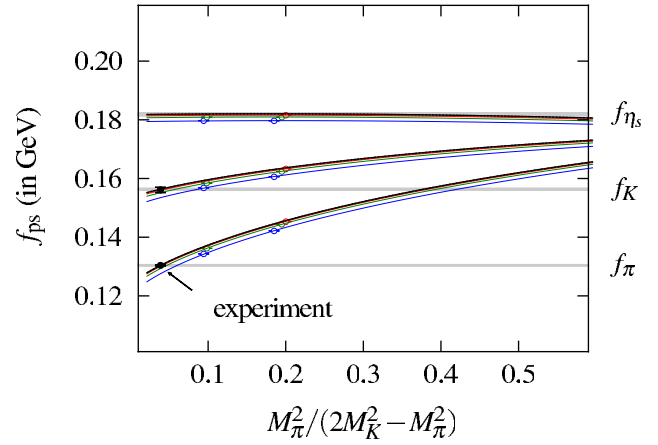


FIG. 15 (color online). The pseudoscalar decay constants plotted against the ratio of squared pseudoscalar masses that is approximately equal to  $m_l/m_s$ . The points have been adjusted for finite-volume effects and for mistuning of the strange quark mass. The lines are from the tuned fit function at each lattice spacing, with results increasing in value from very coarse (blue) to fine (red). The top (black) line is the  $a = 0$  curve and the black leftmost data points give the experimental value for  $f_\pi$  and  $f_K$  given values for  $V_{ud}$  and  $V_{us}$  [35].

in agreement with SU(3) chiral fits using asqtad improved staggered quarks [48]. The resulting physical values for  $f_{\eta_s}$  and  $M_{\eta_s}$  are

$$\begin{aligned} f_{\eta_s} &= 0.1819(5) \text{ GeV} & M_{\eta_s} &= 0.6893(12) \text{ GeV} \\ f_{\eta_s}/M_{\eta_s} &= 0.2638(8). \end{aligned} \quad (29)$$

These are in agreement with the results obtained on  $n_f = 2 + 1$  dynamical asqtad configurations [21] but considerably more accurate because our statistical precision is improved, and we have smaller continuum and chiral extrapolation errors. These last two are reduced because of the improvements in the gluon field configurations and because we are working closer to the chiral limit. Complete error budgets for  $f_{\eta_s}$ ,  $M_{\eta_s}$  and their ratio are given in Table XX.

The results in Eq. (29) are very close, but in fact differ significantly from the expected result from leading order chiral perturbation theory. This is illustrated in Figs. 16 and 17 in which the ratios  $f_{\eta_s}/(2f_K - f_\pi)$  and  $M_{\eta_s}^2/(2M_K^2 - M_\pi^2)$  are plotted against  $x_l/x_s$ . Both ratios are very flat in  $x_l/x_s$ , never differing by as much as 1% from 1. We determine the physical values for the ratios to differ significantly from 1, however, with results:

$$\begin{aligned} f_{\eta_s}/(2f_K - f_\pi) &= 0.9977(6) \\ M_{\eta_s}^2/(2M_K^2 - M_\pi^2) &= 1.0070(18). \end{aligned} \quad (30)$$

Since our fit uses  $r_1/a$  to set the relative lattice spacing we can determine a value for  $r_1$  from the final match with experiment for  $f_\pi$  and  $f_K$ . We obtain

TABLE XX. Complete error budget for  $r_1$ ,  $f_{\eta_s}$ ,  $M_{\eta_s}$  and  $f_{\eta_s}/M_{\eta_s}$ . Errors are given as a percentage of the physical value. Errors which are negligible compared to the others are indicated by “0”.

	$r_1$	$f_{\eta_s}$	$M_{\eta_s}$	$f_{\eta_s}/M_{\eta_s}$
Stats/fitting	0.24	0.16	0.07	0.18
$a$ extrapolation	0.46	0.14	0.03	0.16
$m_l$ extrapolation	0.09	0.12	0.04	0.11
Finite volume	0.04	0	0	0
$r_1/a$	0.73	0.12	0.02	0.12
Initial $r_1$ uncertainty	0.26	0.02	0	0.02
$M_\pi, M_K$	0	0.05	0.14	0.09
Total	0.90	0.28	0.17	0.30

$$r_1(f_{\eta_s}) = 0.3209(29) \text{ fm.} \quad (31)$$

The error budget for  $r_1$  is given in Table XX. This physical result for  $r_1$  agrees with the value obtained from the same analysis on  $n_f = 2 + 1$  dynamical asqtad lattices [21], but is almost twice as accurate.

We can use  $f_{\eta_s}$  and  $M_{\eta_s}$  to determine the  $s$  quark mass and lattice spacing on each ensemble. This is done by tuning the  $s$  quark mass so that  $f_{\eta_s}/M_{\eta_s}$  takes the value in Eq. (29) and then the lattice spacing is read from the value of  $f_{\eta_s}$ . We do this here retrospectively by using our chiral fits to tune the  $s$  quark mass and work out the corresponding changes in  $f_{\eta_s}$  and  $M_{\eta_s}$ . For simplicity the sea light quark masses were also retuned to the physical value. The values of  $a$  obtained are given in Table X.

In Table XII we give tuned values of  $am_s$  on each ensemble as a result of tuning the  $\eta_s$  to the physical value

given in Eq. (29). Over the short range needed for the retuning the relationship  $m_s \propto M_{\eta_s}^2$  works very well. We give results for both the case of using the  $\eta_s$  decay constant to fix the lattice spacing and of using the  $Y 2S - 1S$  splitting. The values of  $am_s$  obtained from the two methods differ substantially on the very coarse lattices but come into agreement on the fine lattices as expected.

The errors in the tuned values of  $am_s$  are dominated by the errors in the lattice spacing. The relative error in  $a$  is doubled in  $am_s$  because the quark mass is proportional to the square of the meson mass. When the quark mass is converted to physical units one factor of the lattice spacing error disappears.

## V. $r_1$

The values of the heavy quark potential parameter,  $r_1$ , can be determined by combining the values for  $r_1/a$  from MILC given in Table I with the values for the lattice spacing given from our two different methods in Table X. We use “unsmoothed” values of  $r_1/a$  which are the results of an independent fit to the heavy quark potential on each ensemble. Figure 18 shows the results for  $r_1$  from each method as a function of the lattice spacing. Differences are evident on the very coarse lattices as a result of discretization errors but there is clear convergence as  $a \rightarrow 0$ . The results are plotted against  $(a/r_1)^4$  since the leading tree-level discretization errors are at  $a^4$ . Note that the behavior of this plot is rather different from that obtained previously on the  $2 + 1$  flavor configurations (Fig. 3 of [21]). There is a little less variation with  $a$ , to be expected because of the various improvements to the discretization of QCD. The main difference however is the

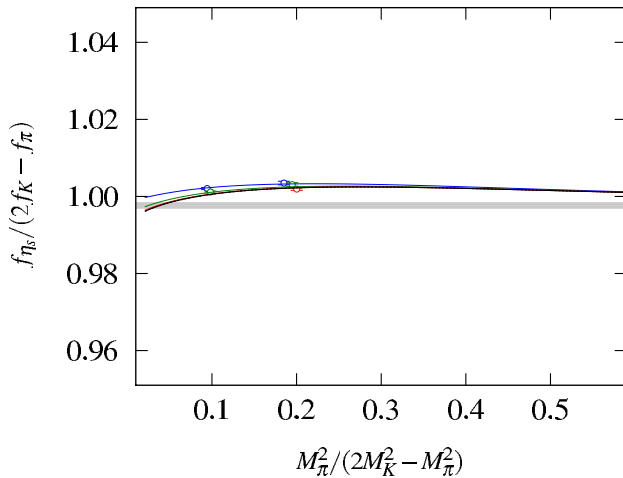


FIG. 16 (color online). The ratio of  $f_{\eta_s}$  to  $2f_K - f_\pi$ , which would be 1 in leading order chiral perturbation theory. The ratio of squared meson masses on the  $x$  axis corresponds approximately to  $m_l/m_s$ . The blue, green and red points and fit curves correspond to very coarse, coarse and fine lattices, respectively. The black line is the continuum,  $a = 0$ , fit curve.

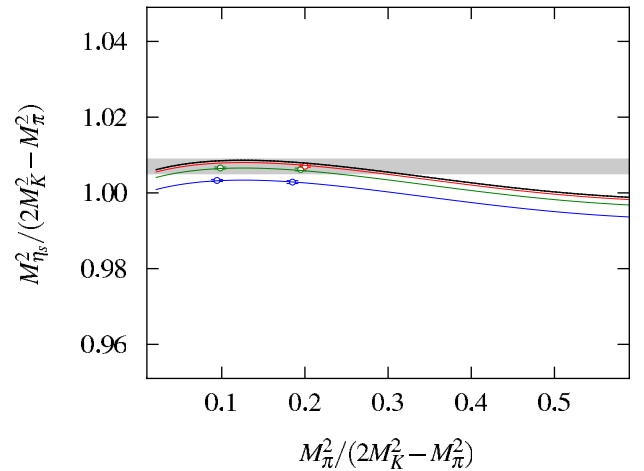


FIG. 17 (color online). The ratio of  $M_{\eta_s}^2$  to  $2M_K^2 - M_\pi^2$ , which would be 1 in leading order chiral perturbation theory. The ratio of squared meson masses on the  $x$  axis corresponds approximately to  $m_l/m_s$ . The blue, green and red points and fit curves correspond to very coarse, coarse and fine lattices, respectively. The black line is the continuum,  $a = 0$ , fit curve.

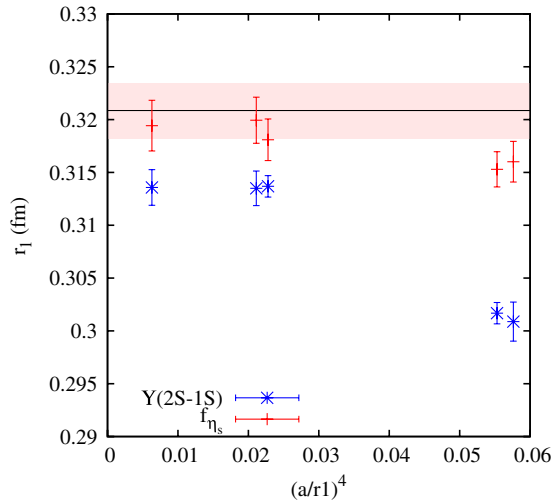


FIG. 18 (color online). Values for the heavy quark potential parameter  $r_1$  obtained by combining values for  $r_1/a$  from MILC with either of our two methods for determining the lattice spacing. The red plus symbols correspond to using the  $\eta_s$  and the blue stars to using the  $Y\ 2S - 1S$  splitting (these points do not include the NRQCD systematic error which is correlated between the points). The black line with light red error band corresponds to the final value for  $r_1$  from the combined fit to the results from both methods and includes the total error.

direction of approach to  $a = 0$ . The results for  $r_1$  from  $f_{\eta_s}$  are now very flat and the results from the  $Y$  approach  $a = 0$  from below. This reflects a change in the relative discretization errors of the quantities involved.

As discussed above, the chiral fits involving the  $\eta_s$  give a result for  $r_1$  of 0.3209(29) fm. We can fit the results from using the  $Y$  method to test if they are consistent with this. Using the  $\eta_s$  result as a prior for the  $Y$  fit then enables us to extract an improved result for  $r_1$  which combines both methods.

To extract a physical value for  $r_1$  using the  $Y$  results we use the same functional form for the fit as was used earlier for  $R_S$  and  $R_P$ , Eq. (17). This includes an allowance for variations as a function of the sea light quark masses, although it is clear from the results that any such dependence is very small. Indeed the quantities being used were chosen for their insensitivity to such effects. We also include an allowance for discretization errors, both of the standard type, varying as  $(a\Lambda)^n$  and the from various  $am_b$ -dependent type coming from radiative corrections in NRQCD. We also allow for the NRQCD systematic error from Tables VI and VII as a correlated error for all 5 ensembles.

The fit to the  $Y$  values using a large width prior for the physical value (0.32(10) fm) gives  $\chi^2/\text{dof} = 0.79$  for 5 degrees of freedom and  $r_1(Y) = 0.310(6)$  fm. This shows the required consistency in the determination of the lattice spacing from the two methods as  $a \rightarrow 0$ . The fit including the prior value from the  $\eta_s$  analysis gives  $\chi^2/\text{dof} = 0.76$  and result:

$$r_1 = 0.3209(26) \text{ fm.} \quad (32)$$

This is slightly improved over the  $\eta_s$  value on its own.

This final value for  $r_1$  can now be used to determine  $a$  on other ensembles if values of  $r_1/a$  are available. We include in Table X the lattice spacing values on sets 1 to 5 from using  $r_1$ .

Our result for  $r_1$  can be compared to our previous result of 0.3133(23) fm on the MILC 2 + 1 flavor dynamical asqtad lattices [21]. This is 2% lower than our current result with a combined uncertainty of 1% and so is not significant. In principle the two results do not have to agree because we are now including  $c$  quarks in the sea. However we expect this to have a small effect and then only in short-distance quantities [14]. We can obtain estimates for the effect on the  $Y\ 2S - 1S$  splitting from the fact that it is proportional to the hyperfine splitting. Missing  $c$  quarks in the sea increases the  $Y$  mass by approximately 5 MeV with a smaller amount for excited states. It therefore reduces the  $2S - 1S$  splitting by approximately 2.5 MeV or 0.4%. This could have led previously to a 0.4% underestimate of  $r_1$  from the  $Y\ 2S - 1S$  splitting if  $r_1/a$  itself was not affected. This effect is no larger than other sources of systematic error in the earlier calculation [2] coming from radiative corrections to  $v^4$  terms that are also now included. Thus we cannot claim to see any strong evidence of an effect from  $c$  quarks in the sea. Indeed if we compare the  $r_1$  values coming from the  $Y$  analysis alone there is a change of 2(2)%, in which a 0.4% effect from  $c$  in the sea would be invisible. Any allowance for an effect on  $r_1$  itself, also a fairly short distance quantity, would reduce this expected variation further. The  $\eta_s$  analysis would be expected to be very insensitive to sea charm because of the low internal momenta inside these light hadrons. For that case we see only a 0.5% change in the value of  $r_1$  obtained, again with a 2% error.

## VI. $m_b/m_s$

From Table XII we can determine the ratio of the bare NRQCD  $b$  quark mass to the bare HISQ  $s$  quark mass on each ensemble. To do this we must use the same determination of the lattice spacing for the tuning of each mass, and so we use the lattice spacing determined from the  $Y\ 2S - 1S$  splitting (columns 2 and 3). The lattice spacing error appears doubled in  $m_s$  and once in  $m_b$  because of their different dependence on the meson masses used to fix them. These errors are correlated in the ratio  $m_b/m_s$  so one factor of the lattice spacing error cancels between numerator and denominator.

The ratio of masses in different schemes (NRQCD and HISQ) is not particularly useful. However, we can convert this using perturbation theory to a ratio of masses in the same mass-independent scheme, such as  $\overline{\text{MS}}$ , at the same scale,  $\mu$ . The ratio then becomes scale-independent and the same in any scheme related to  $\overline{\text{MS}}$  by a simple

renormalization. For both the NRQCD and the HISQ actions the mass renormalization is known to  $\mathcal{O}(\alpha_s)$ .

The lattice to  $\overline{\text{MS}}$  mass renormalization constant is calculated by multiplying the lattice bare mass to pole mass renormalization by the continuum pole mass to  $\overline{\text{MS}}$  renormalization. This latter renormalization is given by:

$$m_q^{\overline{\text{MS}}}(\mu) = m_{q,\text{pole}} \left( 1 + \alpha_s \left[ -\frac{4}{3\pi} - \frac{2}{\pi} \ln \frac{\mu}{m_{q,\text{pole}}} \right] + \dots \right). \quad (33)$$

The lattice bare mass to pole mass renormalization for HISQ quarks is given for small quark masses by [49–51]:

$$m_{s,\text{pole}} = \frac{am_s}{a} \left( 1 + \alpha_s \left[ -\frac{2}{\pi} \ln am_s + 0.5387 \right] \dots \right), \quad (34)$$

where we have written the equation explicitly for the strange quark mass. When Eqs. (33) and (34) are combined to obtain the conversion factor from the lattice bare mass to the  $\overline{\text{MS}}$  mass at scale  $\mu$  and  $\mathcal{O}(\alpha_s)$  the logarithm multiplying  $\alpha_s$  becomes  $\ln(a\mu)$ , and there is a constant given by  $0.5387 - 4/(3\pi)$ .

We can also write the NRQCD mass renormalization in the form

$$m_{b,\text{pole}} = \frac{am_b}{a} \left( 1 + \alpha_s \left[ -\frac{2}{\pi} \ln am_b + A^{\text{NRQCD}} \right] \dots \right). \quad (35)$$

although no  $\ln(am)$  term is explicit in that calculation. On doing this we find that the remainder term,  $A^{\text{NRQCD}}$  given in Table XXIII, has very little  $am_b$  dependence.

Combining Eqs. (33)–(35) it is then clear that the ratio of  $\overline{\text{MS}}$  masses for  $b$  and  $s$  is given to  $\mathcal{O}(\alpha_s)$  by:

$$\frac{m_b^{\overline{\text{MS}}}(\mu)}{m_s^{\overline{\text{MS}}}(\mu)} = \frac{am_b}{am_s} [1 + \alpha_s (A^{\text{NRQCD}} - 0.5387) + \dots] \quad (36)$$

where the  $\mu$  dependence cancels out. The ratio of bare lattice masses from columns 2 and 3 of Table XII varies very little with lattice spacing with values between 51 and 52. The renormalization in Eq. (36) is a relatively mild one, with  $\alpha_s$  coefficient varying between 0.31 and 0.39 with  $am_b$  value. We apply this one-loop renormalization with  $\alpha_s$  values taken as  $\alpha_V(1.8/a)$  from Table XXII. The energy scale for  $\alpha_s$  is then in agreement with the Brodsky-Lepage-Mackenzie scale calculated for the light quark (asqtad) mass renormalization in [49]. This gives the values for the  $\overline{\text{MS}}$   $m_b/m_s$  ratio plotted in Fig. 19.

The results in Fig. 19 show very little dependence on lattice spacing or sea quark mass within the 1% statistical and systematic errors from the lattice calculation. A much larger error is that from missing higher order powers of  $\alpha_s$  in Eq. (36). We take account of this error by allowing a correlated error between the points of  $1 \times \alpha_V(1.8/a)^2$

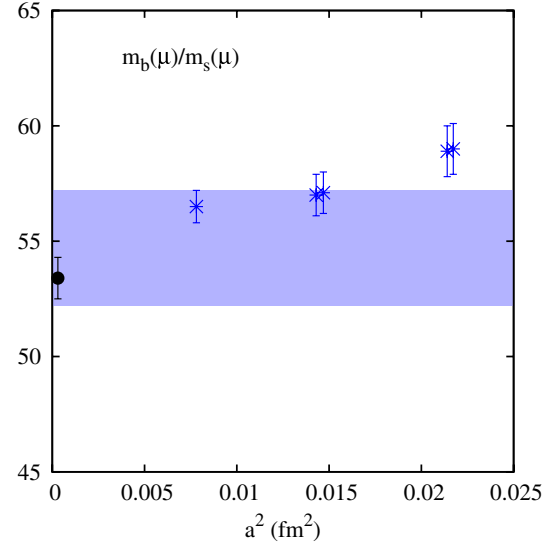


FIG. 19 (color online). Values for the ratio of the  $b$  quark mass to the  $s$  quark mass in the  $\overline{\text{MS}}$  scheme at a given scale plotted against the square of the lattice spacing. Results are obtained from combining NRQCD  $b$  quark masses and HISQ  $s$  quark masses with an  $\mathcal{O}(\alpha_s)$  perturbative renormalization. The errors on the points include statistical/fitting errors, lattice spacing errors and NRQCD systematic errors. The final result, including the  $\mathcal{O}(\alpha_s^2)$  perturbative error is plotted as the shaded blue band. The result from our previous fully nonperturbative calculation on ensembles including  $2 + 1$  flavors of sea quarks [52,53] is given by the black filled circle at  $a = 0$ .

along with a possible variation with  $am_b$  of the form  $\alpha_V(1.8/a)^2 \times \delta x_m/4$  (see Eq. (17) for a definition of  $\delta x_m$ ). This allows the  $\alpha_s^2$  term to have both a coefficient and a mass dependence which is 3 times that of the known  $\alpha_s$  term. We allow for possible dependence on sea quark masses and the lattice spacing by using a fit of the same form as that in Eq. (17). The final fit result is then:

$$\frac{m_b^{\overline{\text{MS}}}(\mu)}{m_s^{\overline{\text{MS}}}(\mu)} = 54.7(2.5), \quad (37)$$

plotted as the shaded blue band in Fig. 19. The error is dominated, not surprisingly, by the error from the unknown  $\alpha_s^2$  term.

We can compare this new result to a combination of our earlier results for  $m_b/m_c$  (4.51(4)) from [52] and  $m_c/m_s$  (11.85(16)) from [53]. These results were obtained entirely nonperturbatively by using the HISQ action for all the quarks. Then the ratio of lattice bare quark masses in the continuum limit is the ratio of  $\overline{\text{MS}}$  masses at a given scale—the renormalization factor cancels completely. From the numbers above we have  $m_b/m_s = 53.4(9)$  which is plotted as the black point at  $a = 0$  on Fig. 19. Our new, completely independent, result agrees well with this earlier value although it is much less accurate.



## VII. CONCLUSIONS

In this paper we have determined the  $Y$  spectrum using the NRQCD formalism for the  $b$  quarks in lattice QCD. We include several improvements over our earlier work. The key improvements are:

- (i) we use gluon field configurations with a fully  $\mathcal{O}(\alpha_s a^2)$  improved gluon action and HISQ quarks in the sea, provided by the MILC Collaboration;
- (ii)  $c$  quarks are now included in the sea;
- (iii) we take the NRQCD action to a new level of accuracy by including radiative corrections to the terms at next-to-leading relativistic order ( $v^4$ );
- (iv) we improve the method for tuning the  $b$  quark mass so that systematic errors are reduced to 0.5%.

With significantly improved systematic errors from NRQCD we are then able to determine the lattice spacing to better than 1% from the  $2S - 1S$  splitting. Using this we obtain  $M(h_b) - M(1\bar{S})$  to 1.4% and  $M(Y'') - M(Y)$  to 2.4% which is a strong test of NRQCD. This gives  $M(h_b) = 9905(7)$  MeV to be compared with the experimental result of 9898.3(1.5) MeV [39] and  $M(Y'') = 10375(22)$  MeV to be compared to the experimental result of 10355.2(5) MeV [35].

We have examined the  $Y$  and  $\eta_b$  dispersion relations in much more detail than before, so that we can quantify the effect of the radiative corrections to the  $v^4$  kinetic terms in the action. We are also able to show how small are the deviations from continuum rotational invariance. This enables us to tune the  $b$  quark mass to 0.5%.

Our result for the hyperfine splitting between the  $\Upsilon$  and  $\eta_b$  states is much more accurate than in our earlier work because we have included the critical renormalization of  $c_4$  (the coefficient of the  $\boldsymbol{\sigma} \cdot \mathbf{B}$  term) in our analysis. We obtain  $M(\Upsilon) - M(\eta_b) = 70(9)$  MeV now with a 13% error. This gives  $M(\eta_b)$  of 9390(9) MeV to be compared to the experimental result of 9390.9(2.8) MeV.

Our result for  $M(Y') - M(\eta'_b)$  is also much more accurate largely because of a huge improvement in the statistical error. We find a  $2S$  hyperfine splitting that is half as big as the  $1S$  hyperfine splitting at  $35(3)$  MeV, predicting  $M(\eta'_b) = 9988(3)$  MeV.

These new results are collected together in a plot of the  $\Upsilon$  spectrum from improved lattice NRQCD in Fig. 20. We mark with different symbols those results used to tune parameters, those which correspond to masses already known from experiment, and those (the  $\eta'_b$ ) which are predictions. We include the  $P$ -wave fine structure from our results for  $c_4 = 1.15$  on the fine lattices, set 5, since this  $c_4$  is close to the perturbative value on those lattices. We include an additional 10% error for missing  $v^6$  terms in our NRQCD action.  $D$ -wave  $\Upsilon$  masses from our calculation will be reported elsewhere.

Light meson ( $\pi$ ,  $K$  and  $\eta_s$ ) masses and decay constants are also given here that enable us to determine the

properties of the  $\eta_s$  meson and give a complementary determination of the lattice spacing to better than 1%. The calculation shows significantly improved discretization errors over our earlier results on ensembles including  $2 + 1$  flavors of asqtad quarks [21]. The results on the properties of the  $\eta_s$  are in agreement with our earlier work. However, our earlier result was not able to distinguish the mass and decay constant of the  $\eta_s$  from that would be obtained in leading order chiral perturbation theory. We now obtain  $M(\eta_s) = 0.6893(12)$  GeV and  $f_{\eta_s} = 0.1819(5)$  GeV. In both cases these values disagree significantly, but by less than 1%, from the leading order expectation. The  $\eta_s$  particle is relatively insensitive to sea  $u/d$  quark masses and so it is very useful to have accurate results for its properties for tuning the  $s$  quark mass and determining the lattice spacing on other lattice ensembles.

The  $Y\ 2S - 1S$  and  $\eta_s$  determinations of the lattice spacing can be compared through a third parameter,  $r_1$ , from the heavy quark potential. We show that both determinations agree in the continuum and chiral limits and give a physical value for  $r_1$  of 0.3209(26) fm. This can also be used to determine the lattice spacing on other lattice ensembles.

We also combine  $\Upsilon$  and  $\eta_s$  calculations through a determination of the ratio of  $\overline{\text{MS}}$   $b$  quark to  $s$  quark masses of  $m_b/m_s = 54.7(2.5)$ , in agreement with our earlier result from HISQ quarks alone of  $53.4(9)$  [52,53].

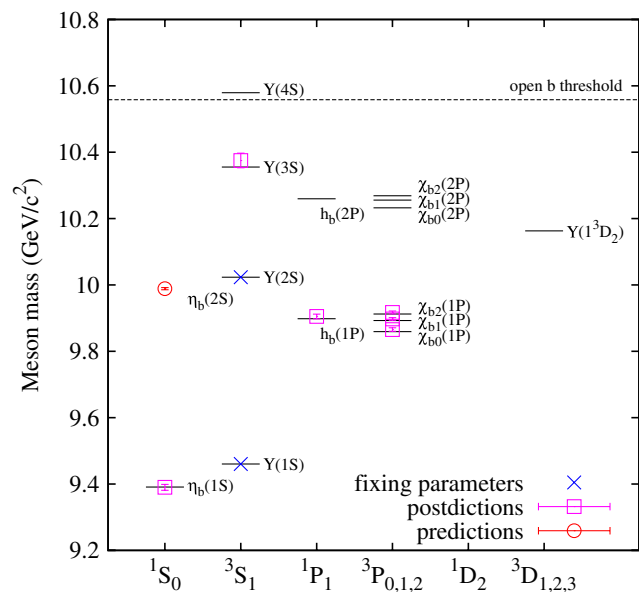


FIG. 20 (color online). The spectrum of bottomonium states from lattice NRQCD (colored symbols with error bars) compared to experiment (black lines). Blue crosses denote results used to tune parameters, pink open squares results to be compared to experiment and red circles predictions ahead of experiment. For simplicity we mark the  $\Upsilon$  with a blue cross although in fact we use the spin average of  $\Upsilon$  and  $\eta_b$  to tune the  $b$  quark mass.

Finally we comment on the effect of including  $c$  quarks in the sea. We have seen no significant effect on any of the observables that we have calculated compared to results obtained with  $2 + 1$  flavors of sea quarks. The results cannot be compared lattice spacing by lattice spacing because of changes to the lattice QCD action that reduce the size of discretization errors in our new results. Final physical results can be compared, however, with and without sea  $c$  quarks to see if there is a difference. In our earlier  $2 + 1$  flavor calculations [14] we estimated that the presence of sea  $c$  quarks would shift the  $Y$  and  $\eta_b$  masses downwards by 5 MeV through an induced additional local potential which was proportional to  $\alpha_s^2 \delta^3(r)/m_c^2$ . This would have a smaller effect on radial excitations of the  $Y$  than on the ground state masses and very little effect on  $P$ -wave states. We then estimate the effect on, for example, the  $Y$   $1P - 1S$  splitting to be  $\mathcal{O}(1\%)$ . This would barely be visible above the errors in our current calculation and the errors in the earlier calculation were somewhat larger, so any comparison certainly has an error of greater than 1%. However, it is clear from our results that no unexpectedly large effect has appeared. For light hadrons we expect even smaller effects and there we can limit any differences in  $M_{\eta_s}$  and  $f_{\eta_s}$  to smaller than 1%, with the main error coming from our earlier calculation [21].

We are now combining  $b$  quark propagators from our improved NRQCD action with  $l$ ,  $s$  and  $c$  propagators on these ensembles to study  $B$ ,  $B_s$  and  $B_c$  meson masses and matrix elements. Significantly improved systematic errors should be possible both from the NRQCD action and because we are working much closer to physical light sea quark masses than before with an improved gluon and sea quark action.

## ACKNOWLEDGMENTS

We are grateful to the MILC Collaboration for the use of their gauge configurations and particularly to D. Toussaint for help in reading them and in providing values for  $r_1/a$ . The results described here were obtained using the Darwin Supercomputer of the University of Cambridge High Performance Computing Service as part of the DiRAC facility jointly funded by STFC, the Large Facilities Capital Fund of BIS and the Universities of Cambridge and Glasgow. This work was funded by STFC, MICINN, DGIID-DGA and NSF with support from the Scottish Universities Physics Alliance and the EU under ITN-STRONGnet.

## APPENDIX A: GAUGE ACTION

For clarity, the gauge action  $S_G$  used in the generation of the MILC ensembles will be summarized in this section. See [19]. The action is a tadpole and one-loop improved Lüscher-Weisz action,

$$S_G = \beta \left[ c_P \sum_P \left( 1 - \frac{1}{3} \text{Re Tr}(P) \right) + c_R \sum_R \left( 1 - \frac{1}{3} \text{Re Tr}(R) \right) + c_T \sum_T \left( 1 - \frac{1}{3} \text{Re Tr}(T) \right) \right], \quad (\text{A1})$$

where the sums are over plaquettes  $P$ , rectangles  $R$  and twisted loops (or parallelograms)  $T$ . The coefficients are calculated perturbatively through  $\mathcal{O}(\alpha_s)$  including both gluonic loops [54] and contributions from HISQ sea quarks [20]. The tadpole improvement parameter was chosen to be the fourth root of the plaquette  $u_{0P} = \left( \frac{1}{3} \text{Re Tr}(P) \right)^{1/4}$  and, via a perturbative calculation of the plaquette, gives an expression for the strong coupling constant  $\alpha_s = -1.303615 \log u_{0P}$ .  $u_{0P}$  also appears in the gauge coupling as  $\beta = 10/(g^2 u_{0P}^4)$ . The coefficients used are

$$\begin{aligned} C_P &= 1.0 \\ C_R &= \frac{-1}{20u_{0P}^2} (1 - (0.6264 - 1.1746N_f) \log(u_{0P}^2)) \\ C_T &= \frac{1}{u_{0P}^2} (0.0433 - 0.0156N_f) \log(u_{0P}^2). \end{aligned} \quad (\text{A2})$$

The inclusion of these terms mean that the gauge action is improved completely through order  $\mathcal{O}(\alpha_s a^2)$ . As mentioned in the text, sea quarks are included using the HISQ action [16] with a  $U(3)$  projection (only) for the intermediate re-unitarization step.

## APPENDIX B: PERTURBATIVE DETERMINATION OF RADIATIVE CORRECTIONS TO $c_i$ COEFFICIENTS IN THE NRQCD ACTION AND THE MASS RENORMALIZATION

*Spin-independent coefficients.* The  $c_i$  coefficients appearing in the NRQCD action, Eq. (2), have expansion  $1 + c_i^{(1)} \alpha_s + \mathcal{O}(\alpha_s^2)$ . The  $c_i^{(1)}$  for the kinetic terms,  $i = 1, 5, 6$ , are determined following the method of [26,55]. The NRQCD quark self-energy is calculated through  $\mathcal{O}(\alpha_s)$  and the  $c_i^{(1)}$  are given by the requirement that the correct energy-momentum relationship be obtained through  $\mathcal{O}(\alpha_s v^4)$ . The terms proportional to  $(\Delta^{(2)})^2$  in Eq. (2) can be merged together so that this term in  $\delta H$  appears as

$$\tilde{c}_1 \left( 1 + \frac{am_b}{2n} \right) \frac{(\Delta^{(2)})^2}{8(am_b)^3}. \quad (\text{B1})$$

Thus only two radiative corrections need to be calculated for the complete set of kinetic terms at  $\mathcal{O}(v^4)$ , i.e. for  $\tilde{c}_1$  and  $c_5$ . The radiative correction for  $\tilde{c}_1$  then applies equally to  $c_1$  and  $c_6$ .

The full inverse NRQCD quark propagator at  $\mathcal{O}(\alpha_s)$  is

$$aG^{-1}(p) = Q^{-1}(p) - \alpha_s a\Sigma(p), \quad (\text{B2})$$

where  $ap = (a\mathbf{p}, ap_4)$  is a 4-vector in lattice Euclidean space. The pole in the propagator is identified as  $a\omega(\mathbf{p}) = ip_4 a$ . The expansion of  $\omega(\mathbf{p})$  in powers of the spatial momentum can be used to identify the quark mass renormalization factor  $Z_m$  and wave-function renormalization factor  $Z_2$  but also to tune  $\tilde{c}_1^{(1)}$  and  $c_5^{(1)}$  to appropriate values.  $Q^{-1}(p)$  is the quark propagator obtained at tree level from the NRQCD action, including the (as yet unknown) radiative corrections to  $\tilde{c}_1$  and  $c_5$ . Its pole is then given by:

$$a\omega_0(p) = \frac{a^2\mathbf{p}^2}{2am_b} - \frac{(a^2\mathbf{p}^2)^2}{8(am_b)^3} + \alpha_s \left\{ c_5^{(1)} \frac{a^4\mathbf{p}^4}{24am_b} - \tilde{c}_1^{(1)} \left( \frac{1}{2n} + \frac{1}{am_b} \right) \frac{(a^2\mathbf{p}^2)^2}{8(am_b)^3} \right\}. \quad (\text{B3})$$

$\Sigma(p)$  is the one-loop self-energy and consists, as shown in Fig. 21, of rainbow and tadpole diagrams as well as diagrams containing insertions of the one-loop piece of the tadpole-improvement factor,  $u_0$ . Writing  $u_0 = 1 + \alpha_s u_0^{(1)}$ , we have  $u_0^{(1)} = 0.750$  for the Landau link tadpole parameter,  $u_{0L}$  [56]. We have

$$\omega(\mathbf{p}) = \omega_0(\mathbf{p}) - \alpha_s \Sigma(\omega_0(\mathbf{p}), \mathbf{p}) \quad (\text{B4})$$

and can expand  $\Sigma$  to  $v^4$  as

$$a\Sigma(p) = \Sigma_0(\omega) + \Sigma_1(\omega) \frac{a^2\mathbf{p}^2}{2am_b} + \Sigma_2(\omega) \frac{(a^2\mathbf{p}^2)^2}{8(am_b)^3} + \Sigma_3(\omega) a^4\mathbf{p}^4. \quad (\text{B5})$$

The  $\Sigma_i$  are extracted from suitable combinations of partial derivatives of  $\Sigma$ :

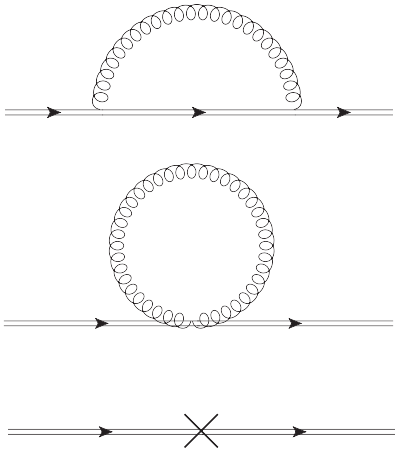


FIG. 21. The Feynman diagrams needed for the calculation of  $\mathcal{O}(\alpha_s)$  corrections to the heavy quark self-energy. From top to bottom, rainbow, tadpole and  $u_0$  counterterm diagrams.

$$\begin{aligned} \Sigma_0 &= a\Sigma(\mathbf{p}=0) & \Sigma_1 &= am_b \left. \frac{\partial^2 a\Sigma}{\partial a^2 p_z^2} \right|_{\mathbf{p}=0} \\ \Sigma_2 &= (am_b)^3 \left. \frac{\partial^4 a\Sigma}{\partial a^2 p_z^2 \partial a^2 p_y^2} \right|_{\mathbf{p}=0} & (\text{B6}) \\ \Sigma_3 &= \frac{1}{24} \left( \frac{\partial^4 a\Sigma}{\partial a^4 p_z^4} - 3 \frac{\partial^4 \Sigma}{\partial a^2 p_y^2 \partial a^2 p_z^2} \right)_{\mathbf{p}=0}. \end{aligned}$$

Each of the  $\Sigma_i$  also has an expansion in powers of  $\omega$  as  $\Sigma_i = \Sigma_{i=0}^\infty \Sigma_i^{(l)} \omega^l$ . Then

$$a\omega(\mathbf{p}) = \frac{a^2\mathbf{p}^2}{2am_{b,r}} - \frac{(a^2\mathbf{p}^2)^2}{8(am_{b,r})^3} - \alpha_s a\delta\omega(\mathbf{p}), \quad (\text{B7})$$

where  $m_{b,r} = Z_m m_b$  and

$$Z_m = 1 + \alpha_s Z_m^{(1)} = 1 + \alpha_s (\Sigma_0^{(1)} + \Sigma_1^{(0)}) \quad (\text{B8})$$

to this order. The correction term  $\delta\omega$  is given by:

$$\begin{aligned} a\delta\omega &= W_0 + \left( W_1 + \tilde{c}_1^{(1)} \left( \frac{1}{2n} + \frac{1}{am_b} \right) \right) \frac{(a^2\mathbf{p}^2)^2}{8(am_b)^3} \\ &+ \left( W_2 - \frac{c_5^{(1)}}{24am_b} \right) a^4\mathbf{p}^4, \end{aligned} \quad (\text{B9})$$

with

$$\begin{aligned} W_0 &= \Sigma_0^{(0)} \\ W_1 &= \frac{2\Sigma_0^{(1)}}{am_b} + 2\Sigma_0^{(2)} + \frac{3\Sigma_1^{(0)}}{am_b} + 2\Sigma_1^{(1)} + \Sigma_2^{(0)} \\ W_2 &= \Sigma_3^{(0)}. \end{aligned} \quad (\text{B10})$$

The requirement that lattice NRQCD reproduce the low-energy physics of full QCD means that  $\delta\omega$  can only be a pure energy shift independent of spatial momentum, i.e. the coefficients of  $(\mathbf{p}^2)^2$  and  $\mathbf{p}^4$  in Eq. (B10) must be zero. Thus

$$\tilde{c}_1^{(1)} = -\left( \frac{1}{2n} + \frac{1}{am_b} \right)^{-1} W_1 \quad c_5^{(1)} = 24am_b W_2. \quad (\text{B11})$$

The Feynman rules were generated automatically using the HIPPY package and the Feynman lattice integrals for  $\Sigma$  and its derivatives were constructed and evaluated numerically using the HPSRC package and VEGAS contained therein [57,58]. We use analytic differentiation using the TAYLUR package in the HPSRC Fortran code together with numerical differentiation which, for sufficiently smooth functions, can be up to an order of magnitude faster than analytic differentiation.

Because the kinetic  $(a^2\mathbf{p}^2)^2$  term is included at tree level both  $W_1$  and  $W_2$  are infrared (IR) finite and so no IR regulation is needed although a gluon mass was used to regularize intermediate divergences. However, the integrals arising from the rainbow diagram still have large

peaks in the IR region. These peaks arise because the differentiation generates extra powers of the heavy quark NRQCD propagator in the integrand. In this case to use numerical differentiation alone proves to be unstable and it is imperative to use a mixture of analytic and numerical approaches and also to introduce a suitable subtraction function to remove the most severe behavior of the integrand. In contrast, the integrals arising from the tadpole diagram are well behaved because they contain no quark propagators but they are expensive to evaluate since the two-gluon vertex contains a large number of terms. In this case, numerical differentiation proved to be the most efficient for the higher order mixed derivatives without compromising accuracy. In all cases the temporal derivatives were done using the analytic method.

We checked that the results agree well with those of Morningstar [26,55] for his gluon and NRQCD actions. For the simplest gluon and NRQCD actions the results agree with the analytic calculation of Monahan [59].

The contribution to the  $c_i^{(1)}$  from the  $u_0^{(1)}$  insertions of Fig. 21 can be calculated analytically. This gives:

$$\begin{aligned} \frac{\tilde{c}_1^{(1)}}{u_0^{(1)}} &= -\frac{1}{8} \left(1 + \frac{am_b}{2n}\right)^{-1} \left[ \frac{12}{n^2} - \frac{1}{n} + \frac{1}{2am_b} \left( \frac{3}{n^2} - 4 \right) \right. \\ &\quad \left. + \frac{6}{(am_b)^2} \left( \frac{1}{n} - 12 \right) + \frac{6}{(am_b)^3} \right] \frac{c_5^{(1)}}{u_0^{(1)}} \\ &= -\frac{4}{3} + \frac{1}{4am_b} + \frac{3}{(am_b)^2} - \frac{3}{8n(am_b)^2} - \frac{3}{4(am_b)^3}. \end{aligned} \quad (\text{B12})$$

These contributions are sizeable and act to cancel contributions coming from the other diagrams, as part of the “tadpole-improvement” mechanism [5,26]. This is particularly true for  $c_5^{(1)}$ ; less so for  $\tilde{c}_1^{(1)}$ , as in [26]. The  $c_i^{(1)}$  values will then change depending on the tadpole-improvement parameter chosen, for example  $u_{0P}$  or  $u_{0L}$ , because the  $c_i$  must compensate perturbatively for changes in  $u_0$ . Here we use  $u_{0L}$  in the NRQCD action and this is the only  $u_0$  that affects the  $c_i$  to  $\mathcal{O}(\alpha_s)$ .  $u_{0P}$  is used in the gluon action and counterterms from this will appear in the  $c_i$  at higher order.

Table XXI gives the results for  $\tilde{c}_1^{(1)}$  and  $c_5^{(1)}$  for 3 different values of  $am_b$  and stability parameter  $n = 4$ . The mass

TABLE XXI. Coefficients  $\tilde{c}_1^{(1)}$  and  $c_5^{(1)}$  that multiply  $\alpha_s$  in the one-loop correction to the kinetic terms in the NRQCD action used here in conjunction with the improved gluon action described in Appendix A.

$am_b$	n	$\tilde{c}_1^{(1)}$	$c_5^{(1)}$
1.95	4	0.774(21)	0.392(17)
2.8	4	0.951(26)	0.406(11)
3.4	4	0.952(30)	0.445(10)

values are not exactly the  $am_b$  values used for the numerical work in this paper but the  $c_i^{(1)}$  show very mild dependence on  $am_b$ , so we can simply interpolate to the  $am_b$  values we are using. The results are different from those of [26] because both the gluon action and the NRQCD action have changed. However, qualitative features are the same in that the values are not large and only mild dependence on  $am_b$  is seen for  $am_b$  larger than 1. We note that the  $c_i^{(1)}$  coefficients will change if higher order terms are added to the NRQCD action. For example [27] tests were done with an NRQCD action which included a term in  $\delta H$  of  $-\Delta^{(6)}/(180am_b)$ , removing  $\mathcal{O}(a^6)$  discretization errors from  $H_0$ . This changes  $c_5^{(1)}$  to 0.017(4) for  $am_b = 1.95$  and  $n = 4$  to be compared with the result of 0.392(17) in Table XXI.

The coefficients in Table XXI need to be combined with a value for  $\alpha_s$  to give final results for  $c_1$ ,  $c_5$  and  $c_6$ . The scale,  $q^*$ , used for  $\alpha_s$  was taken as that calculated for the Brodsky-Lepage-Mackenzie scheme in Fig. 10 of [26], assuming that this does not change significantly with the changes in the action used. This gives  $q^* \approx 1.4/a$  for  $c_5$  and  $q^* \approx 1.8/a$  for  $\tilde{c}_1$ . We take  $\alpha_s$  from [52], specifically the value  $\alpha_{\overline{\text{MS}}}(M_z, n_f = 5) = 0.1183$ . We convert this to  $\alpha_V$  [60] and run perturbatively to values using  $n_f = 4$  and appropriate scales  $q^*$ . The  $q^*$  values are calculated for the very coarse, coarse and fine ensembles using  $a^{-1} \approx 1.3, 1.6$  and  $2.2$  GeV, respectively, from Table X. The  $\alpha_V$  values obtained are listed in Table XXII. These are combined with the coefficients in Table XXI to give the values used in Table II. The coefficient  $\tilde{c}_1^{(1)}$  was reduced slightly on the fine lattices (to 0.766) to account for the fact that the value

TABLE XXII. Values for  $\alpha_V$  used in calculating the  $\mathcal{O}(\alpha_s)$ -corrected coefficients  $c_1$ ,  $c_5$ ,  $c_6$  and  $c_4$ .

Sets	$1/a$ GeV	$\alpha_V^{(4)}(1.4/a)$	$\alpha_V^{(4)}(1.8/a)$	$\alpha_V^{(4)}(\pi/a)$
Fine	2.2	0.32	0.28	0.225
Coarse	1.6	0.39	0.33	0.255
Very coarse	1.3	0.46	0.38	0.275

TABLE XXIII. Coefficients  $Z_m^{(1)}$  and  $c_4^{(1)}$  that multiply  $\alpha_s$  in the one-loop correction to the mass renormalization and the  $\sigma \cdot \mathbf{B}$  term in the NRQCD action, respectively. These are calculated with the NRQCD action used here and the improved gluon action described in Appendix A.  $A^{\text{NRQCD}}$  in column 4 is  $Z_m^{(1)} + 2 \ln(am_b)/\pi$ , as described in the text.

$am_b$	n	$Z_m^{(1)}$	$A^{\text{NRQCD}}$	$c_4^{(1)}$
1.9	4	0.439(3)	0.848(3)	0.691(7)
2.65	4	0.263(5)	0.883(5)	0.775(8)
3.4	4	0.150(3)	0.929(3)	0.818(4)



of  $am_b$  used was slightly smaller than that for which the coefficient was calculated.

The remaining errors in the kinetic  $c_i$  coefficients after this one-loop correction has been made will be  $\mathcal{O}(\alpha_s^2)$ . From Table XXII we can see that  $0.5\alpha_s^2$  ranges from 0.1 on the very coarse ensembles to 0.05 on fine. The impact of these errors can then be estimated from the size of the effect that we see on physical observables from the  $\mathcal{O}(\alpha_s)$  corrections.

We have not corrected the coefficient of the Darwin term,  $c_2$ , in our NRQCD Hamiltonian. We have however assessed the effect of taking  $c_2$  to be as large as 1.25 on the meson kinetic mass and on the hyperfine splitting and we find the effects to be small.

*Mass renormalization.* In Table XXIII we give values for  $Z_m^{(1)}$ , the coefficient of  $\alpha_s$  in the mass renormalization of Eq. (B8).  $Z_m$  was calculated previously for different parameter values in [61]. We also show the result of adding  $2\ln(am_b)/\pi$  to  $Z_m^{(1)}$  as  $A^{\text{NRQCD}}$ .  $A^{\text{NRQCD}}$  will be used in Sec. VI to derive the ratio  $m_b/m_s$  in the  $\overline{\text{MS}}$  scheme. Only mild dependence on  $am_b$  is seen in  $A^{\text{NRQCD}}$ .

*Spin-dependent terms.* The perturbative renormalization of field-dependent terms has to be done in a different way and this includes all the spin-dependent terms. Recently the radiative corrections to  $c_4$  have become available [28]. They were calculated by matching the effective action in NRQCD to continuum QCD using the background field method. We give values for  $c_4^{(1)}$  in Table XXIII appropriate to the  $am_b$  and  $n$  values we are using here.

A number of pieces go in to the calculation of  $c_4^{(1)}$ . These include renormalization of the chromomagnetic moment, renormalization of the wave function and, because  $c_4$  multiplies a term in the bare lattice NRQCD Hamiltonian which includes the bare lattice quark mass, the mass renormalization.  $c_4^{(1)}$  is the sum of two pieces, one of which has polynomial dependence on the bare quark mass  $am_b$  and the other is proportional to  $\ln(am_b)$ . The logarithmic term has coefficient  $-3/(2\pi)$  [28]. Both terms are included in the total result given in Table XXIII—the logarithmic term is of similar size to the polynomial term over the range of  $am_b$  that we are using. The  $c_4^{(1)}$  values are combined with values for  $\alpha_s^{(4)}(\pi/a)$  (given in Table XXII) to give the results for the 1-loop corrected  $c_4$  coefficients given in Table XIII.

Figure 22 gives a more complete picture of  $c_4^{(1)}$  by plotting values as a function of  $am_b$ . We see relatively little  $am_b$  dependence until  $am_b$  becomes smaller than 1 when  $c_4^{(1)}$  starts to diverge. This is typical of the behavior of radiative corrections to coefficients in the NRQCD action.

Finally we give results for the coefficients of the spin-dependent 4-quark operators that contribute to the hyperfine splitting. These terms have coefficients  $d_1$  and  $d_2$  that multiply terms that would appear in the NRQCD action at order  $\mathcal{O}(\alpha_s^2 v^3)$ :

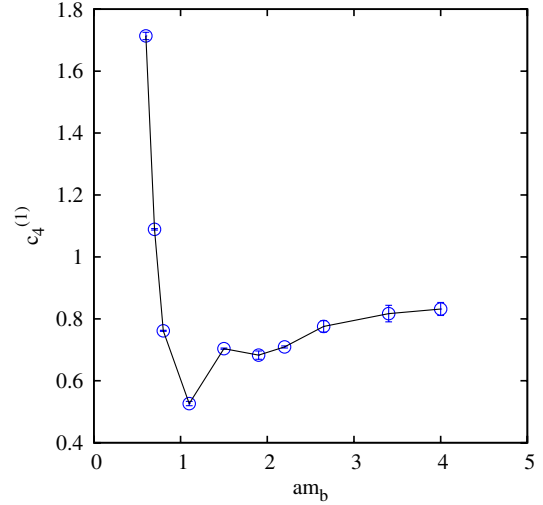


FIG. 22 (color online). The  $\mathcal{O}(\alpha_s)$  coefficient in the perturbative expansion of  $c_4$ , coefficient of the  $\sigma \cdot \mathbf{B}$  term, plotted against the bare  $b$  quark mass.

$$S_{4q} = d_1 \frac{\alpha_s^2}{(am_b)^2} (\psi^\dagger \chi^*) (\chi^T \psi) + d_2 \frac{\alpha_s^2}{(am_b)^2} (\psi^\dagger \sigma \chi^*) \cdot (\chi^T \sigma \psi). \quad (\text{B13})$$

These terms are subleading compared to tree-level  $v^4$  operators but contribute to the hyperfine splitting at the same order as  $\alpha_s$  corrections to  $c_4$  [28]. We do not include these 4-quark terms in our NRQCD action but we can estimate their effect because they give rise a shift in the relative energies of the  $\Upsilon$  and  $\eta_b$  which is proportional to the “wave-function-at-the-origin”, and given by:

$$\Delta E_{\text{hyp}} = \frac{6\alpha_s^2(d_2 - d_1)}{m_b^2} |\psi(0)|^2. \quad (\text{B14})$$

The relevant coefficients,  $d_1$  and  $d_2$  are given in Table XXIV. They were calculated previously for a slightly different NRQCD action in [28]. The coefficients are related by:

$$d_1 = -3d_2 - \frac{4}{9}(1 - \ln(2)), \quad (\text{B15})$$

where the term proportional to  $(\ln 2 - 1)$  is from  $\eta_b$  annihilation to 2 gluons. This term increases the hyperfine

TABLE XXIV. Coefficients  $d_1$  and  $d_2$  of spin-dependent 4-quark operators that give rise to a correction to the hyperfine splitting. These are calculated with the NRQCD action used here with the parameters given in columns 1 and 2 and the improved gluon action described in Appendix A.

$am_b$	$n$	$d_1$	$d_2$
1.9	4	$-\ln(1.9) + 0.796(4)$	$\ln(1.9)/3 - 0.311(1)$
2.65	4	$-\ln(2.65) + 0.448(6)$	$\ln(2.65)/3 - 0.195(2)$
3.4	4	$-\ln(3.4) + 0.038(8)$	$\ln(3.4)/3 - 0.058(2)$

splitting from Eq. (B14) since it pushes the  $\eta_b$  mass down. When Eq. (B14) is applied for just this piece we obtain an estimate of its size of about 1 MeV. This is smaller, but in agreement with, the earlier estimate of 2.4(2.4) MeV applied in Sec. III C in deriving an appropriate spin-averaged  $1S$  meson mass to tune the  $b$  quark mass against. For that purpose the shift is completely negligible, representing a tiny fraction of the  $\eta_b$  mass. For the hyperfine splitting it is a more important issue. For this we take the results from Eq. (B14) because that provides a consistent treatment of all the 4-quark operator effects.

$d_1$  and  $d_2$  are separated into logarithmic and nonlogarithmic pieces in Table XXIV. The nonlogarithmic piece has significant mass dependence here, becoming small at large  $ma$ . The logarithmic and nonlogarithmic terms in fact cancel for  $ma$  around 1.9. In assessing the error in the hyperfine splitting from missing higher order terms multiplying the 4-quark operators we are careful not to assume that this is generic behavior.

We combine the  $d_1$  and  $d_2$  coefficients with  $\alpha_V(\pi/a)$  values from Table XXII and values for  $|\psi(0)|^2$  from our fits to obtain corrections to the hyperfine splitting that are applied in Sec. III E 3.

### APPENDIX C: NONPERTURBATIVE DETERMINATION OF RADIATIVE CORRECTIONS TO $c_3$ AND $c_4$ COEFFICIENTS IN THE NRQCD ACTION

An alternative approach to tuning the spin-dependent coefficients  $c_3$  and  $c_4$  is from matching fine structure in the spectrum to experiment. Here we use the  $P$ -wave fine structure in the  $Y$  spectrum to do this [2,12]. The  $P$ -wave masses are shifted from the spin average by amounts that depend on spin-spin coupling terms proportional to  $\mathbf{S} \cdot \mathbf{S}$  or  $S_{ij}$  and spin-orbit terms proportional to  $\mathbf{L} \cdot \mathbf{S}$ . The spin-spin terms are proportional to  $c_4^2$  and the spin-orbit terms to  $c_3$ . We can make a combinations of the  $^3P$  state masses in which the eigenvalues of  $S_{ij}$  and  $\mathbf{S} \cdot \mathbf{S}$  cancel, and a separate combination in which the eigenvalues of  $\mathbf{S} \cdot \mathbf{S}$  and  $\mathbf{L} \cdot \mathbf{S}$  cancel. Thus each of these combinations gives a result which should depend on only one of the spin-dependent couplings in our current NRQCD action. Comparing these combinations to experiment allows us to tune  $c_3$  and  $c_4$ . Note that 4-quark operators, discussed in Appendix B with reference to their effect on  $S$ -wave hyperfine splittings, have negligible effect on  $P$ -wave states, and they therefore give a very clean determination of  $c_3$  and  $c_4$ .

The eigenvalues for  $\mathbf{L} \cdot \mathbf{S}$ ,  $S_{ij}$  and  $\mathbf{S} \cdot \mathbf{S}$  for  $^{2S+1}L_J$  states  $\{^3P_0, ^3P_1, ^3P_2, ^1P_1\}$  (i.e.  $\{\chi_{b0}, \chi_{b1}, \chi_{b2}, h_b\}$ ) are

$$\begin{aligned} \mathbf{L} \cdot \mathbf{S}: & \{-2, -1, 1, 0\}; & S_{ij}: & \{-4, 2, -2/5, 0\}; \\ \mathbf{S} \cdot \mathbf{S}: & \{1/4, 1/4, 1/4, -3/4\}. \end{aligned} \quad (C1)$$

We see that the  $\mathbf{S} \cdot \mathbf{S}$  terms affect the splitting between the  $^1P_1$  and the spin average of the  $^3P$  states. We expect this

splitting to be small because, in a potential model approach, the accompanying spin-dependent potential would be a delta function at the origin with very little overlap for  $P$ -wave states. Both  $S_{ij}$  and  $\mathbf{L} \cdot \mathbf{S}$  terms affect the splittings within the  $^3P$  sector but not the splitting between  $^1P_1$  and  $^3P$ . The  $\mathbf{L} \cdot \mathbf{S}$  terms give the conventional ordering of  $^3P_0$ ,  $^3P_1$  and  $^3P_2$ , but with the  $^3P_2$  splitting from the  $^3P_1$  larger than that between the  $^3P_1$  and  $^3P_0$ . The  $S_{ij}$  terms will push down the  $^3P_2$  relative to the others. Thus the final splittings depend on the relative strength of the accompanying potentials for these terms and, in NRQCD language, the coefficients  $c_3$  and  $c_4$ .

The combination of spin-splittings that depends on  $c_4^2$  (through  $S_{ij}$ ) and is independent of  $c_3$  is [2]

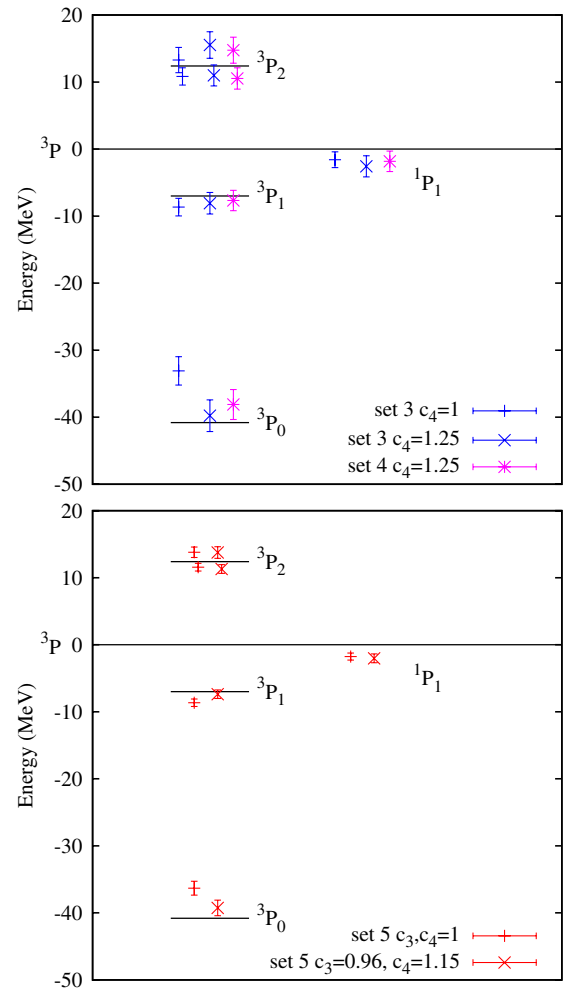


FIG. 23 (color online). The masses of the lowest-lying  $P$ -wave states in the  $Y$  spectrum plotted relative to the spin average of the  $^3P$  states for the coarse lattices, sets 3 and 4 (top plot) and the fine lattices, set 5 (lower plot). In each plot we compare mass splittings for  $c_4 = 1$  with a nonperturbatively tuned value for  $c_4$  chosen to match a combination of mass splittings to experiment (see text).  $c_3 = 1$  in all cases. For the  $^3P_2$  states the  $^3P_E$  is plotted to the left of the  $^3P_T$ .

TABLE XXV. Fitted energies for  $P$ -wave states on sets 3, 4 and 5 for the NRQCD parameters given. The last two rows give the combination of energies used to determine  $c_3$  and  $c_4$ . Errors are from statistics/fitting only.

	Set 3	Set 3	Set 4	Set 5	Set 5
	$am_b = 2.66$	$am_b = 2.66$	$am_b = 2.62$	$am_b = 1.91$	$am_b = 1.91$
	$c_4 = 1.0$	$c_4 = 1.25$	$c_4 = 1.25$	$c_4 = 1.0$	$c_4 = 1.15$
	$c_3 = 1.0$	$c_3 = 1.0$	$c_3 = 1.0$	$c_3 = 1.0$	$c_3 = 0.96$
$aE(1^1P_1)$	0.5655(23)	0.5247(22)	0.5253(20)	0.4833(10)	0.4478(11)
$aE(1^3P_0)$	0.5460(20)	0.5017(20)	0.5034(18)	0.4678(9)	0.4312(9)
$aE(1^3P_1)$	0.5611(24)	0.5213(26)	0.5218(24)	0.4802(10)	0.4454(11)
$aE(1^3P_E)$	0.5747(30)	0.5359(28)	0.5354(25)	0.4903(11)	0.4549(12)
$aE(1^3P_{T_2})$	0.5732(28)	0.5331(28)	0.5328(27)	0.4893(11)	0.4538(12)
$aE(1^1P_1) - aE(^3\bar{P})$	-0.0010(7)	-0.0016(10)	-0.0011(9)	-0.0008(2)	-0.0009(2)
$aE(1^3P_0) - aE(^3\bar{P})$	-0.0204(13)	-0.0246(14)	-0.0231(13)	-0.0163(4)	-0.0176(5)
$aE(1^3P_1) - aE(^3\bar{P})$	-0.0053(8)	-0.0050(10)	-0.0046(9)	-0.0039(2)	-0.0033(3)
$aE(1^3P_E) - aE(^3\bar{P})$	0.0082(12)	0.0096(12)	0.0089(11)	0.0062(3)	0.0062(4)
$aE(1^3P_{T_2}) - aE(^3\bar{P})$	0.0067(8)	0.0068(10)	0.0064(10)	0.0052(3)	0.0051(3)
$2aE(1^3P_2E) + 3aE(1^3P_2T_2)$	0.093(8)	0.104(9)	0.097(8)	0.072(3)	0.073(3)
$-3aE(1^3P_1) - 2aE(1^3P_0)$					
$0.4aE(1^3P_2E) + 0.6aE(1^3P_2T_2)$	-0.018(2)	-0.026(4)	-0.025(3)	-0.0153(7)	-0.0198(9)
$-3aE(1^3P_1) + 2aE(1^3P_0)$					

TABLE XXVI. Combinations of  $P$ -wave energies needed to fix  $c_3$  and  $c_4$  in GeV. Lattice spacing values are taken from Table X. Errors are statistical/fitting only.

	3	3	4	5	5
	$c_4 = 1$	$c_4 = 1.25$	$c_4 = 1.25$	$c_4 = 1$	$c_4 = 1.15$
	$c_3 = 1.0$	$c_3 = 1.0$	$c_3 = 1.0$	$c_3 = 1.0$	$c_3 = 0.96$
$5E(1^3P_2) - 3E(1^3P_1) - 2E(1^3P_0)$	0.151(13)	0.168(14)	0.160(13)	0.161(6)	0.162(7)
$E(1^3P_2) - 3E(1^3P_1) + 2E(1^3P_0)$	-0.028(4)	-0.042(6)	-0.041(5)	-0.0342(16)	-0.0442(20)

TABLE XXVII.  $\Upsilon$  and  $\eta_b$  energies and kinetic masses in lattice units for various lattice momenta on coarse set 3 for  $b$  quark mass  $am_b = 2.66$  and  $c_{1,5,6}$  set to 1.

	(0, 0, 0)	(1, 0, 0)	(1, 1, 1)	(2, 0, 0)	(2, 2, 1)	(3, 0, 0)
$aE(1S_0, \mathbf{P})$	0.255 29(4)	0.261 19(4)	0.273 09(4)	0.278 90(4)	0.308 30(8)	0.308 14(6)
$aE(3S_1, \mathbf{P})$	0.286 26(6)	0.292 20(7)	0.304 26(7)	0.310 07(9)	0.339 77(17)	0.339 57(14)
$aM_{\text{Kin}}(\eta_b)$	...	5.773(10)	5.767(7)	5.788(2)	5.787(7)	5.805(3)
$aM_{\text{Kin}}(\Upsilon)$	...	5.716(25)	5.703(17)	5.739(7)	5.732(15)	5.753(11)
$a\tilde{M}_{\text{Kin}}(1S)$	...	5.730(20)	5.719(14)	5.751(6)	5.746(12)	5.766(8)

TABLE XXVIII.  $\Upsilon$  and  $\eta_b$  energies and kinetic masses in lattice units for various lattice momenta on coarse set 3 for  $b$  quark mass  $am_b = 2.66$  and  $c_{1,5,6}$  set to their  $\mathcal{O}(\alpha_s)$  improved values. Slight differences with Table VIII for zero momentum energies arise because we fit a single zero momentum correlator rather than a  $5 \times 5$  matrix.

	(0, 0, 0)	(1, 0, 0)	(1, 1, 0)	(1, 1, 1)	(2, 0, 0)	(2, 1, 1)	(2, 2, 1)	(3, 0, 0)
$aE(1S_0, \mathbf{P})$	0.260 96(4)	0.266 84(4)	0.272 73(4)	0.278 60(4)	0.284 38(4)	0.296 10(4)	0.313 48(6)	0.313 35(6)
$aE(3S_1, \mathbf{P})$	0.292 43(6)	0.298 38(6)	0.304 34(6)	0.310 30(7)	0.316 11(8)	0.327 99(8)	0.345 55(14)	0.345 36(14)
$aM_{\text{Kin}}(\eta_b)$	...	5.818(7)	5.819(7)	5.817(7)	5.839(3)	5.834(4)	5.844(7)	5.859(4)
$aM_{\text{Kin}}(\Upsilon)$	...	5.747(18)	5.748(17)	5.742(17)	5.778(7)	5.764(9)	5.778(13)	5.798(12)
$a\tilde{M}_{\text{Kin}}(1S)$	...	5.764(15)	5.766(14)	5.761(14)	5.793(5)	5.782(8)	5.795(11)	5.813(10)

TABLE XXIX.  $\Upsilon$  and  $\eta_b$  energies and kinetic masses in lattice units for various lattice momenta on fine set 5 for  $b$  quark mass  $am_b = 1.91$  and  $c_{1,5,6}$  set to 1.

	(0, 0, 0)	(1, 0, 0)	(1, 1, 1)	(2, 0, 0)	(2, 2, 1)	(3, 0, 0)
$aE(^1S_0, \mathbf{P})$	0.246 52(3)	0.251 07(3)	0.260 10(3)	0.264 61(3)	0.287 13(4)	0.287 12(4)
$aE(^3S_1, \mathbf{P})$	0.271 53(5)	0.276 10(4)	0.285 18(5)	0.289 74(5)	0.312 44(6)	0.312 46(7)
$aM_{\text{Kin}}(\eta_b)$	...	4.244(6)	4.252(6)	4.2548(14)	4.2516(23)	4.251(3)
$aM_{\text{Kin}}(\Upsilon)$	...	4.222(14)	4.230(13)	4.225(3)	4.223(4)	4.215(6)
$a\bar{M}_{\text{Kin}}(1S)$	...	4.228(12)	4.236(11)	4.2327(24)	4.230(4)	4.224(5)

TABLE XXX.  $\Upsilon$  and  $\eta_b$  energies and kinetic masses in lattice units for various lattice momenta on fine set 5 for  $b$  quark mass  $am_b = 1.91$  and  $c_{1,5,6}$  set to their  $\mathcal{O}(\alpha_s)$  improved values. Slight differences in zero momentum energies are seen compared to Table VIII because we used  $u_{0L} = 0.85246$  rather than 0.8525 and are fitting to single correlators rather than a  $5 \times 5$  matrix.

	(0, 0, 0)	(1, 0, 0)	(1, 1, 0)	(1, 1, 1)	(2, 0, 0)	(2, 2, 1)	(3, 0, 0)
$aE(^1S_0, \mathbf{P})$	0.258 27(3)	0.262 78(3)	0.267 27(4)	0.271 73(3)	0.276 20(3)	0.298 50(4)	0.298 47(3)
$aE(^3S_1, \mathbf{P})$	0.283 90(5)	0.288 44(4)	0.292 99(6)	0.297 47(5)	0.301 99(5)	0.324 51(6)	0.324 47(6)
$aM_{\text{Kin}}(\eta_b)$	...	4.278(7)	4.286(9)	4.287(6)	4.2914(14)	4.2920(23)	4.2951(19)
$aM_{\text{Kin}}(\Upsilon)$	...	4.245(15)	4.251(17)	4.256(14)	4.2515(29)	4.2523(44)	4.2538(41)
$aM_{\text{Kin}}(1S)$	...	4.253(12)	4.260(15)	4.264(11)	4.2615(24)	4.2622(37)	4.2641(35)

$$M(\chi_{b2}) - 3M(\chi_{b1}) + 2M(\chi_{b0}) \quad (\text{C2})$$

with experimental value:  $-47.4(1.3)$  MeV [35], determining the errors on mass differences by adding the errors on the masses in quadrature. Likewise the combination that depends on  $c_3$  only

$$5M(\chi_{b2}) - 3M(\chi_{b1}) - 2M(\chi_{b0}) \quad (\text{C3})$$

with experimental value:  $163.8(3.2)$  MeV [35]. Comparison of our results with experiment for these combinations then allows us to fix  $c_3$  and  $c_4$ .

Table XXV gives the results for the energies in lattice units of the lowest-lying  $P$ -wave states for the  $am_b$  values given in Table III on the coarse (sets 3 and 4) and fine (set 5) lattices. The results were obtained from 5 exponential fits of the form given in Eq. (7) to the  $2 \times 2$  matrix of correlators for each  $P$ -wave meson done as a single simultaneous fit. This enables us to extract mass differences more precisely from the fit than the individual masses and the splitting between each state and the spin average of all the  $^3P$  states is also given. Note that we give separate values for  $^3P_2E$  and  $^3P_2T_2$  lattice representations of the  $J = 2$  state. Differences between the values obtained for  $T_2$  and  $E$  would be a sign of discretization errors. We do not have a significant signal for this but the  $E$  state is higher than the  $T_2$  in all of our fits. The difference is about 3 (2) MeV on the coarse lattices and 2(1) MeV on the fine lattices.

Results are given for the case  $c_4 = 1$  and a nonzero value of  $c_4$  chosen to give reasonable agreement with the experimental value of the combination in Eq. (C2). Results in GeV for the two combinations tested are given in Table XXVI using values of the lattice spacing from the

( $2S - 1S$ ) splitting in Table X, and combining the  $E$  and  $T_2$  representations for the  $^3P_2$  state with the appropriate number of spin states. We see that  $c_3 = 1$  within our errors, but  $c_4$  needs to be larger than 1, more so on the coarse lattices than the fine. We take the same value of  $c_4$  on both coarse sets since the tuning should not depend on the sea quark masses and indeed our results demonstrate that it does not.

Figure 23 shows the spectrum of  $P$ -wave states relative to the  $^3P$  spin average ( $5M(\chi_{b2}) + 3M(\chi_{b1}) + M(\chi_{b0})$ ). The results with  $c_4 > 1$  clearly agree better with experiment than for  $c_4 = 1$ . The main effect of increasing  $c_4$  is to push the  $\chi_{b0}$  state down relative to the spin average. Very little else changes. In particular we see that the splitting between the  $^1P_1$  and the  $^3P$  spin average is very small and negative in all cases. It increases with increasing  $c_4$  but, because the splitting itself is so small, this is not significant. We obtain a  $P$ -wave hyperfine splitting of 2(2) MeV on both coarse and fine lattices, where the experimental result is  $1.6 \pm 1.5$  MeV [39].

On the fine lattices we took  $c_4 = 1.15$ , based on initial calculations. From Table XXVI and Fig. 23 this appears to be an underestimate and an improved value would be 1.18. We also used  $c_3 = 0.96$  but that value is indistinguishable within our errors from  $c_3 = 1.0$ . On the coarse lattices,  $c_4 = 1.25$  is also a slight underestimate, although it agrees within statistical errors with the correct answer.

The final nonperturbatively tuned values for  $c_3$  and  $c_4$  that we obtain are then:  $c_3 = 1.00(9)(2)(10)$  on coarse lattices and  $1.00(4)(2)(10)$  on fine lattices. Our best estimates for  $c_4$  are

$$c_4(\text{coarse}) = 1.28(7)(1)(5) \quad c_4(\text{fine}) = 1.18(2)(1)(5). \quad (\text{C4})$$



The first error is from the statistical/fitting error on the  $P$ -wave masses along with the lattice spacing error. The second error is from experiment. The third error is a systematic error from  $v^6$  terms in NRQCD that are missing from our calculation but that have effectively been absorbed into the value of  $c_3/c_4$  from matching to experiment. The spin splittings could change by  $\mathcal{O}(10\%)$  from  $v^6$  terms. Note that  $c_4$  gets closer to 1 as the lattice gets finer as we expect. Note also that the relationship between  $c_3$  and  $c_4$  that holds in potential models or NRQCD in the continuum because of Lorentz covariance [37] is not applicable to lattice NRQCD in this formulation.

The agreement between the  $c_4$  coefficients obtained nonperturbatively and the  $c_4$  coefficients obtained at  $\mathcal{O}(\alpha_s)$  in Appendix B is good, and certainly within possible  $\alpha_s^2$  variation of the perturbative coefficients (see Table XIII).

Our nonperturbative results for  $c_4$  and  $c_3$  agree well with those derived for the same NRQCD action on different gluon configurations at similar lattice spacing in [12]. There spin-dependent terms at  $v_b^6$  are also included in a separate calculation and then the values derived for the  $v^4$  coefficients  $c_3$  and  $c_4$  change (both increasing). Note that in that paper the calculations were

done with tree-level coefficients for all  $c_i$  and the results rescaled for the derived values of  $c_4$ .

## APPENDIX D: RESULTS FOR THE KINETIC MASS

Tables XXVII, XXVIII, XXIX, and XXX give the results for the ground-state energies and kinetic masses [as defined in Eq. (10)] of the  $Y$  and  $\eta_b$  mesons for different lattice meson momenta in units of  $2\pi a/L$ . We also give the spin-averaged  $1S$  kinetic mass. Results are taken from simultaneous fits to local correlators with the given momentum and with momentum zero using the fit form in Eq. (7). The energies for each momentum and the energy difference which yields the kinetic mass are given directly by the fit. Correlations between the correlators mean that the error on the energy difference is typically smaller than the combined errors from the separate energies. This is particularly true of the “on-axis” momenta which have only one nonzero component. So, for example, the kinetic mass for momentum  $(2, 0, 0)$  is more precise than that for  $(1, 1, 1)$ .

The results are given for coarse ensemble set 3 and fine ensemble set 5 with separate results for the case where  $c_{1,5,6}$  are taken to be 1 and the case where  $c_{1,5,6}$  are  $\alpha_s$  improved. We take 9 exponential fits on set 3 and 7 exponential fits on set 5.

- 
- [1] C. T. H. Davies *et al.* (HPQCD, MILC and Fermilab Lattice), *Phys. Rev. Lett.* **92**, 022001 (2004).
  - [2] A. Gray *et al.* (HPQCD Collaboration), *Phys. Rev. D* **72**, 094507 (2005).
  - [3] A. Gray, Ph. D. thesis, University of Glasgow, 2004.
  - [4] G. Lepage, L. Magnea, C. Nakhleh, U. Magnea, and K. Hornbostel, *Phys. Rev. D* **46**, 4052 (1992).
  - [5] G. Lepage and P. B. Mackenzie, *Phys. Rev. D* **48**, 2250 (1993); arXiv:hep-lat/9209022 [Phys. Lett. B. (to be published)].
  - [6] A. Bazavov *et al.*, *Rev. Mod. Phys.* **82**, 1349 (2010).
  - [7] Z. Hao, G. M. von Hippel, R. R. Horgan, Q. J. Mason, and H. D. Trottier, *Phys. Rev. D* **76**, 034507 (2007).
  - [8] K. Orginos and D. Toussaint (MILC Collaboration), *Phys. Rev. D* **59**, 014501 (1998).
  - [9] K. Orginos, D. Toussaint, and R. L. Sugar (MILC Collaboration), *Phys. Rev. D* **60**, 054503 (1999).
  - [10] G. P. Lepage, *Phys. Rev. D* **59**, 074502 (1999).
  - [11] S. Meinel, *Phys. Rev. D* **79**, 094501 (2009).
  - [12] S. Meinel, *Phys. Rev. D* **82**, 114502 (2010).
  - [13] C. T. H. Davies *et al.* (HPQCD Collaboration), *Phys. Rev. D* **82**, 114504 (2010).
  - [14] E. B. Gregory *et al.* (HPQCD Collaboration), *Phys. Rev. D* **83**, 014506 (2011).
  - [15] E. B. Gregory *et al.* (HPQCD Collaboration), *Phys. Rev. Lett.* **104**, 022001 (2010).
  - [16] E. Follana *et al.* (HPQCD Collaboration), *Phys. Rev. D* **75**, 054502 (2007).
  - [17] E. Follana, C. T. H. Davies, G. P. Lepage, and J. Shigemitsu (HPQCD Collaboration), *Phys. Rev. Lett.* **100**, 062002 (2008).
  - [18] C. McNeile, C. T. H. Davies, E. Follana, K. Hornbostel, and G. P. Lepage (HPQCD Collaboration), *Phys. Rev. D* **85**, 031503 (2012).
  - [19] A. Bazavov *et al.* (MILC Collaboration), *Phys. Rev. D* **82**, 074501 (2010).
  - [20] A. Hart, G. M. von Hippel, and R. R. Horgan (HPQCD Collaboration), *Phys. Rev. D* **79**, 074008 (2009).
  - [21] C. Davies, E. Follana, I. Kendall, G. Lepage, and C. McNeile (HPQCD Collaboration), *Phys. Rev. D* **81**, 034506 (2010).
  - [22] C. Aubin *et al.* (MILC Collaboration), *Phys. Rev. D* **70**, 094505 (2004).
  - [23] R. Sommer, *Nucl. Phys.* **B411**, 839 (1994).
  - [24] D. Toussaint (private communication).
  - [25] B. Thacker and G. Lepage, *Phys. Rev. D* **43**, 196 (1991).
  - [26] C. J. Morningstar, *Phys. Rev. D* **50**, 5902 (1994).
  - [27] E. Mueller, Ph. D., thesis University of Edinburgh, 2009.
  - [28] T. C. Hammant, A. G. Hart, G. M. von Hippel, R. R. Horgan, and C. J. Monahan, *Phys. Rev. Lett.* **107**, 112002 (2011).
  - [29] C. T. H. Davies *et al.*, *Phys. Rev. D* **37**, 1581 (1988).

- [30] C. T. H. Davies *et al.*, *Phys. Rev. D* **50**, 6963 (1994).
- [31] I. D. Kendall, Ph. D., thesis University of Glasgow, 2010.
- [32] C. Gattringer and C. B. Lang, *Lect. Notes Phys.* **788**, 1 (2010).
- [33] G. P. Lepage *et al.*, *Nucl. Phys. B, Proc. Suppl.* **106**, 12 (2002).
- [34] C. Bernard *et al.* (Fermilab Lattice and MILC), *Phys. Rev. D* **83**, 034503 (2011).
- [35] K. Nakamura *et al.* (Particle Data Group), *J. Phys. G* **37**, 075021 (2010).
- [36] Note that in our previous work [14] we had to allow for a mass shift from missing  $c$  quarks in the sea. That is no longer necessary here.
- [37] G. S. Bali, K. Schilling, and A. Wachter, *Phys. Rev. D* **56**, 2566 (1997).
- [38] T. Burch *et al.* (Fermilab Lattice and MILC), *Phys. Rev. D* **81**, 034508 (2010).
- [39] I. Adachi *et al.* (Belle Collaboration), *Phys. Rev. Lett.* **108**, 032001 (2012).
- [40] B. Aubert *et al.* (BABAR Collaboration), *Phys. Rev. Lett.* **101**, 071801 (2008).
- [41] B. Aubert *et al.* (BABAR Collaboration), *Phys. Rev. Lett.* **103**, 161801 (2009).
- [42] G. Bonvicini *et al.* (CLEO Collaboration), *Phys. Rev. D* **81**, 031104 (2010).
- [43] R. Mizuk (Belle), Quarkonium Working Group meeting, 2011.
- [44] B. A. Kniehl, A. A. Penin, A. Pineda, V. A. Smirnov, and M. Steinhauser, *Phys. Rev. Lett.* **92**, 242001 (2004); **104**, 199901(E) (2010).
- [45] A. A. Penin, [arXiv:0905.4296](https://arxiv.org/abs/0905.4296).
- [46] C. Aubin *et al.* (MILC Collaboration), *Phys. Rev. D* **70**, 114501 (2004).
- [47] S. R. Sharpe and N. Shores, *Phys. Rev. D* **62**, 094503 (2000).
- [48] A. Bazavov *et al.* (MILC Collaboration), *Proc. Sci., LAT2009* (2009) 079.
- [49] Q. Mason, H. D. Trotter, R. Horgan, C. T. H. Davies, and G. P. Lepage (HPQCD Collaboration), *Phys. Rev. D* **73**, 114501 (2006).
- [50] Q. Mason (private communication).
- [51] Note that there is a typographical error in [49] so that the lattice logarithm is given the wrong sign in Eq. (11).
- [52] C. McNeile, C. T. H. Davies, E. Follana, K. Hornbostel, and G. P. Lepage (HPQCD Collaboration), *Phys. Rev. D* **82**, 034512 (2010).
- [53] C. T. H. Davies *et al.* (HPQCD Collaboration), *Phys. Rev. Lett.* **104**, 132003 (2010).
- [54] M. G. Alford, W. Dimm, G. P. Lepage, G. Hockney, and P. B. Mackenzie, *Phys. Lett. B* **361**, 87 (1995).
- [55] C. J. Morningstar, *Phys. Rev. D* **48**, 2265 (1993).
- [56] M. A. Nobes, H. D. Trotter, G. P. Lepage, and Q. Mason, *Nucl. Phys. B, Proc. Suppl.* **106**, 838 (2002).
- [57] A. Hart, G. M. von Hippel, R. R. Horgan, and L. C. Stoneri, *J. Comput. Phys.* **209**, 340 (2005).
- [58] A. Hart, G. M. von Hippel, R. R. Horgan, and E. H. Müller, *Comput. Phys. Commun.* **180**, 2698 (2009).
- [59] C. Monahan, Ph. D. thesis, University of Cambridge, 2011.
- [60] C. T. H. Davies *et al.* (HPQCD Collaboration), *Phys. Rev. D* **78**, 114507 (2008).
- [61] E. Dalgic, J. Shigemitsu, and M. Wingate, *Phys. Rev. D* **69**, 074501 (2004).